DYNAMIC STABILITY OF QUADRUPEDAL LOCOMOTION: ANIMAL MODEL, CORTICAL CONTROL AND PROSTHETIC GAIT

A Dissertation
Presented to
The Academic Faculty

by

Bradley J Farrell

In Partial Fulfillment
of the Requirements for the Degree
Doctor of Philosophy in the
School of Applied Physiology

Georgia Institute of Technology
December 2012

DYNAMIC STABILITY OF QUADRUPEDAL LOCOMOTION: ANIMAL MODEL, CORTICAL CONTROL AND PROSTHETIC GAIT

Approved by:

Dr. Boris I Prilutsky, Advisor
School of Applied Physiology
Georgia Institute of Technology

Dr. Irina Beloozerova, Co-advisor
Division of Neurobiology
Barrow Neurological Institute

Dr. Young-Hui Chang
School of Applied Physiology
Georgia Institute of Technology

Dr. Robert Guldberg
School of Mechanical Engineering
Georgia Institute of Technology

Dr. T Richard Nichols
School of Applied Physiology
Georgia Institute of Technology

Dr. Minoru Shinohara
School of Applied Physiology
Georgia Institute of Technology

Date Approved: November 11, 2012

This dissertation is dedicated to Jennifer and Luke. Thank you!

ACKNOWLEDGEMENTS

I wish to thank first and foremost my wife and family for always being throughout this endeavor. I would also like to thank everyone who encouraged me and never stopped believing in me; without your support I would not be here. I would also like to thank my advisor, Dr. Boris Prilutsky, for his guidance. I would like to thank my committee members for their help and support. I would also like to thank everyone who helped me in my research: Dr. Margarita Bulgakova for help with EMG and cortical activity analysis, Drs. Irina Beloozerova and Mikhail Sirota for help with cortical activity recording and analysis, Dr. Jana Ritter for help with histopathology, Dr. Ketul Popat for help with nanotextured implants, Dr. Mark Pitkin for providing implants, Dr. Ashley Strong for veterinary assistance, Dr. John Dalton IV for surgical assistance, Rob Kistenberg for prosthesis design, Juan Cave II, Shivani Shah, and Zengqin Fan for help with data analysis, Allison Cerutti for help with prosthesis parameters, Tim Kunz for help with prosthesis design and everyone else who gave me feedback along the way. Lastly I thank everyone who encouraged me and helped me get through to the end.

TABLE OF CONTENTS

LIST OF TABLES

Page

LIST OF FIGURES

Page

LIST OF SYMBOLS AND ABBREVIATIONS

⊕ or CoM	Center of Mass
✣ or XCoM	Extrapolated Center of Mass
BoS	Base of Support
EMG	Electromyography
DSA	Direct Skeletal Attachment
TA	Tibialis Anterior
MG	Medial Gastrocnemius
LG	Lateral Gastrocnemius
SO	Soleus
VM	Vastus Medialis
VL	Vastus Lateralis
RF	Rectus Femoris
BFA	Biceps Femoris Anterior
BFP	Biceps Femoris Posterior
IP	Iliopsoas
SAM	Sartorius Medial
PTN	Pyramidal Tract Neuron
PEF	Period of Elevated Firing
dM	Depth of Modulation
MTP	Metatarsal Phalangeal
MCP	Metacarpal Phanalgeal
IDS	Index of Dynamic Stability
ISS	Index of Static Stability
SD	Sprague Dawley

SUMMARY

The ability to control balance and stability are essential to prevent falls during locomotion. Maintenance of stable locomotion is challenging especially when complicated by amputation and prosthesis use. Humans employ several motor strategies to maintain stability during walking on complex terrain: decreasing walking speed, adjusting stride length and stance width, lowering the center of mass, and prolonging the double support time. The mechanisms of selecting these motor strategies by the primary motor cortex are unknown and cannot be studied directly in humans. There is also little information about dynamic stability of prosthetic gait with bone-anchored prostheses, which are thought to provide sensory feedback to the amputee through osseoperception. Therefore, the Specific Aims of my research were to (1) evaluate dynamic stability and the activity of the primary motor cortex during walking with different constraints on the base of support and (2) develop an animal model to evaluate mechanics and stability of prosthetic gait with a bone-anchored prosthesis. To address these aims, I developed a feline model that allows for investigating (1) the role of the primary motor cortex in regulation of dynamic stability of intact locomotion, (2) skin and bone integration with a percutaneous porous titanium implant facilitating prosthetic attachment, and (3) dynamic stability of walking on a bone-anchored prosthesis. The results of Specific Aim 1 demonstrated that the area and shape of the base of support influence the margins of dynamic stability during quadrupedal walking. For example, I found that the animal is dynamically unstable in the sagittal plane and frontal plane (although to a lesser degree) during a double-support by a forelimb and the contralateral hindlimb. Elevated neuronal

activity from the right forelimb representation in the primary motor cortex during these phases suggests that the motor cortex may contribute to selection of paw placement location and thus to regulation of stability. The results of Specific Aim 2 on the development of skin-integrated bone-anchored prostheses demonstrated the following. Skin ingrowth into 3 types of porous titanium pylons (pore sizes 40-100 μm and 100-160 μm and nano-tubular surface treatment) implanted under skin of rats was seen 3 and 6 weeks after implantation, and skin filled at least 30% of available implant space. The duration of implantation, but not implant pore size (in the studied range) or surface treatment statistically influenced skin ingrowth; pore size and time of implantation affected the implant extrusion length ($p<0.05$). The implant type with the slowest extrusion rate (pore size 40-100 μm) was used in a feline model of prosthetic gait with skin-integrated bone-anchored prosthesis. The developed implantation methods, rehabilitation procedures and feline prostheses allowed 2 animals to utilize skin- and bone-integrated prostheses for dynamically stable locomotion. Prosthetic gait analysis demonstrated that the animals loaded the prosthetic limb, but increased reliance on intact limbs for weight support and propulsion. The obtained results and developed animal model improve the understanding of locomotor stability control and integration of skin with percutaneous implants.

CHAPTER 1

INTRODUCTION

The ease with which people and animals move is not merely a stereotypical, robot-like movement but an ever changing, precise coordination of limbs, joints and muscles which results in elegant, fluid movement. Specifically, locomotion is the primary way in which people and animals move from place to place. It is exhibited in many different forms (walking, running, hopping, swimming, crawling, etc. (Gray, 1968)) and has been studied for many years using a variety of models (Matthews, 2004). Of the different modes of locomotion, walking is perhaps the most common and is typically defined for humans and other terrestrial animals by the absence of an aerial phase during which none of the legs are in contact with the ground (Hildebrand, 1965). During walking the legs provide the propulsive forces needed for movement, however, it is imperative to understand that control of the other body segments (e.g. arms, trunk and head) are necessary to maintain posture and balance thus preventing falls (MacKinnon & Winter, 1993). When the sensory and motor systems are intact and functioning properly falls are generally prevented. However, in the presence of sudden perturbations, neurological disease, musculoskeletal conditions or declining sensorimotor performance especially with age, falls occur more readily.

While not all falls cause injury, unintentional falls are the leading cause of injury among the US population. In 2007, unintentional falls caused 8 million injuries resulting in a net cost (medical plus work loss) of $29 billion and in 2009 unintentional falls caused approximately 25,000 fatalities (Centers for Disease Control and Prevention, 2003). Unintentional falls are especially problematic in elderly persons and persons with

disabilities who may already be at a disadvantage in terms of maintaining balance (Miller *et al.*, 2001a; Miller *et al.*, 2001b; Viswanathan & Sudarsky, 2012). Specifically, in lower limb amputees, the risks of falling increases due to the lack of feedback from the neuromuscular system and a decrease in the ability to produce corrective movements in the amputated limb. On top of that, the falls not only cause physical injury but can also cause damage to an expensive prosthesis. Therefore it is important to understand how balance and stability are controlled during uninjured and injured states and what improvements can be made to prevent falls.

1.1 Balance and Stability

Balance and stability are complicated terms each with multiple meanings. Balance can refer to the state of equilibrium of the system, the position of the center of mass relative to the base of support, the zero sum of forces and moments about the center of mass, and the ability not to fall (MacKinnon & Winter, 1993; Maki & McIlroy, 1997; Pollock *et al.*, 2000). Furthermore, definitions of dynamic balance, where the body is moving and the resultant force and moment acting at the center of mass (CoM) are not zero (i.e. the body is accelerating), are less established. Stability, in postural control terms, typically refers to the ability of the system to respond to a perturbation. There are multiple ways to quantify stability, e.g. using the mathematical stability theory describing stability of solution of differential equations (through Floquet multipliers (Hurmuzlu & Basdogan, 1994; McAndrew *et al.*, 2011) or Lyapunov coefficients (Full *et al.*, 2002; Hasan, 2005)) or using the experimentally determined margins of stability, i.e. the distance from the projection of the CoM on to the ground to the edge of area of support (Hof *et al.*, 2005). For the purposes of this work, balance is considered as the ability of

the system to maintain the performance of a task (i.e. not to fall) and stability is defined based on the margins of stability, i.e. the location of the projection of the center of mass (or extrapolated center of mass, defined below) on to the walking surface relative to the base of support (BoS) (Fig 1.1).

In accordance with this definition, a mechanical system is statically stable when its CoM is within the BoS. The level of stability (or stability margin) can be quantified as the shortest distance from the CoM projection to the edge of BoS (Fig 1.2). If the CoM projection is within BoS (the stability margin is positive), the body is statically stable, otherwise the stability margin is negative and the body is unstable (Ting *et al.*, 1994). For instance, during quiet standing the CoM has zero velocity and acceleration (static position; i.e. the resultant force at and moment about the CoM are zero); as a result the CoM projection onto the ground lies within the BoS. Thus, according to this definition, quiet standing is a balanced and statically stable condition. However, during locomotion this is not the case. The CoM has a non-zero velocity and the sum of the forces and moments applied to the body is not zero (i.e. the body is accelerating). As such, stability cannot be described solely by the static position of the CoM and needs to be defined differently. Hof et al (2005) proposed to measure dynamic stability of a moving mechanical system using the notion of the extrapolated center of mass ($XCoM = P_{CoM} + v_{CoM}/\omega_o$, where P_{CoM} is the position and v_{CoM} is the velocity of the CoM and $\omega_o = \sqrt{g/l}$ is the natural frequency of the (inverted) pendulum with mass, equal to body mass, balancing on a massless stick of length *l* equaled leg length). According to this approach, a body is dynamically stable if the projection of XCoM onto the ground is within the BoS, and it is unstable otherwise. Other methods of evaluating dynamic stability of

locomotion that are based on the mathematical stability theory, such as Floquet multipliers, use similar assumptions (i.e., rigid struts for legs and a rigid torso (Hurmuzlu & Basdogan, 1994)) and lead to similar conclusions about the effects of wide and narrow base of support on dynamic stability of human walking (McAndrew Young & Dingwell, 2012b, a). Thus, the chosen method of estimating margins of dynamic stability of locomotion using the extrapolated CoM (Hof et al., 2005) evaluates the dynamic stability of the system and might have a simpler mechanical meaning.

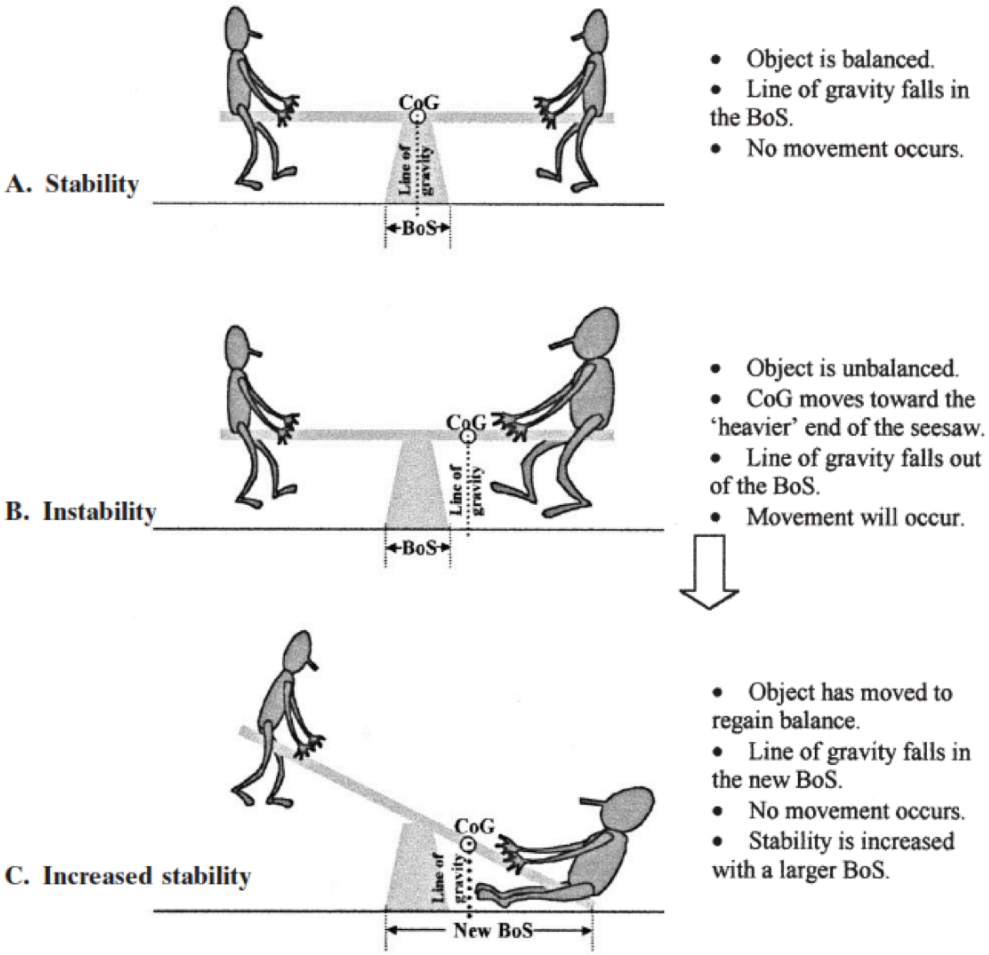

Figure 1.1 Relationship between base of support, center of mass (CoM or Center of Gravity, CoG) and stability. Reproduced with permission (Pollock et al., 2000)

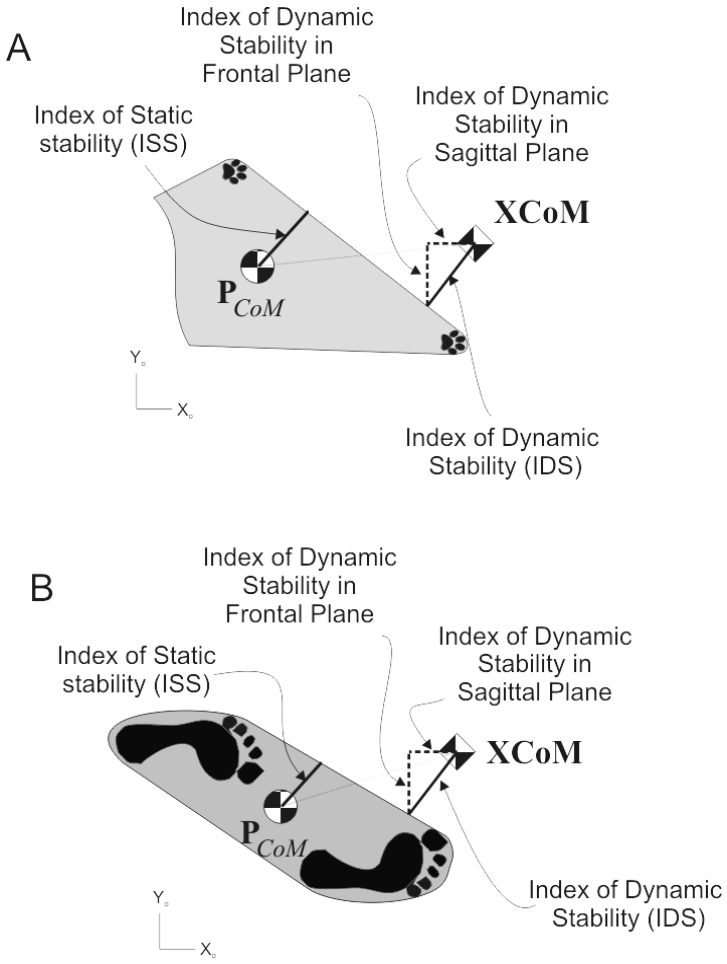

Figure 1.2 Definitions of margins of stability for a quadrupedal animal (A) and human (B). View from above; axis x defines direction of progression and axis y, the medial-lateral direction. P_{CoM} is the projection of the center of mass onto the support surface. XCoM is the extrapolated center of mass (see text for further explanations). Shaded areas represent the base of support. In A only part of support area is shown.

Controlling the margins of stability is important. During bipedal gait initiation the CoM must be shifted toward the trailing leg, i.e. prepared for a reduction of the BoS while the leading leg loses contact with the ground during the first step. In addition, the body is destabilized in the direction of progression to initiate locomotion and this destabilization occurs in each step in both the anterior -posterior and medial -lateral direction to maintain forward progression (Jayes & Alexander, 1980; Winter, 1995; Hof *et al.*, 2005). In quadrupeds, however, the increased base of support in the sagittal plane

may allow the CoM to remain within the BoS during some phases of locomotion. Thereby the least stable (most unstable) direction for the quadruped would be the lateral direction in the frontal plane based on the ratio of support width (frontal plane) to support length (sagittal plane) Misiaszek (2006).

1.2 Mechanisms of balance and stability control during locomotion

Maintaining balance and stability during locomotion involves a complex network of neural pathways with multiple levels of control (Fig 1.3). The lowest level of stability control is the passive mechanics of the musculoskeletal system (e.g.(Loram *et al.*, 2007; Bunderson *et al.*, 2010). Passive mechanics provides joint and limb stiffness, which results in the force necessary to stabilize the system after perturbations. The next level of stability control involves spinal reflexes. These reflexes originate from muscle stretch (e.g. monosynaptic stretch reflex), Golgi tendon organs or mechanoreceptors in skin and other soft tissues. A combination of muscle stretch and force related spinal responses regulate muscle and joint stiffness (Nichols & Houk, 1976) and assist in stabilizing the body after perturbations. Previous evidence suggests that these responses are only short-term compensation strategies (Lalonde & Strazielle, 2007) and that delayed responses to larger postural perturbations involve coordination through the spinal and lower brain stem (Fung & Macpherson, 1999; Honeycutt & Nichols, 2010), vestibular (Macpherson *et al.*, 2007) and visual (Hallemans *et al.*, 2010) systems, cerebellum (Dichgans & Fetter, 1993), reticular formation (Deliagina *et al.*, 2008; Stapley & Drew, 2009) and the cortical areas (Jacobs & Horak, 2007), including the primary motor cortex (Karayannidou *et al.*, 2008; Karayannidou *et al.*, 2009).

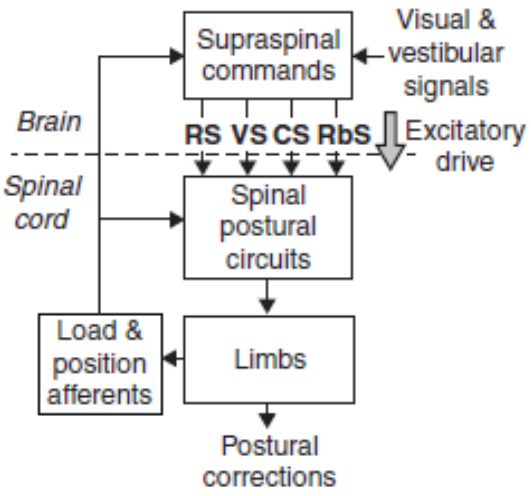

Figure 1.3 Main components of the postural system in quadrupeds. Two closed-loop mechanisms participate in postural control. Spinal circuits generate postural limb reflexes, and their effects are added to the effects of supraspinal commands, which are generated on the basis of sensory information and transmitted by the major descending tracts - reticulospinal (RS), vestibulospinal (VS), corticospinal (CS) and rubrospinal (RbS) Reproduced with permission (Deliagina *et al.*, 2008)

During unconstrained, level walking with no perturbations, the gait biomechanics of the premammillary decerebrated cat preparations are similar to the intact cat (Mori, 1987; Whelan, 1996; Musienko *et al.*, 2012) and do not require external support for lateral stability that spinalized cats (Macpherson & Fung, 1999) or cats decerebrated more caudally require. Thus, the responses, elicited from the spinal cord and brain stem, allow for maintenance of posture and simple postural corrections required for "normal" gait. However, recovery of posture is typically much slower illustrating deficits to the control system (Musienko *et al.*, 2008; Musienko *et al.*, 2012).

Therefore, higher brain centers, such as the motor cortex, may alter responses to the sensory feedback, adjust muscle synergies and overall alter movements as needed for the given perturbation to avoid falling. This involves processing sensory information

from multiple sources including visual, vestibular and somatosensory feedback and activating the correct spinal centers in the correct pattern to produce the appropriate reaction to prevent falling. Processing and responding to the input information takes time and thus a longer delay before action (that is, spinal reflexes and pathways are first to respond followed later by supraspinal responses). The central component of proper responses to postural perturbations is the sensory feedback from the somatosensory system. Previous research has shown that without somatosensory feedback, postural perturbations cause a greater loss of balance (Bolton & Misiaszek, 2009) because the system is relying on visual and vestibular feedback only, which does not provide a fast enough response time. The rapid feedback may be a key role of the spinal reflexes; providing initial corrective response to perturbations and giving the supraspinal mechanisms, including the cortical ones, increased time for planning. Nevertheless, visual and vestibular inputs cannot be discounted because these inputs are needed to maintain balance (Hallemans *et al.*, 2010); e.g. loss of vestibular feedback leads to falls during head turns in the cat (Stapley *et al.*, 2006). Furthermore, cognitive tasks, performed during postural tasks, exacerbate balance control. For instance, when a subject is asked to solve a complex problem overall stability decreases and this decrease is exaggerated with age (Maki & McIlroy, 2007; Schmid *et al.*, 2007).

In reality, balance control is a combination of the mechanisms at all levels of the nervous system and incorporates other processing areas such as the cerebellum (Ioffe *et al.*, 2007), basal ganglia and other brain centers (Lalonde & Strazielle, 2007) and further is dependent on the nature of the perturbation. It has been suggested that the general control strategy for balance is set by the supraspinal centers and then the lower spinal

networks and reflexes implement the rules (Misiaszek, 2006b). For instance, if the set state is quiet standing, then signals from the supraspinal centers may move specific spinal reflexes closer to threshold such that a smaller movement or perturbation will result in a corrective response. For instance, in the sagittal plane the triceps surae and tibialis anterior muscle stretch reflexes may be preferentially activated in response to backward or forward body perturbations.

Much of the research on postural coordination and balance has been performed in animal models, especially the cat. Given that the cat has four legs providing support, one must ask if the human control systems react in a similar way. There are many similarities in balance control between these two models, e.g. reflex pathways, timing, and patterns of muscle postural responses (Fung & Macpherson, 1999; Torres-Oviedo *et al.*, 2006; Macpherson *et al.*, 2007; Torres-Oviedo & Ting, 2010). However, the human, being bipedal, has a much smaller area of support and margins of stability. Further, humans have a higher center of mass than most animals due to the bipedal stance and upright posture. Therefore, based solely on height, the projection of their CoM on the ground would reach the border of the area of support sooner at the same angular displacement of the line connecting the CoM and the center of the base of support from the vertical.

1.3 Balance Control in the Amputee

As with most technologies, the field of prosthetics has undergone many advances since the first wooden leg was implemented (Wilson, 1992). Today's prostheses incorporate microprocessor damped and powered joints (Bellmann *et al.*, 2010), carbon fiber components, and many more advances. However, even with the technological advances, given the insult to the neuromuscular system, maintaining balance can be

difficult and the difficulties tend to increase with more proximal and invasive amputations (e.g. bilateral transfemoral amputation). The many muscles, which were typically active to correct posture after perturbations, are lost after amputations. In the sagittal plane, postural corrections after transtibial and higher amputations are impacted substantially as the ankle recovery strategy is the most common postural response to relatively small perturbations (Maki & McIlroy, 1997; Curtze *et al.*, 2012). In the frontal plane balance may not be as adversely affected because postural corrections generally involve the proximal muscles around the hip. However postural responses that arise from tactile sensation in the feet or muscles that have been amputated are lost. In general, amputees tend to have a bias towards the intact leg. Perhaps this is due to inherent "trust" in the intact limb and the fact that the residual limb cannot provide sensory information about the load or position of the prosthesis. Consequently amputees typically have standing and gait asymmetry where the intact leg supports more load, is on the ground longer and overall does more work (Hurley *et al.*, 1990; Burkett *et al.*, 2003; Nederhand *et al.*, 2012).

There are several possibilities for improving balance in amputees. Efforts have been made to restore symmetry of posture and locomotion in the amputees through training more symmetrical loading during standing (Nederhand *et al.*, 2012), but other results suggest that weight bearing and balance have different control centers (Macpherson & Fung, 1999). Further, training and experience improves amputee balance however amputees rely heavily on vision to maintain balance (Barnett *et al.*, 2012). Balance is also generally better with a longer residual limb as there is more direct interface with the prosthetic socket (Murdoch, 1969); thus, improved diagnostic and

surgical techniques could help salvage as much residual limb length as possible. Alignment of the prosthesis is also a key factor in determining the quality of both prosthetic use and balance. For instance, in persons with transfemoral amputations, the anterior/posterior alignment of the knee joint can create either an extension or flexion moment at the knee during stance. A knee joint placed anterior to the line to the ground reaction force vector can cause the knee to buckle unexpectedly, whereas placing the knee joint posterior to this line adds stability during stance. Similarly, frontal plane alignments are important if frontal plane motion is allowed. External rotation of the foot could provide the amputee with an increased base of support laterally. However, amputees often adapt by internally rotating the hip to allow for easier shank progression and push-off during stance, therefore any improvements in balance are lost by internal hip rotation (Fridman *et al.*, 2003). Other improvements in balance could be complicated by injury to the intact joints or loss of symmetry between limbs (though it is unclear if symmetry leads to better balance) (Hurley *et al.*, 1990). Finally, one of the largest contributors to control of balance in the amputee is the fit of the prosthesis. A loose socket provides an unstable connection between the limb and the device making application of force to the socket wall difficult. Therefore, if the body is perturbed, correction forces are not immediately applied to the socket wall because they are required to move the limb into apposition with the socket wall and deform soft tissues. Thus, reaction time needed to respond (and possibly the pain associated) increases making the risk of falling greater.

1.4 Direct Skeletal Attachment

One solution to improve prosthetic fit is to eliminate the socket and directly attach the prosthesis to the residual bone. Direct skeletal attachment (DSA) of an external prosthesis, often referred to as an osseointegrated or bone anchored prosthesis, is achieved via a percutaneous implant that is anchored in the bone. Direct skeletal attachment was first documented around the 1850's, when Malgaigne attached a screw through the skin into the tibia to secure a brace (Murphy, 1973). After World War II further efforts were made in Germany and the US to directly attach a limb prosthesis to the residual limb, however infection was a major issue (Murphy, 1973). In the 1950's Per-Ingvar Branemark unintentionally discovered that titanium would integrate with bone (Branemark, 1983) and developed implantation procedures for titanium dental implants (Brånemark *et al.*, 1969; Adell *et al.*, 1970). Since then there have been more than 800,000 people implanted with titanium anchors in the jaw (Brånemark *et al.*, 2001). Additional uses of direct skeletal attachment has been in bone anchored hearing aids (BAHAs)(Tjellström & Håkansson, 1995) which have been FDA approved for over 25 years and 90% of patients remain free of infection (Snik *et al.*, 2005). More recently DSA procedures have been adapted for attachment of limb (Brånemark *et al.*, 2001; Staubach & Grundei, 2001) and digit prostheses (Lundborg *et al.*, 1996; Manurangsee *et al.*, 2000) however there is still room to improve DSA devices.

DSA removes the common cause of problems in amputees, the socket. Ill fitted sockets can limit wear time because of pain (Sherman, 1999), skin irritation, (Levy, 1992; Levy, 1995; Koc *et al.*, 2008), infection (Köhler *et al.*, 1989) or feelings of discomfort during sitting or standing (Pezzin, 2004). They can also "piston" (movement of the socket relative to the skin of the residual limb) which can lead to soft tissue breakdown.

Combined, these problems result in approximately 25% of amputees dissatisfied with the fit of their prosthesis (Pezzin, 2004). Furthermore, there are instances in which the residual limb is too short to provide stable attachment for a socket prosthesis, e.g. cases involving high transfemoral amputations or high upper arm or finger amputations (Manurangsee *et al.*, 2000; Hagberg *et al.*, 2005; Cervelli *et al.*, 2008). Thus, the biggest advantage of DSA prostheses is the removal of the socket and the transmission of load directly to the bone avoiding pressure on the skin. In addition, an increase in range of motion (Sullivan *et al.*, 2003; Hagberg *et al.*, 2005) and osseoperception (a sense of loading) have been associated with DSA prostheses (Jacobs *et al.*, 2000). The origin of osseoperception is currently unknown. It may originate in mechanoreceptor neurons within the residual bone or it may be a result of joint capsule mechanoreceptors. Presently it has only been described as based on subjective response from the amputee. While DSA procedures are currently approved for use in patients or undergoing clinical evaluations in a few countries, they are not FDA approved in the US due to high risks of infection (Tillander *et al.*, 2010) and lack of long-term research. Therefore improvements of the procedures and implants are needed to provide a safer and more reliable direct attachment of prosthesis to the bone.

Optimal direct skeletal attachment for limb prostheses relies on an implant that is integrated with the bone and skin. Bone integration is a well-established phenomenon necessary to prevent implant loosening over the lifetime of the device and provide a secure attachment for performing various motor activities including locomotion. Skin integration, on the other hand, is equally important to provide a natural protective barrier

against bacteria and other pathogens but has yet to be achieved. A brief review of the physiology of bone and skin interaction with implants is presented next.

1.4.1 Bone Integration

Bone integration with an implant, which has been termed osseointegration, is growth of bone tissue into and/or around the implant. The term osseointegration initially referred to an intimate implant surface to bone contact where the implant was pure titanium (Brånemark *et al.*, 2001). This term has since been expanded to incorporate other materials, such as plastics, other metals, and ceramics (Albrektsson & Johansson, 2001), and describe their "fusion" with bone (Kienapfel *et al.*, 1999). Osseointegration has been more formally defined as the growth and formation of bone tissue around an implant without the presence of fibrous tissue at the bone–implant interface (Dorland's Illustrated Medical Dictionary, 2007). The term *bone ingrowth* refers to the growth of bone tissue into pores and/or surface modifications/defects of the implant (Kienapfel *et al.*, 1999). Implants that are solid and have a smooth finish prevent bone ingrowth as the bone can only grow around the implant and not directly into it. Implants with porosity or a rough surface texture tend to be better integrated because the bone ingrowth secures the implant through additional contact surface area. Today most implants used for osseointegration have porous or roughened surfaces to provide areas for bone ingrowth and attachment (Ehrenfest *et al.*, 2010).

Optimal porosity for bone integration has been well established. Previous reports indicate that pore sizes between 100-400 μm are of the optimal range (Kienapfel *et al.*, 1999) for osseointegration (with a trend toward the higher range). However, osseointegration has also been shown in implants with pores ranging from 25μm to 100

μm (Itala *et al.*, 2001). The main advantage of larger pores is that they allow for reduction of shear stress due to a greater contact area with bone. Smaller pores, however, may be more beneficial for skin integration and thus eventually implants with different pore sizes in different regions may be necessary for bone and skin integration. Further, the fact that small pore implants, which are preferable for skin integration (see below), do show bone integration (Itala *et al.*, 2001; Pitkin *et al.*, 2009) could make these implants suitable for use in bone anchored limb prostheses. Another benefit to implants with small pore size is that increasing pore size decreases the strength of the implant thus increasing the probability of its failure.

The overall process of osseointegration is, in general, better understood and documented than skin integration. Principally this is due to the fact that, unlike skin, bone readily integrates with implants made of certain materials. Additionally, osseointegration is stable and its properties for the most part do not rapidly change. Bone growth into and/or around the implants is slow, so each stage of bone remodeling and osseointegration can be isolated and identified. The stages resemble those of bone fracture healing with the lack of a cartilaginous stage (Kienapfel *et al.*, 1999). Immediately after implantation there is the formation of a hematoma around the implant. This is followed by the development of a mesenchymal tissue layer, which provides the progenitor cells that will develop into mature osteocytes. As healing continues the mesenchymal layer is replaced by woven bone, which is stronger but still fragile and less stable than compact or cortical bone. Finally, the woven bone is replaced by compact bone through remodeling, and restoration of bone marrow proceeds if space is available.

One of the most important factors to achieve successful osseointegration of an implant is stability of the implant-bone interface (Kienapfel *et al.*, 1999). If the implant is loaded and shifts during the early phases of remodeling, this could cause a breakdown of the developing bone-implant interface leading to prolong recovery or the interface damage. Therefore, an implant must be protected from external loads during the relatively slow healing process to yield mechanically sound integration. Typically, several months of no-load bearing are recommended for patients receiving an osseointegrated implant in both the lower and upper extremities (Brånemark *et al.*, 2001; Sullivan *et al.*, 2003; Snik *et al.*, 2005). After the no-loading period the implants are loaded slowly such that the bone will slowly align with the stresses that are applied (Frossard *et al.*, 2002; Frossard, 2010). Nevertheless, in total hip arthroplasty, some research suggests that early loading of uncemented implants produces no ill effect several years post-surgery (Hol *et al.*, 2010). This, however, is most likely due to the orientation of loading and the geometry of the marrow cavity. When the femoral components of the hip implants are loaded early before osseointegration can occur, they are forced deeper into the femoral marrow cavity. The cone-like shaft of the implant and the decreasing radius of the marrow cavity prevent movement and allow the implant to become more secure with compressive loading. Furthermore, hip arthroplasties are generally performed in elderly patients who are less active compared to younger traumatic amputees. Therefore, considerations must be made concerning the life of the implant and how the body will respond to the implant over the course of several years.

1.4.2 Skin Integration

Skin integration has a unique set of challenges compared to bone integration, some of which stem from the wound healing process itself and others from the dynamic processes of skin growth and regeneration. First, consider typical wound healing of damaged skin and the distinct steps of this process. Similar to bone, initially there is development of a hematoma at the site of the dermal interruption. This helps to seal off the wound from the external environment and prevent excessive blood loss. Following hematoma there is an infiltration of macrophages and fibroblasts in the wound area to remove foreign debris and lay down connective tissue, respectively. Finally there is infiltration by keratinocytes throughout the wound space and reformation of the dermal and epidermal layers (von Recum & Park, 1981). During the healing processes, dermal and epidermal continuity seems to be a primary goal. This means that the skin tends to be a continuous layer with no interruptions. This is achieved by the skin following the deep border of the scab along the capillary beds until it has reestablished connections with the other side of the skin opening and thus regaining continuity (von Recum, 1984). Afterwards the skin will slowly reestablish collagen and connective tissues and finally align them according to the stresses in the skin, however, this section of skin typically known as the scar will never regain its original strength (Schreuders *et al.*, 1988).

During the wound healing process, one main feature that hinders proper skin integration with a percutaneous device is dermal continuity. As the wound heals around the implant, the skin grows down, away from the exterior surface of the skin, along the borders of the implant until dermal continuity is reached. This often results in a thick fibrous capsule forming around the perimeter of the implant known as a sinus tract. In solid non-porous implants this has been termed marsupialization. In marsupialized

implants, the empty space between the tissue and implant become filled with dead cells and debris over time and results in a haven for bacteria. The implant is either extruded through normal skin growth or through application of external forces (e.g. scratching or biting). Infection in the space between the implant and capsule often leads to faster extrusion and/or infection in deeper tissues. In light of these and other reasons for extrusion of percutaneous implants, four main mechanisms of implant loss or extrusion from the skin have been identified: marsupialization, permigration, infection, or avulsion (von Recum, 1984).

As opposed to marsupialization, permigration, is extrusion of a porous implant though a process more complex than marsupialization. Given sufficient pore size of the implant, the surrounding tissue and cells can venture into the pores of implants with pore sizes larger than 40 μm (Winter, 1974). Typically, the porous implant is filled with skin cells and connective tissue and in many cases skin cells are viable although small pores (< 40 μm) can limit nutrient availability and survivability. The infiltration into the pores appears, according to literature, to inhibit the downward epidermal migration preventing typical marsupialization (Winter, 1974; Hall *et al.*, 1975). Instead, the problem arises due to the skin attachment and fibrous infiltration into the porous implant. When the epidermal cells are constantly moving superdermally (or externally), an extrusion force develops and can carry the implant towards the surface with the attached skin cells (Hall *et al.*, 1975). In other words, the fact that skin cells are frequently divided, pushed to the surface and sloughed off means that any skin-implant bonds will either be broken or create a force that tends to extrude the implant (Hall & Ghidoni, 1978; von Recum & Park, 1981). Further, even though connective tissue is developed in the pores, it is

typically immature and the extrusion force overtakes any securing force that may have developed. Additionally, connective tissue levels present can vary within the same animal (Schreuders *et al.*, 1988).

The final two mechanisms of percutaneous implant extrusion, infection and avulsion, have similar underlying processes though the initial causes are of differing origins. Similar mechanisms are utilized during infection around either solid or porous implants. Inflammatory cells heavily invade the area and any tissue attached to or surrounding the implant is broken down until a thick fibrous capsule is formed. The implant is then extruded in a manner similar to marsupialization (von Recum & Park, 1981). Avulsion, on the other hand, is primarily due to mechanical stresses at the tissue implant interface. Through small movements the mechanical attachments between skin and implant are broken down. After sufficient breakdown and injury, focal inflammation occurs and the surrounding tissue can become necrotic. From this point, extrusion is similar to infection. Both types of extrusion, infection and avulsion, can result in deep infection and overall faster extrusion time rate. Therefore, similar to osseointegration, a stable skin-implant interface is needed to prevent avulsion (von Recum & Park, 1981).

Based on the above mechanisms, a few simple guidelines for skin integration of percutaneous implants have been developed, mainly focusing on the skin-implant interface (Grosse-Siestrup & Affeld, 1984). The main consideration is skin movement. If skin movement is expected around the implant, the interface needs to be flexible and elastic since skin is flexible and elastic. This type of interface will reduce stress around the typically more rigid implant leading to less avulsion and breakdown. However, in the case of natural skin protrusion (e.g. horns and antlers), the skin shows relatively little

movement. Therefore, if a protruding implant is rigidly fixed in bone and provides stable interface with skin, one could expect a good skin adherence with implant. To date however, perfect skin integration with a percutaneous implant has yet to be accomplished. The reasons explaining failures of purely percutaneous implants is best summarized by Hall and Ghidoni; "if good skin interfacing is accomplished the percutaneous implant will eventually become extruded. If good skin interfacing is not accomplished, a sinus tract will form through which bacteria can gain entrance" (Hall & Ghidoni, 1978). With regard to current research, the best possibilities for skin integration appear to be with porous implants because of the absence of epidermal migration and presence of some cellular infiltration.

1.5 Current state of DSA

1.5.1 Skin implant interface

DSA research for limb prostheses has been aimed primarily at the skin-implant interface and infection prevention. Research is divided primarily between porous implants and solid implants and presently there is no consensus about which type performs better. Porous implants appear to mimic biological percutaneous devices. For instance, one investigation into deer antlers was undertaken to understand the naturally occurring percutaneous device (Pendegrass *et al.*, 2006b). The results from that study have demonstrated that the skin-antler interface is achieved through a tight subdermal attachment to the protruding bone which led investigators to develop the intraosseous transcutaneous prosthesis (ITAP) (Pendegrass *et al.*, 2006a) (Kang *et al.*, 2010). Pitkin and colleagues investigated cell survivability inside the porous titanium implants *in–vitro* using human fibroblasts *(Galibin et al., 2007)* and *in-vivo* in rats and one cat (Pitkin *et*

al., 2006; Pitkin *et al.*, 2009). Results have demonstrated in principle that skin cells can invade the porous structures; however, there have been several limitations (principally spontaneous or self-implant removal) with these studies and improved experimental design is needed. Other researchers have investigated porous implants for skin and bone integration composed of metals (including titanium, tantilum and stainless steel) (Nilles & Lapitsky, 1973; Müller *et al.*, 2006; Pitkin *et al.*, 2006; Pitkin *et al.*, 2007a; Pitkin *et al.*, 2009; Chou *et al.*, 2010; Isackson *et al.*, 2011) and other materials (including carbon, poly(Hema) and others) (Davis *et al.*, 1972; Krouskop *et al.*, 1988; Schreuders *et al.*, 1988; Fukano *et al.*, 2010), most of which demonstrate ingrowth into the implants.

In contrast to the idea of porous percutaneous implants, smooth surface or solid implants have been clinically used since the inception of DSA (Brånemark *et al.*, 2001; Tillander *et al.*, 2010). These implants cause less mechanical damage to the abutting skin if movement is allowed, but prevent any tissue ingrowth. There is some evidence that they allow better cellular attachment (Pendegrass *et al.*, 2008), though *in vivo* studies have not been performed. Other research has shown that when percutaneous implants are securely attached to bone the risk of infection is reduced due to the increased stability of the skin–implant interface, possibly through reduced avulsion (Jansen & de Groot, 1988; Jansen *et al.*, 1990).

Further tests have been performed at eliminating bacteria at the skin implant interface. Cationic steroid antimicrobial impregnated pads surrounding the exit site of a percutaneous solid titanium rod in sheep have been tested; unfortunately, the animal model had large amounts of skin motion at the implantation site and resulted in torn skin and the loss of an intimate skin-implant interface (Perry *et al.*, 2009). This was

complicated by the fact that 85% of all implants (17 of 20) showed bacteria in cultures. Therefore the antimicrobial pads did not significantly reduce infection rates; though a better antimicrobial medication might have shown better results.

A limiting factor in percutaneous implant research is a small number of methods available for analysis of skin-implant integration and barrier formation. Histology is probably the most frequently used method, but has flaws. First, materials choices are limited for simple histological analysis (Knowles *et al.*, 2005). Thus, many hard materials such as metals and ceramics have not been studied in-depth. Another problem is that histology only captures a single instant in time making it difficult to understand the dynamic nature of the skin-implant integration process. Other than histology, there are few reports testing the actual skin attachment force (von Recum & Park, 1981; Pitkin *et al.*, 2009) or dermal barrier formation (Isackson *et al.*, 2011).

1.5.2 Balance and mechanics using DSA prostheses

Another factor limiting DSA acceptance is lack of biomechanical research. For prosthetic attachment, DSA makes a compelling argument; however there is a lack of knowledge regarding changes in gait or balance with a DSA prosthesis compared to a traditional prosthesis. The fact that DSA provides a direct connection with the residual limb suggests that mechanical interactions (i.e. the force transmission to the skeleton) are faster compared to traditional prostheses, as no soft tissue deformation is required. Consequently, reaction time to perturbations may improve due to the faster feedback and force transmission to the support surface. Further, osseoperception, or sense of loading that has been associated with DSA (Jacobs *et al.*, 2000), may improve overall balance and coordination through biofeedback mechanisms, which has not been tested. It is

unclear where osseoperception arises (potentially the mechanoreceptors in the bone and/or joint capsule receptors) but it appears to be activated by direct loading of the bone. Another consideration is the total force and moment that these implants can withstand and still remain functional is unknown. Since current clinical DSA procedures involve threaded implants, under appropriate torque they can loosen (Manurangsee *et al.*, 2000) resulting in bone-implant interface damage, implant removal or injury (Roy Bloebaum, personal communication). While some limited information is available (Lee *et al.*, 2007), further evaluations of DSA loading and mechanics are needed in both postural and locomotor tasks

1.8 Animal Model

Given the need for DSA prostheses in human populations, human testing is not approved in the US. Thus, an animal model is needed to further investigate the physiology and biomechanics of DSA prostheses. The animal research model may also provide new insight into clinical veterinary practice for animals with limb loss. Of the many animal models available, the two models chosen for my studies were the hairless rat model and the cat model. The hairless rat (CD hairless) model was chosen for studying skin integration, as skin in this animal model is more analogous to human dermal tissue (Rougier, 1987; Lauer *et al.*, 1997).

For biomechanical evaluation and investigation into both skin and bone implant integration a cat model was chosen. Although other models have been used in the past (rat, rabbit, guinea pig, dog, sheep), the cat model was chosen because there is extensive knowledge of the cat neuromuscular physiology and biomechanics. Furthermore, the cat uses an upright posture, has ground reaction forces that are similar in pattern to human

forces and while larger than rodents, the cat is still relatively small and can fit into a typical gait analysis laboratory setting. Biomechanics of the intact and injured (sans amputation) cat model have been studied in depth. Sagittal plane full body mechanics have been described (Manter, 1938; Prilutsky *et al.*, 2005; Beloozerova *et al.*, 2010) however, frontal plane analyses of the cat and the associated EMG patterns during cat walking have been described only sparsely (Bolton *et al.*, 2006; Misiaszek, 2006a) as well as studies looking at lateral stability for standing (Henry *et al.*, 2001; Karayannidou *et al.*, 2009) and walking (Bolton & Misiaszek, 2009; Karayannidou *et al.*, 2009). However, these studies lack a quantitative approach to understanding stability and therefore it is difficult to determine how stability changes during the locomotion.

1.9 Objectives and Specific Aims

The overarching goal of my dissertation is to provide insight into control of locomotor stability during intact and prosthetic gait. Specifically, the objectives of my research are to examine stability control during intact gait and gait with a direct skeletally attached prosthesis. Since balance and stability control are tightly regulated by the central nervous system during gait, the central hypothesis is that perturbations to gait will demonstrate quantifiable alterations in the stability measures as well as changes in overall motor cortex activity. Therefore, I investigated the following specific aims:

Specific Aim 1: Evaluate dynamic stability and motor cortex activity of the cat during three conditions:

(1a) Normal walking

(1b) Walking with increased base of support

(1c) Walking with reduced base of support.

Specific Aim 2: Develop an animal model to study dynamic stability during gait with a DSA prosthesis.

(2a) Investigate the effects of implantation time, pore size, and nano-textured surfaces of porous titanium implants on skin integration in the rat.

(2b) Develop procedures for implantation, rehabilitation and attachment of DSA prosthesis in the feline model.

(2c) Evaluate dynamic stability during feline prosthetic gait.

Specific Aim 1 - Evaluate dynamic stability and motor cortex activity of the cat during three locomotion conditions.

People and animals constantly regulate their center of mass (CoM) position to maintain upright posture during gait. If the CoM is not properly controlled, a trip or fall can occur and lead to injury. My experimental approach is to understand the biomechanical mechanisms of balance in an animal with intact afferent feedback during walking with different stance widths. Balance or body stability can be quantified both statically, when the CoM is positioned inside the base of support (Ting, Blickhan, & Full, 1994), and dynamically, using the extrapolated center of mass (XCoM) (Hof *et al.*, 2005). A feline model is chosen to address Specific Aim 1, because it has been the model of choice for biomechanics and neuroscience research for many years and thus background information about the system (e.g. body segment inertial characteristics (Hoy & Zernicke, 1985), spinal reflexes (Jankowska, 2008), etc) are known. In addition, feline gait

characteristics and muscle activity resemble human characteristics more than those of rodents. Quadrupedal gait has another important feature for studying locomotor stability control – the afferent control of the hindlimbs is mediated by proprioception exclusively without visual feedback. I hypothesize that body stability will decrease during walking on a narrow path and increase during walking on a wide paw separation. During narrow walking, it is likely that the CoM or XCoM will fall outside the small support area. Therefore, this will result in a less stable gait. During wide walking, the area of support is quite large and therefore the CoM or XCoM will fall inside the support area creating a stable gait. I further hypothesize that motor cortex activity will increase during walking on a narrow path and decrease during walking with wide paw separation. The rationale for this hypothesis is that with a smaller base of support, the CoM and XCoM will be further outside the base of support and thus passive spinal postural mechanisms will be insufficient for maintaining balance and supraspinal adjustments will be necessary to accomplish the task. The opposite is true for the wide walking task.

Specific Aim 2 - Develop an animal model to study dynamic stability during gait with a DSA prosthesis.

Direct skeletal attachment (DSA) is an alternative to traditional socket prostheses where the prosthesis is attached directly to the residual bone. Unfortunately there are many complications currently with DSA and further study is needed to understand DSA physiology and biomechanics. Therefore, I plan to a) investigate the effects of implantation time, pore size, and nano-textured surfaces of porous titanium implants on skin integration in the rat, b) develop procedures for implantation, rehabilitation and

attachment of DSA prosthesis in the feline model and c) evaluate dynamic stability during feline prosthetic gait. For specific aim 2a, hairless rats will be used, as their skin is a good analog for human dermal tissue. Based on my preliminary results and published literature, I hypothesized that increasing pore size will, histologically, increase skin ingrowth due to the increased available implant volume for skin-cell distribution. Furthermore, based on results of Puckett et al (2010), I expect to see increased skin ingrowth and reduced extrusion rate in implants that have a nanotextured surface. I will evaluate skin ingrowth using three groups of implants at two time points: 3 and 6 weeks. Small pore implants (pore size 40-100 μm) will be compared to large pore implants of (100-160 μm) and to small pore implants with nanotextured surface modifications.

In experiment 2b, I will develop an animal model to study gait on a direct skeletally attached prosthesis. As these procedures have not been thoroughly investigated (2005; Drygas *et al.*, 2008; 2010), it is necessary to formulate an implantation and rehabilitation protocol to allow the animals full use of the new technology. In addition, it is important to determine procedures to ensure implant survival and prosthesis rehabilitation. The objective for this aim is to develop procedures that will provide accurate and valid methods for implanting DSA prosthetic technology in the feline model.

For aim 2c, I will use a feline animal model (similar to aim 1) to examine the mechanics of gait on a DSA prosthesis and the stability of walking before and after implantation. I hypothesized that loading of the prosthesis will be reduced similar to results in sheep (Shelton *et al.*, 2011) and compensated for through the intact limbs.

Further, given the insult to limb and loss of primary sensory feedback (e.g. muscle spindles and paw pad receptors) I expect body stability to be decreased.

A note about the order of chapters

In the following chapters I will present the results of my research. Chapters 2 and 3 will address Aim 1, whereas Chapters 4 and 5 will address Aim 2. The flow from Chapter 3 to Chapter 4 may not seem directly related to my investigation of dynamic stability during locomotion. To explain, it was necessary to demonstrate skin ingrowth into porous titanium prior to beginning the animal DSA prosthetic model development in Chapter 5. Therefore, Chapter 4 details this endeavor and does in fact directly relate to the experiments in Chapter 5.

CHAPTER 2

MECHANICS, EMG AND MOTOR CORTEX ACTIVITY DURING WALKING WITH INCREASED STANCE WIDTH: DO STABILITY AND ACCURACY HAVE CONFLICTING DEMANDS?

2.1 Introduction

The ability to control body balance and stability are essential to prevent falls and recover from perturbations during locomotion. Maintenance of stable standing and locomotion is complicated by injury (Holder-Powell & Rutherford, 2000; Duong *et al.*, 2004; Day *et al.*, 2012), aging (Schrager *et al.*, 2008) and fear of falling (Chamberlin *et al.*, 2005; Dunlap *et al.*, 2012). Several motor strategies have been found to help maintain stability while walking on complex terrain. They include (1) decreasing walking velocity (Maki, 1997; Dingwell *et al.*, 2000; Chamberlin *et al.*, 2005; Galvez-Lopez *et al.*, 2011), (2) adjusting stride length and stance width (Maki, 1997; Misiaszek, 2006a; Dunlap *et al.*, 2012; McAndrew Young & Dingwell, 2012b, a), (3) lowering the center of mass (Beloozerova *et al.*, 2010; Schmidt & Fischer, 2010; Galvez-Lopez *et al.*, 2011) and prolonging the double support time (Maki, 1997; Chamberlin *et al.*, 2005). Of these strategies, stance width can be easily manipulated and is thought to influence stability in the frontal plane. Decreasing stance width (e.g. walking on a narrow path) destabilizes gait in humans (McAndrew Young & Dingwell, 2012b), rats (Schmidt & Fischer, 2010) and dogs (but not in cats, see Chapter 3), whereas a larger stance width increases support area and may improve gait stability (e.g. (Hof *et al.*, 2005; McAndrew Young & Dingwell, 2012b)). For example, during quiet standing, increased stance width allows the

center of mass a greater range of motion within the base of support thereby increasing margins of stability (Hof *et al.*, 2005). Modeling results show that with a larger base of support less active regulation of postural stability is needed due to passive body mechanics (Scrivens *et al.*, 2006).

Although the contribution of passive body mechanics to regulation of stability during standing and locomotion may be substantial (Ting *et al.*, 2009; Bunderson *et al.*, 2010), active mechanisms of the spinal cord, brain stem and primary motor cortex are pervasive (Macpherson & Fung, 1999; Beloozerova *et al.*, 2005; Karayannidou *et al.*, 2009; Stapley & Drew, 2009; Honeycutt & Nichols, 2010; Zelenin *et al.*, 2010; Musienko *et al.*, 2012). Neurons from fore- and hindlimb representations in the primary motor cortex have been shown to modulate their activity in response to postural perturbations in the frontal plane in the cat (Beloozerova *et al.*, 2005; Karayannidou *et al.*, 2009). This finding suggests that the primary motor cortex is involved in control of postural stability and that changes in lateral stability demands, especially during gait, may affect its involvement in postural control. As discussed above, increasing stance width increases margins of stability in the frontal plane during human standing and walking (Hof *et al.*, 2005; McAndrew Young & Dingwell, 2012b) and thus reduces lateral stability demands and may simplify postural control.

The contribution of the primary motor cortex to maintenance of lateral stability of gait with increased stance width (wide walking) is not known. Therefore, the purpose of this study was to examine the effects of increased stance width on static and dynamic stability, muscle activity and motor cortex activity during walking. First, I hypothesized that wider stance width would increase margins of lateral stability compared to walking

with self-selected, unconstrained paw placement. Second, the activity of neurons from the forelimb representation in the primary motor cortex would show little difference compared to unrestrained walking because relatively low demands of wide walking on lateral stability and accuracy. Although paw placement was restricted in the medial direction, the animal did not have to select specific areas on the floor for stepping; thus accuracy demands of wide walking did not appear significant. Interestingly, I found that sagittal stability was substantially compromised during double support by contralateral fore- and hindlimbs in unconstrained walking. During wide walking, there were periods (2/8 support phases) of elevated margins of stability, however, surprisingly 6/8 support phases of the wide walking cycle showed compromised stability (increased instability) compared to unconstrained walking. For the most part the increased instability was related to the frontal plane. Despite substantial changes in lateral stability and mechanics during wide walking, changes in the magnitude and modulation of motor cortex activity were rather modest. During wide walking, the activity of 93% (57/61) of recorded neurons was stride-related, and the activity of 85% (52/61) of neurons was different from that of unconstrained walking. The average discharge rate of 26% of neurons was higher (by 7±1 imp/s), whereas in 25% of them it was lower (by 6±2 imp/sec) than during unconstrained walking. The depth of frequency modulation was different from that during unconstrained walking in 55% (34/61) of neurons: it was higher in 34% (by 54±7%) and lower in 21% of cells (by 32±3%). I concluded that wide walking involves a greater involvement of the motor cortex than unconstrained walking due to increased lateral instability of wide walking. Preliminary results have been published in abstract form (Farrell et al, 2008; Farrell et al 2011).

2.2 Methods

2.2.1 Ethical approval

All experimental and surgical procedures were consistent with US Public Health Service Policy on Humane Care and Use of Laboratory Animals and approved by the Institutional Animal Care and Use Committee of Georgia Institute of Technology and Barrow Neurological Institute.

2.2.2 Animal characteristics and locomotion tasks

In total 7 cats (3.5 $\pm$ 0.5 kg; Table 2.1) were trained to walk on Plexiglas enclosed walkway (3.0 m x 0.25 m) with unrestrained stance width (unconstrained walking) and a wide separation of paws (>9 cm, wide walking) using food reward. Several cats (Table 2.1) were trained to perform the same tasks on a treadmill. The path for wide walking was created by placing a 9-cm wide triangular prism in the center of the walkway or treadmill, creating a 9-cm wide obstacle whereby leaving space on either side of it for paw placement (Fig 2.1A). Cats that participated in cortical recording experiments were trained to wear a cotton jacket, a light backpack with connectors, and an electro-mechanical sensor on the right fore paw for determining swing and stance phases of the walking cycle (Beloozerova & Siorta, 1993) (Fig. 2.2 C,D).

2.2.3 Experimental procedures

Surgical procedures

After animals were trained to perform experimental tasks, 5 cats participating in mechanical analysis of unconstrained and wide overground locomotion (Table 2.1) were

implanted with EMG electrodes in selected hindlimb muscles under general anesthesia and aseptic conditions (for details see (Prilutsky *et al.*, 2011)). In summary, the cat was anesthetized using ketamine (10 mg/kg, subcutaneously, SC), atropine (0.05 mg/kg, SC) and isoflurane (inhalation; induction at 5%, maintained at 1-3%) and the right hindlimb and skull were shaved and cleaned with a surgical disinfectant. The animal was continuously monitored for temperature, respiration, heart rate and blood pressure throughout the surgery. Skin incisions were made in the skull, lower back and right thigh and shank. Teflon-insulated multi-stranded stainless-steel wires (100 mm diameter, Cooner Wire, USA) were passed subcutaneously along the back from two 24-pin amphenol connectors mounted on the skull with stainless-steel screws and dental cement

Table 2.1 Animal characteristics and analyses conducted.

Cat	Gender	Mass, kg	Forelimb Length, cm	Hindlimb length, cm	Full-Body Mechanics	EMG	Motor Cortex
Az	Female	4.2	21.1	24.4	x	x	
In	Female	3.2	19.1	25.8	x	x	
Kr	Female	3.0	19.4	25.1	x	x	
Ma	Female	2.8	21.4	27.6	x	x	
Sv	Female	3.8	19.5	26.0	x	x	
10	Female	4.0					x
11	Female	3.7				x	x

Note: Hindlimb length is defined as the sum of tarsals, shank and thigh length. Forelimb length is defined as the sum of carpals, forearm, and arm lengths.

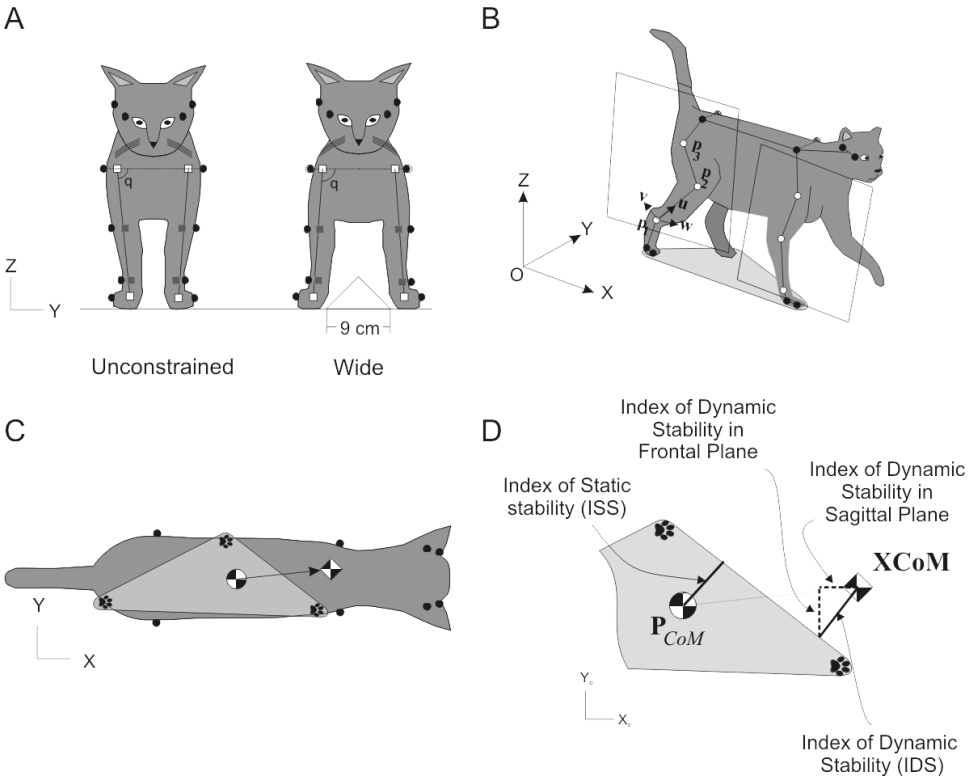

Figure 2.1 Determining static and dynamic stability of locomotion. A) Frontal view of the cat demonstrating experimental conditions with unconstrained and wide walking. Gray and open squares indicate estimated centers of the joints or paw. Angle q is the hip and shoulder angle in the frontal plane. B) Perspective view of the cat during walking showing how the hindlimb plane was defined (the forelimb plane was defined in the same way). Three open markers on each limb were used to define unit vectors v, u and w and the limb plane (see text for further explanations). C) Dorsal view of the cat during walking: ◔, center of mass (CoM) and ✣, extrapolated center of mass (XCoM). Paw prints indicate the paws on the ground, which form the base of support (light gray area). Filled circles are markers on iliac crests and scapulars, and at the corner of each eye and ear. D) Definitions of the base of support, index of static stability (ISS), index of dynamic stability (IDS, in panel IDS < 0) and its components, i.e. index of dynamic stability in the frontal plane (IDS_f) and index of dynamic stability in the sagittal plane (IDS_s) (see text for further explanations).

to muscles of interest, and pairs of wires with a small strip of insulation removed were secured in mid-belly of each muscle 3-5 mm apart. The implanted muscles included soleus, ankle extensor, SO; medial, MG and lateral, LG gastrocnemii, ankle extensors and knee flexors; tibialis anterior, ankle flexor, TA; vastus medialis, knee extensor, VM; rectus femoris, knee extensor and hip flexor, RF; sartorius medial, knee and hip flexor, SAM; iliopsoas, hip flexor, IP; biceps femoris anterior, hip extensor, BFA; biceps femoris posterior, hip extensor and knee flexor, BFP; and adductor magnus, hip adductor

and extensor, AM. EMG electrode implantations were verified by mild electrical stimulation through the head connectors. After implantation skin incisions were closed and pain medication administered (fentanyl transdermal patch, 2-25 mg/hour and/or buprenorphine, SC, 0.01 mg/kg or ketoprofen, 2 mg/kg, SC) and anesthesia stopped. At the end of surgery, length of each limb segment and width of limb joints were measured using a caliper.

In 2 separate cats another aseptic surgery under Isoflourane anesthesia was performed to prepare these animals for cortical activity recordings (Table 2.1). This surgical procedure and neuron identification methods have been described in detail previously (Beloozerova & Siorta, 1993; Prilutsky *et al.*, 2005; Beloozerova *et al.*, 2010) and only briefly outlined here. A portion of the skull and dura above the motor cortex were removed and the motor cortex was identified by the surface features and photographed. The exposed motor cortex area was covered by a 1-mm thick acrylic plate with pre-drilled holes of 0.36 mm in diameter spaced 0.5 mm apart, and then the plate holes were filled with bone wax. For the purpose of physiological identification of pyramidal tract neurons (PTNs) in the awake animal, two 26 gauge hypodermic guide tubes were implanted above the medullary pyramids so that their tips were approximately at the Horsley-Clarke coordinates (P7.5, L0.5) and (P7.5, L1.5), and the depth of H0. A ring-shaped metal base covered with a plastic cap surrounded and protected all implants.

After completion of the experiments, the animals were deeply anaesthetized and euthanized with pentobarbital sodium. In cats used for cortical recordings several reference lesions were made in the motor cortex in the vicinity of areas from which neurons were recorded. These cats were subsequently perfused with isotonic saline

followed by a 3% formalin solution. The brains were frozen before sectioning them through the regions of recording and stimulating electrodes to 50-μm thickness. The tissue was stained for Nissl substance with cresyl violet. Based on the obtained histological images the positions of recording and stimulation electrodes were verified.

The cadavers of cats participating in biomechanical and electromyographic recordings were used to verify segment length and joint width as well as locations of implanted EMG wires.

Cell recording and identification

Following recovery after surgery, extracellular recordings were obtained using tungsten varnish-insulated microelectrodes (120 μm OD; Frederick Haer & Co, USA) or platinum-tungsten quartz insulated microelectrodes (40 μm OD) pulled to a fine tip and mechanically sharpened using a diamond-grinding wheel. The impedance of both types of electrodes was 1-3 MΩ at 1000 Hz. Electrodes were inserted into cortex through 0.36 mm holes in a plastic plate implanted above the cortex as explained above. The electrode was advanced into the tissue by means of a custom-made miniature manual micro-drive (2.5 g) secured on the head cap. The signals recorded at 30 kHz were pre-amplified by a miniature custom made preamplifier on the cat's head connector, and subsequently further amplified with a stationary amplifier CyberAmp 380 (Axon Instruments, USA). The amplified signals were filtered (0.3-10 kHz band pass), fed to a screen and audio monitor, and saved on the hard drive of a PC using a data acquisition system Power-1401/Spike-2 System (Cambridge Electronic Design, UK). Examples of recordings from a pyramidal tract neuron during unconstrained and wide walking are shown in Fig 2.2 C, D.

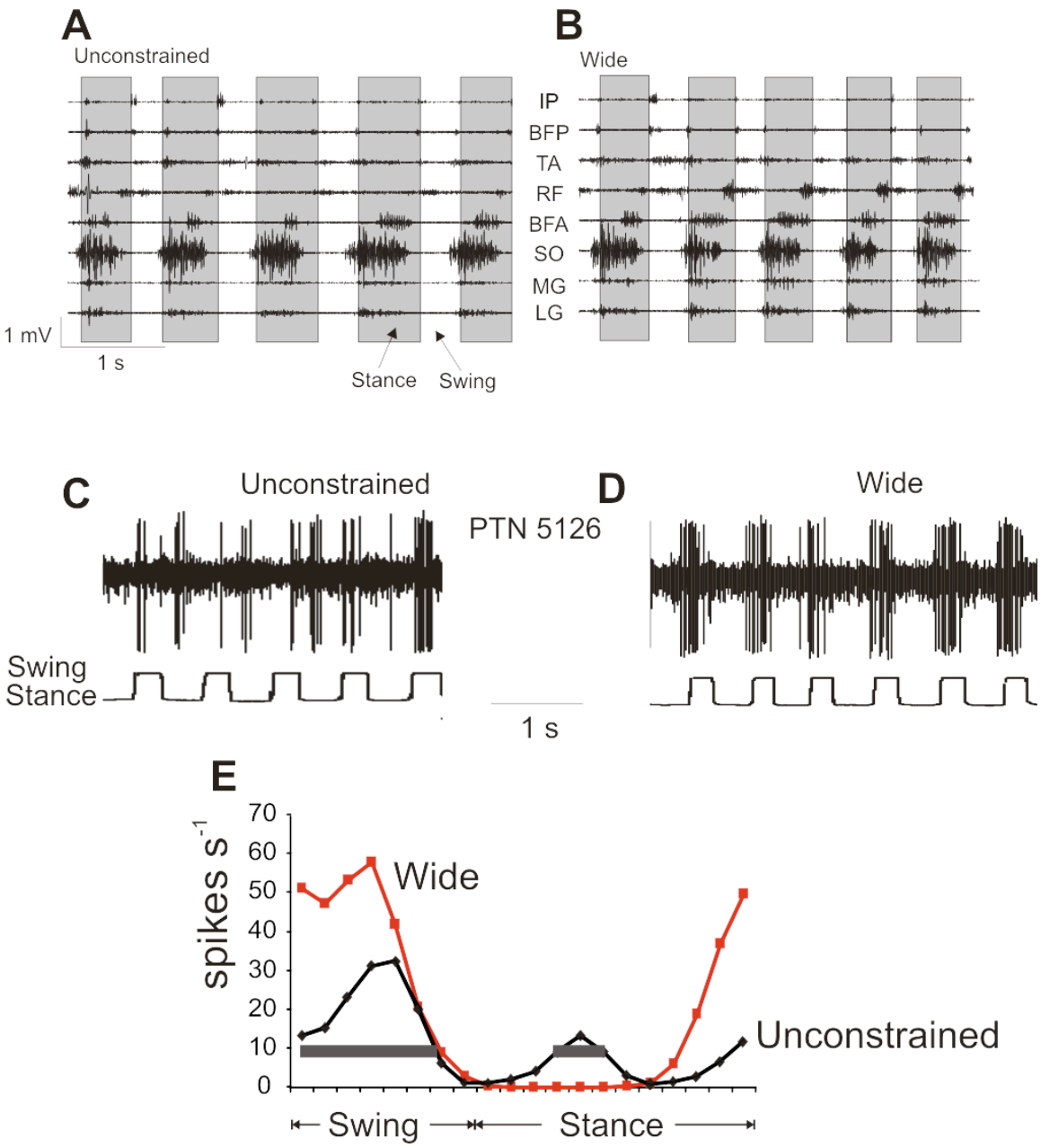

Figure 2.2 Examples of typical hindlimb muscle activity and cortical activity of during walking with unconstrained and wide stance width. A, B) EMG activity of hindlimb muscles during unconstrained and wide walking, respectively. IP, iliopsoas; BFP, biceps femoris posterior; TA, tibialis anterior; RF, rectus femoris; BFA, biceps femoris anterior; SO, soleus; MG, medial gastrocnemius; and LG, lateral gastrocnemius. C, D) Activity of a pyramidal tract neuron PTN during unconstrained and wide walking (the lower trace shows Swing (deflection up) and Stance (deflection down) phase of the stride). E) Activity of the same neuron is presented as a histogram during unconstrained wide walking. Horizontal black bars indicate two periods of elevated firing (PEF) during unconstrained locomotion (see text for more details).

Each encountered neuron was tested for antidromic activation using pulses of graded intensity (0.2 ms duration, up to 0.5 mA) delivered through the bipolar stimulating electrode in the medullary pyramidal tract. The cells that passed the test for collision of spikes (Bishop *et al.*, 1962; Fuller & Schlag, 1976) were identified as PTNs. Each recorded neuron was tested for antidromic activation before, during, and after each locomotion test.

The somatic receptive fields of the PTNs were examined by listening to cell responses elicited by palpation of limbs and passive joint movements via the audio monitor while the animal was sitting on a comfort pad with the head restrained.

Biomechanical and electromyographic recordings

Full-body kinematics and ground reaction forces were collected during unrestrained overground locomotion as described previously (Prilutsky *et al.*, 2005; Beloozerova *et al.*, 2010). Briefly, three-dimensional positions of 28 light reflective markers on the cat body were recorded at 120 frames/s using a 6-camera motion capture system (Vicon Motion Systems, UK). The markers were attached by a double sided adhesive tape to the shaved lateral aspects of the limb joints (left and right hip, knee, ankle, metatarsophalangeal (MTP) joint, 5^{th} hind digit, shoulder, elbow, wrist, metacarpophalangeal (MCP) joint and 5^{th} fore digit), trunk anatomical landmarks (left and right iliac crest and top aspect of left and right scapula) and lateral aspects of the head (Figure 1A, B, D; for further details see (Prilutsky *et al.*, 2005)). The three components of the ground reaction force vector and point of force application to the paw were recorded by 3 small force platforms (0.16 x 0.11 m and 0.11 x 0.07 m; Bertec Corporation, USA) at sampling rate 360 Hz. Cats participating in cortical recording

experiments walked on the walkway floor covered with an electro-conductive rubberized material, which allowed to measure the electrical resistance between the electromechanical sensor on the right fore paw and the floor and thus detect the stance and swing phases (Fig. 2C, D).

EMG recordings were synchronized with motion capture. Prior to recordings reflective markers were placed on the anatomical landmarks as described above and a 16-conductor shielded flexible cable was attached to the head mounted connectors. The cat initiated each walking trial, which consisted of 4-6 walking cycles, and the researcher followed behind the animal supporting the cable so that the cable would not interfere with locomotion. When the cat reached the end of walkway, it stopped, received food, and started a next trial. During each experimental session, both the unconstrained and wide walking tasks were recorded without changing markers or the EMG cable. The order of tasks was randomized between sessions and animals. Recordings lasted for several weeks; 5 days a week until a sufficient number of good trials (as defined below) were collected.

The EMG signals were sampled at 3000 Hz, amplified and saved on a hard drive of a PC for subsequent analysis. Examples of raw myoelectric signals recorded during unconstrained and wide walking are shown in Fig. 2.2A, B.

2.2.4 Data analysis

Kinematic and kinetic analysis

Recorded trials were examined for steady, constant speed of walking, and trials in which cats slowed down, accelerated or demonstrated atypical walking pattern were discarded. Recorded 3D positions of body markers were low pass filtered (4^{th} order, zero-

lag Butterworth filter, cut-off frequency 6 Hz). To estimate locations of joint centers from skin markers on the fore- and hindlimbs, limb planes were defined for each video frame based on the hip, knee and ankle markers for the hindlimbs and on the shoulder, elbow and wrist markers for the forelimbs (Fig. 2.1B, white circles indicate markers used to define limb planes). Each limb plane was associated with the unit vector triad $\mathbf{u}_l\mathbf{v}_l\mathbf{w}_l$:

$$\mathbf{u}_l = (\mathbf{p}_{l2} - \mathbf{p}_{l1}) / \left|(\mathbf{p}_{l2} - \mathbf{p}_{l1})\right|,\ \mathbf{w}_l = (\mathbf{p}_{l3} - \mathbf{p}_{l1}) \times (\mathbf{p}_{l2} - \mathbf{p}_{l1}) / \left|(\mathbf{p}_{l3} - \mathbf{p}_{l1}) \times (\mathbf{p}_{l2} - \mathbf{p}_{l1})\right|,$$

$$\mathbf{v}_l = \mathbf{w}_l \times \mathbf{u}_l \quad , \qquad \text{(Eq. 2.1)}$$

where $\mathbf{u}_l$ and $\mathbf{v}_l$ are orthogonal unit vectors in the limb plane, and $\mathbf{w}_l$ is a unit vector orthogonal to the limb plane *l* (Fig. 2.1B); $\mathbf{p}_{l1}$, $\mathbf{p}_{l2}$ and $\mathbf{p}_{l3}$ are position vectors defining locations of 3 limb markers in the global coordinate frame OXYZ. To minimize errors caused by skin movement around knee and elbow joints (Miller *et al.*, 1975), positions of knee and elbow markers within the limb planes were recalculated using measured positions of hip and ankle, shoulder and wrist markers, respectively, and the corresponding segment lengths (thigh, shank and upper arm, forearm). Location of centers at distal limb joints (MTP, ankle, knee, MCP, wrist, elbow) and center location of paws were calculated by shifting the joint marker position along the line passing through the marker and parallel to unit vector $\mathbf{w}_l$, which is perpendicular to the limb plane (Fig 2.1B, D). The shift distance was equal to the radius of the marker plus half the measured width of the joint. Hip and shoulder joint center locations were determined by shifting the marker position medially along the line connecting the two hip and two shoulder markers, respectively. For the hip joints, the shift length was equal to the radius of the marker plus the distance from the greater trochanter to the femoral head center; for the shoulder, the radius of the marker plus the distance from the greater humerus tuberosity to the humeral

head center (Fig. 2.1D). The joint and bone dimensions were measured while the animal was sedated during surgery or postmortem.

To determine displacement of the center of mass (CoM) of an 18-segment model of the cat in three-dimensions (Fig. 2.1A, B), segment mass (m_i) and relative location of segment center of mass on the long segment axis (λ_i) were calculated for each segment based on measured cat mass (M) and segment length (Table 2.1) using the regression equations developed in (Hoy & Zernicke, 1985). Position of center-of-mass location for each segment in the global coordinate system was computed as

$$\mathbf{p}_{CoMi} = \mathbf{p}_{pi} + \lambda_i(\mathbf{p}_{di} - \mathbf{p}_{pi}), \qquad \text{(Eq. 2.2)}$$

where $\mathbf{p}_{CoMi}$, $\mathbf{p}_{pi}$ and $\mathbf{p}_{di}$ are vectors describing positions of the CoM, proximal and distal joint centers of segment *i*, respectively. The 3D position of the general CoM of the full-body model $\mathbf{p}_{CoM}$ for each video frame was then computed as:

$$\mathbf{p}_{CoM} = \frac{\sum_{i=1}^{18} m_i \mathbf{p}_{CoMi}}{M} \qquad \text{(Eq. 2.3)}$$

or in scalar form

$$X_{CoM} = \frac{\sum_{i=1}^{18} m_i x_i}{M}\ ,\ Y_{CoM} = \frac{\sum_{i=1}^{18} m_i y_i}{M}\ ,\ Z_{CoM} = \frac{\sum_{i=1}^{18} m_i z_i}{M}, \qquad \text{(Eq. 2.3a)}$$

where x_i, y_i, and z_i are the coordinates of the *i*th segment CoM, m_i is the mass of the *i*th segment, M is the total mass of the cat and X_{CoM}, Y_{CoM}, and Z_{CoM} are the coordinates of the general CoM. The 3D CoM velocity and acceleration were calculated as the first and second derivative of CoM position, respectively.

The frontal plane shoulder angles were defined as the angle between the line connecting the two shoulder joint centers and the line from the shoulder center to the MCP joint center (Fig 2.1 D; see also (Misiaszek, 2006a)). The hip frontal plane angles were determined similarly. Stride parameters such as stride length, stance width, mean forward velocity of the general CoM, stance and swing duration, and duty factor (the ratio of stance duration over stride duration) were calculated based on recorded waking kinematics. Stance width for fore- and hindlimbs was defined as the distance between the left and right paw centers during stance. The timing of stance onset (paw contact with the ground) and offset (paw lift-off) was determined based on ground reaction force (when the paw contacted a force platform) or using the paw forward velocity (for details see (Pantall *et al.*, 2012), Method 2).

The frontal plane resultant muscle moments at the hip and shoulder joints ($\mathbf{M}_j$) were computed as the cross product of the position vector from the joint center to point of force application ($\mathbf{p}_j$) and the ground reaction force vector applied to the paw ($\mathbf{F}_j$):

$$\mathbf{M}_j = -(\mathbf{p}_j \times \mathbf{F}_j) \ , \qquad \text{(Eq. 2.4)}$$

where subscript *j* designates the joint number. This simplified equation that does not include inertial terms $m\mathbf{a}$ and $I\boldsymbol{\alpha}$ (m and I, segment mass and moment of inertia; $\mathbf{a}$ and $\boldsymbol{\alpha}$, segment linear and angular acceleration; for details see, for example, (Zatsiorsky, 2002)) was used because moments of inertia for cat segments in the frontal plane are not known and because frontal segment accelerations are relatively small (see Discussion and Fig. 2.10).

Analysis of body dynamic stability

The animal is considered statically stable if the vertical projection of its general CoM is within the support area. During locomotion this condition is satisfied in hexapedal terrestrial insects (Ting *et al.*, 1994), whereas in humans the CoM projection is outside the support area for most of the cycle making human locomotion statically unstable (Winter, 1995; Hof *et al.*, 2005; Hof, 2008). To extend the notion of static stability to dynamic situations including locomotion, Hof introduced the notion of the 'extrapolated center of mass position' (XCoM) and a measure of dynamic stability, i.e. the minimum distance from XCoM to the boundaries of the base of support (Hof *et al.*, 2005; Hof, 2008). The dynamic stability measure and its components were computed in the frontal and sagittal plane for unconstrained and wide walking. The **XCoM** vector in the horizontal plane was calculated as:

$$\mathbf{XCoM} = \mathbf{p}_{CoM} + \frac{\mathbf{v}_{CoM}}{\omega_0}, \qquad \text{(Eq. 2.5)}$$

where $\mathbf{p}_{CoM}$ and $\mathbf{v}_{CoM}$ are the general CoM position and velocity vectors in the horizontal plane, $\omega = \sqrt{g/l}$ is the eigen (natural) frequency of the (inverted) pendulum with mass equaled cat mass *M* balancing on a massless stick of length *l* equaled leg length (Table 2.1), and *g* is acceleration of gravity. The index of dynamic stability, *IDS*, was calculated as the perpendicular distance between **XCoM** and the edge of the base of support (Fig. 2.1C). The animal was considered dynamically stable if **XCoM** was inside the base of support (IDS≥0), and the animal was dynamically unstable if **XCoM** was outside the base of support ((IDS<0). The IDS was decomposed into two perpendicular line segments representing indices of dynamic stability in the frontal and sagittal planes, respectively (Fig. 2.1C). In addition, index of static stability (ISS) was calculated as the

perpendicular distance between $\mathbf{p}_{CoM}$ and the edge of the base of support (Fig. 2.1C). All mechanical variables were time normalized with respect to the stride duration.

EMG analysis

Five cats taking part in mechanical analysis of unconstrained and wide walking were implanted with fine wire EMG electrodes and myoelectric signals were recorded simultaneously with motion capture as described above. Raw EMGs sampled at 3000 Hz were band-pass filtered (30-1000 Hz, 3DB) and full-wave rectified. EMG burst onset and offset times were determined using a threshold EMG value defined as the mean EMG in-between burst periods plus 2 SD ((Gregor *et al.*, 2006; Prilutsky *et al.*, 2011). The mean burst EMG was calculated for all analyzed strides and normalized to the maximum mean EMG value found across all strides of unconstrained walking within each cat.

Analysis of cortical activity

The stride duration of the right forelimb detected with an electro-mechanical sensor on the paw (Fig. 2.2C, D) was divided into 20 equal bins. For each neuron, a histogram of spike activity in the walking cycle was generated for each walking condition (e.g., Fig. 2.2, E). The following parameters were calculated for each recorded neuron (for details see (Beloozerova & Siorta, 1993; Beloozerova *et al.*, 2010)): mean discharge frequency, coefficient of frequency modulation (dM), preferred cycle phase, and duration of the period of elevated firing (PEF). The coefficient of modulation was calculated as:

$$dM = (Nmax - Nmin)/N \times 100\%, \quad \text{(Eq. 2.6)}$$

where *Nmax* and *Nmin* are the number of spikes in the maximal and minimal histogram bin, and *N* is the total number of spikes in the histogram. Period of elevated firing was

defined as the portion of the cycle, in which the activity level exceeds 25% of the difference between the maximal and minimal frequencies in the histogram (Fig 2.2). For the population of neurons the following parameters were calculated: distribution of discharge frequency over walking cycle, range of coefficients of modulation, widths of PEFs. The difference between the mean frequency, the coefficient of frequency modulation, and the preferred phase for unconstrained and wide walking were compared.

Statistical analysis

Time histories of mechanical variables of individual limbs were time normalized to 100% of the limb stride duration; mechanical variables describing motion of the general center of mass and stability measures were time normalized to stride duration of the right forelimb. All time normalized mechanical variables were averaged across walking cycles of individual cats and then across cats for unconstrained and wide walking conditions. The effects of walking conditions on time normalized mechanical variables were tested using the Student's t-test at each percent of walking cycle. The Student's t-test was also used to compare stride parameters, mean EMG burst activity, and parameters of PTN activity between the two walking conditions. The significance level was set at 0.05.

2.3 Results

Overall 241 strides from 5 cats were included for analysis of mechanics, 167 strides for EMG analysis and 61 cortical neurons from 2 cats were recorded during wide and unconstrained walking.

2.3.1 Mechanics of Wide Walking

General stride parameters of wide walking

The mean forward speed for wide walking tended to be slower when compared to unconstrained walking, but the difference was not significant ($p=0.06$, Table 2.2). Similarly, stance, swing and cycle times for wide walking tended to be longer compared to unconstrained, however the differences did not reach the significance level ($p > 0.05$, Table 2.2). Duty factor for the hindlimbs, but not for the forelimbs, was significantly higher for wide walking compared to unconstrained walking (wide, 0.62 ± 0.01; unconstrained, 0.59 ± 0.01, $p < 0.01$). The average stance width (measured from the ipsilateral paw center to the contralateral paw center) for wide walking (forelimbs: 12.45 ± 0.59 cm, hindlimbs 13.07 ± 0.52 cm) was significantly ($p < 0.05$) larger than that of unconstrained walking (forelimbs: 2.68 ± 1.32 cm; hindlimbs: 2.50 ± 1.06 cm). Stance width variance was lower for wide walking compared to unconstrained even though wide walking had a higher mean stance width. Stride length was shorter for both the fore- and hindlimbs during wide walking, but the difference was significant only for the hindlimbs (Table 2.2).

The general pattern of limb support seen during wide walking was consistent with that of quadrupedal gait at moderate walking speeds in general (e.g. Gray, 1968)) and unconstrained and narrow walking exhibited similar patterns; 3-2-3-2-3-2-3-2 (Fig 2.3). While the overall limb support pattern and stride timing parameters showed no significant differences between wide and unconstrained walking (Table 2.2), the duration of each phase of limb support (see Fig 2.3 for definition of limb support phases) did show significant differences (Table 2.3). During the cycle of wide walking, the cats spent more time in 3-legged support phases and less time in 2-legged support phases than during

Table 2.2. Stride characteristics (mean ± SD) of unconstrained and wide walking.

Stride parameter	Limb	Unconstrained	Wide	p-value
Stance time (s)	Fore	0.47 ± 0.03	0.51 ± 0.09	0.29
	Hind	0.44 ± 0.03	0.49 ± 0.07	0.11
Swing time (s)	Fore	0.26 ± 0.02	0.28 ± 0.03	0.33
	Hind	0.30 ± 0.03	0.29 ± 0.03	0.25
Cycle time (s)	Fore	0.73 ± 0.05	0.79 ± 0.11	0.28
	Hind	0.74 ± 0.05	0.78 ± 0.10	0.32
Duty factor	Fore	0.63 ± 0.02	0.64 ± 0.03	0.40
	Hind	0.59 ± 0.01	0.62 ± 0.01	<0.01*
Stride length (cm)	Fore	43.72 ± 3.27	41.25 ± 2.50	0.053
	Hind	44.73± 2.90	41.17 ± 2.40	0.02*
Stance width (cm)	Fore	2.73 ± 1.23	12.45 ± 0.59	<0.01*
	Hind	2.50 ± 1.06	13.07 ± 0.52	<0.01*
Swing height (cm)	Fore	3.91 ± 0.89	4.70 ± 0.94	0.01*
	Hind	3.66 ± 0.28	4.61 ± 0.45	<0.01*
Forward Speed (ms^{-1})		0.61 ± 0.05	0.54 ± 0.09	0.06
Maximal IDS (cm)		1.63 ± 0.30	5.29 ± 0.69	<0.01*
Minimal IDS (cm)		-6.53 ± 1.50	-8.46 ± 1.91	<0.01*
Peak lateral CoM acceleration (cms^{-2})		-59.80 ± 14.62	-174.79 ± 32.60	<0.01*
Max BoS Area (cm^2)		146.5 ± 23.5	355.57 ± 19.61	<0.01*
Min BoS Area (cm^2)		31.7 ± 1.5	39.51 ± 2.73	<0.01*

* Significant difference between unconstrained and wide walking

Table 2.3 Area of support and phase duration (mean ± SD) during limb support phases of unconstrained and wide walking

Limb Support Phase	Base of Support Area (cm^2)			Phase Duration (Gait Cycle %)		
	Unconstrained	Wide	p-value	Unconstrained	Wide	p-value
1	131.9 ± 28.4	320.1 ± 10.5	<0.01*	8.6 ± 1.7	10.8 ± 3.3	0.09
2	72.1 ± 2.6	69.5 ± 2.3	0.14	17.2 ± 1.1	14.2 ± 4.0	0.08
3	125.1 ± 16.4	322.7 ± 19.9	<0.01*	6.4 ± 1.2	11.6 ± 3.1	<0.01*
4	35.0 ± 2.5	42.5 ± 3.9	<0.05*	17.0 ± 1.2	12.2 ± 2.9	<0.01*
5	128.6 ± 21.7	325.0 ± 32.7	<0.01*	8.6 ± 2.1	11.6 ± 3.7	<0.05*
6	74.7 ± 5.3	70.4 ± 4.3	0.23	17.8 ± 2.5	14.8 ± 4.0	0.058
7	124.0 ± 31.5	318.0 ± 37.1	<0.01*	5.6 ± 1.7	9.8 ± 2.9	<0.05*
8	35.8 ± 2.6	41.2 ± 2.3	<0.01*	18.8 ± 2.1	15.0 ± 3.7	0.106

* Significant difference between unconstrained and wide walking. Limb support phases correspond to those in Fig 2.3.

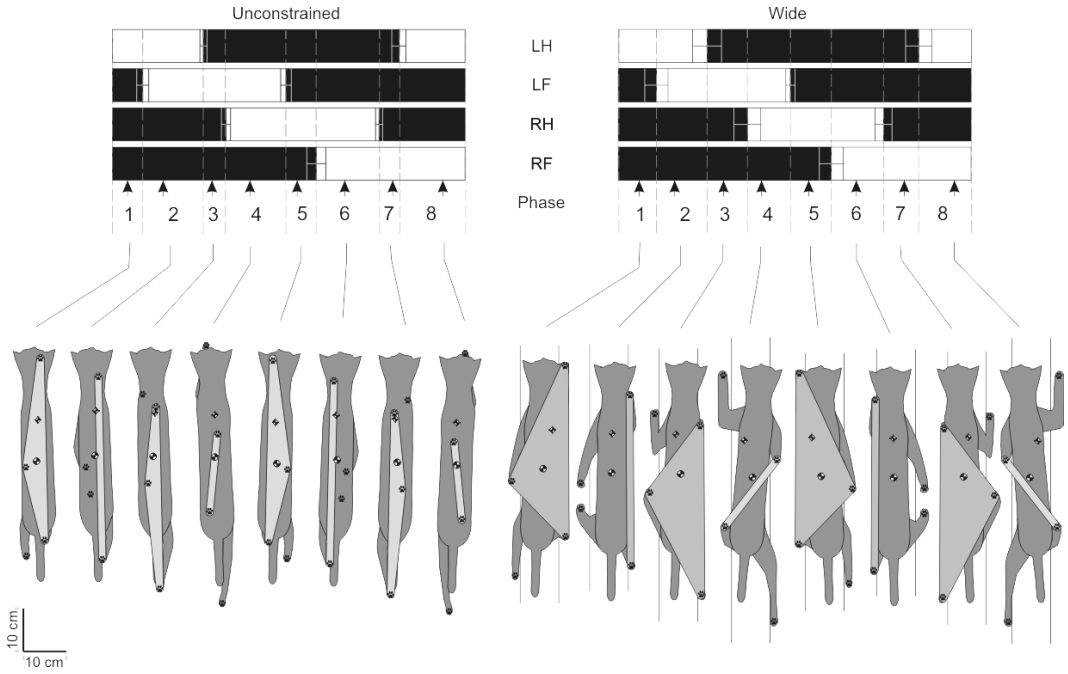

Figure 2.3 Phases of gait (top panel) and representative base of support, center of mass and extrapolated center of mass in each phase (bottom panel). Top Panel: Stance phase is shown by black filled rectangles, swing by open rectangles; vertical bars indicate standard deviations of phase onset and offset. Bottom panels: Base of support is shown in light gray. Stride phases follow a limb support pattern 3-2-3-2-3-2-3-2; each phase is indicated by numbers 1-8.

unconstrained walking. The total normalized cycle time spent in 3-legged support for wide walking was 43.8%, whereas it was significantly shorter for unconstrained walking (29.2%,,$p < 0.05$). Conversely, 56.2% of the wide walking cycle was spent in 2-legged support as opposed to 70.8% during unconstrained walking, a difference of 14.6% ($p<0.05$).

The number and position of the limbs in contact with the ground determined the base of support area for each phase. During 3-legged support phases (phases 1, 3, 5 and 7) of wide walking, the base of support area was several times larger than during unconstrained walking ($p<0.05$, Table 2.3, Fig 2.4). Also, during diagonal double support with a forelimb and contralateral hindlimb (phases 4 and 8) base of support was larger during wide walking ($p <0.05$, Table 2.3, Fig 2.4).

Margins of stability patterns in unconstrained and wide walking

Indices of static (ISS) and dynamic stability (IDS) followed similar patterns for the first and second half of the gait cycle and were closely tied to the base of support area and the support phases of the cycle (Figs 2.3 and 2.4) for both unconstrained and wide walking. During 3-legged support phases formed by 2 fore- and 1 hindlimb (phases 1 and 5), the cats were statically and dynamically stable – ISS and IDS, including both the frontal (IDS_f) and sagittal (IDS_s) components, were significantly greater than zero during both unconstrained and wide walking. All these stability indices were significantly higher for wide walking than for unconstrained walking ($p < 0.05$, Fig 2.4), indicating greater margins of static and dynamic stability for wide walking during phases 1 and 5. During 2-legged support phases 2 and 6 (ipsilateral support by a fore- and hindlimb), the cats were statically and dynamically unstable during wide walking (both ISS and IDS stability

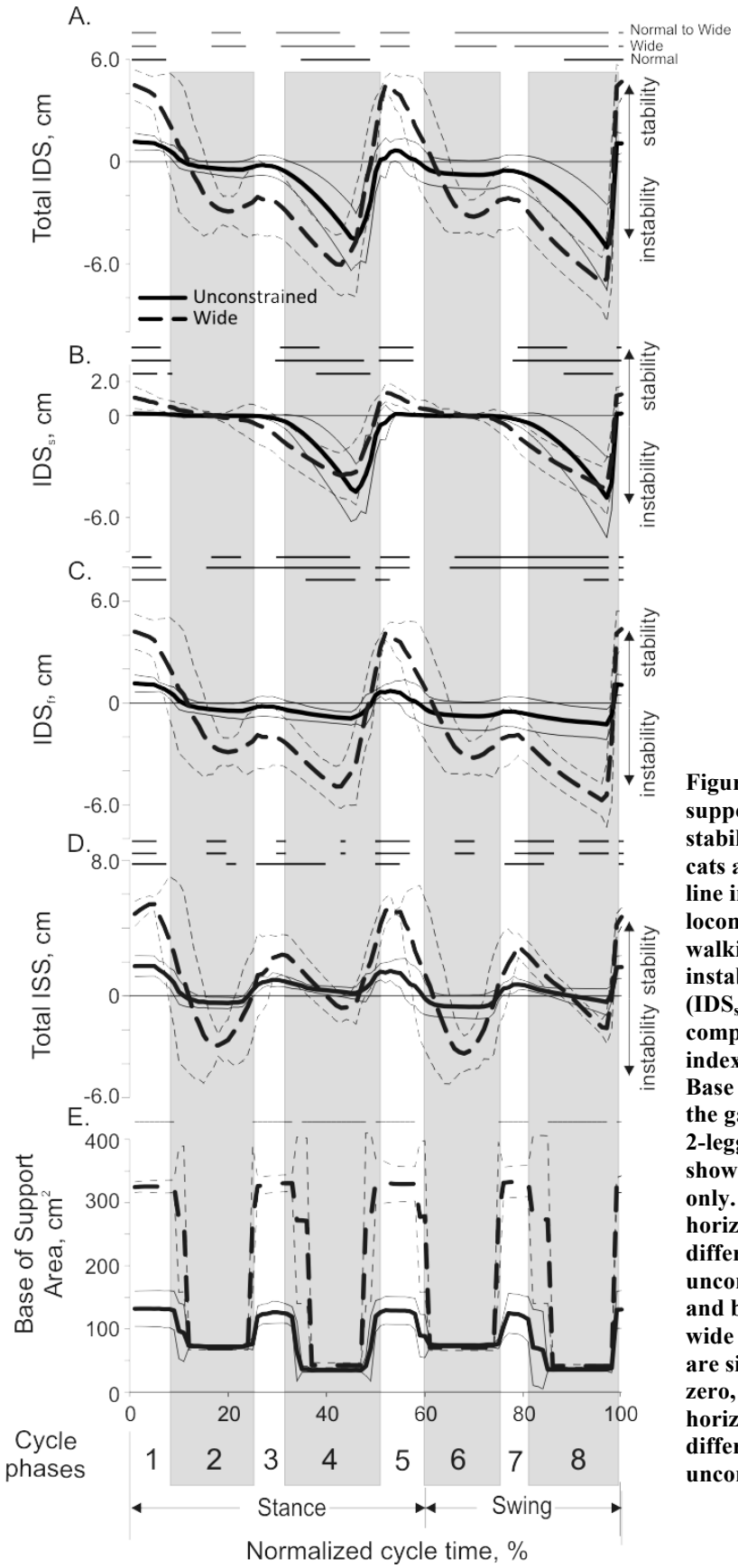

Figure 2.4 Stability and base of support area. A) Index of dynamic stability (IDS) averaged across 5 cats and shown as mean ± SD. Solid line indicates unconstrained locomotion and dashed lines wide walking. Negative values indicate instability. B) Sagittal component (IDS_s) of IDS. C) Frontal component (IDS_f) of IDS. D) Total index of static stability (ISS). E) Base of support area throughout the gait cycle. Gray areas indicate 2-legged support phases and are shown for unconstrained walking only. In panels A-D the top horizontal bar indicates significant difference between wide and unconstrained walking; the middle and bottom bars indicate where wide and unconstrained stability are significantly different from zero, respectively. In panel E, the horizontal bar indicates significant difference between wide and unconstrained base of support area

indices became significantly less than zero, $p<0.05$), whereas during unconstrained walking the cats were dynamically unstable only in the sagittal plane (IDS_f was significantly different from zero, $p<0.05$).

During phases 3 and 7 (3-legged; 1 fore- and 2 hindlimbs), ISS became positive for both wide and unconstrained walking, but only wide walking showed ISS to be significantly greater than zero, indicating greater margins of static stability. During these phases, total IDS increased slightly, however it remained negative including its two components IDS_s and IDS_f of which only IDS_f was significantly less than zero, indicating dynamic instability of the body in the frontal plane. During support phases 4 and 8 (2-legged support; contralateral fore- and hindlimb), ISS decreased during wide walking, but remained insignificantly different from zero. Total IDS however, decreased and was significantly less than zero during wide and unconstrained walking. Further, IDS_s was significantly lower than zero for wide and unconstrained walking due to negative IDS_f for wide walking ($p<0.05$, Fig. 2.4).

Considering the entire gait cycle, cats were dynamically unstable during phases 4 and 8 of unconstrained walking and during at least some portion of phases 2, 3, 4, 6, 7 and 8 of wide walking. During unconstrained walking, the unstable phases were primarily due to the XCoM progressing ahead to the base of support (Fig 2.3C). In phases 2, 3, 6 and 7 of wide walking, the major contributing factor to the instability was IDS_f. In phases 4 and 8, both sagittal and frontal components were negative and contributed to the total instability, but frontal instability (IDS_s) was smaller compared to sagittal instability (IDS_f).

The position of the center of mass calculated for all walking cycles was used to compute the indices of static stability with respect to the paws on the ground. The left-right displacement of the CoM during wide walking was significantly greater than unconstrained walking – the displacement range was close to 4.0 cm for wide and 2.0 cm for unconstrained walking (Fig 2.5A). The vertical position of the CoM showed no significant difference between conditions (not shown). The CoM acceleration showed correspondingly substantially greater values in left and right direction during wide than unconstrained walking ($p<0.05$, Fig. 2.5B). There was no statistical difference in vertical acceleration of the CoM between wide and unconstrained walking (not shown).

Kinetics of wide walking

The ground reaction forces determined the acceleration and displacement of the CoM during walking. The patterns of the vertical and anterior-posterior ground reaction forces were generally similar between unconstrained and wide walking (Fig. 2.6). There were, however, several notable differences between wide and unconstrained walking. For the wide walking, both the fore- and hindlimbs had smaller braking forces in the anterior-posterior direction than for unconstrained walking ($p<0.05$). The forelimbs also exerted smaller vertical forces during the first half of stance and a longer time to the first peak. Especially large differences between wide and unconstrained walking occurred in the medial-lateral forces – the peak lateral forces were about 10 times greater during wide walking for both fore- and hindlimb ($p<0.05$, Fig 2.6).

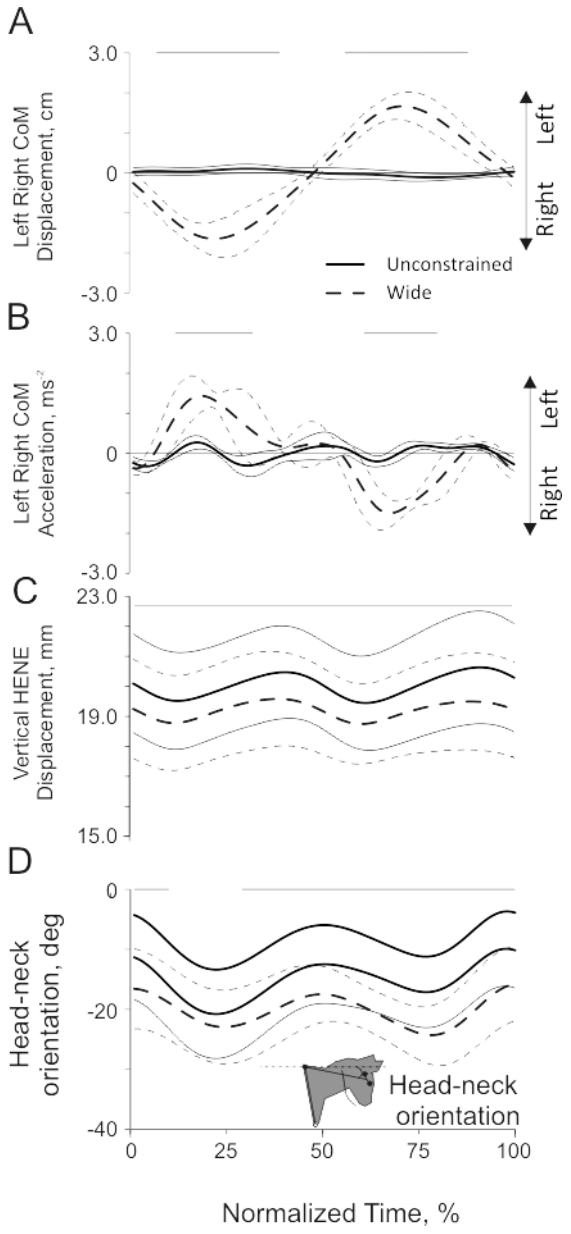

Figure 2.5. Selected mechanical variables of walking with wide and unconstrained paws separation as a function of the normalized cycle time of the right forelimb (see Fig. 2.4 for definition of lines and the horizontal axis). Mean data of 5 cats (Table 2.1). A) Displacement of the CoM in the left and right direction; left direction corresponds to the left side of the body. B) Acceleration of the CoM in the left and right direction. C) Vertical displacement of the head-neck segment. D) Head-neck segment orientation; clockwise segment rotation from the horizontal is defined as negative. Horizontal lines on top of each panel indicate statistically significant differences ($p < 0.05$) between unconstrained and wide walking

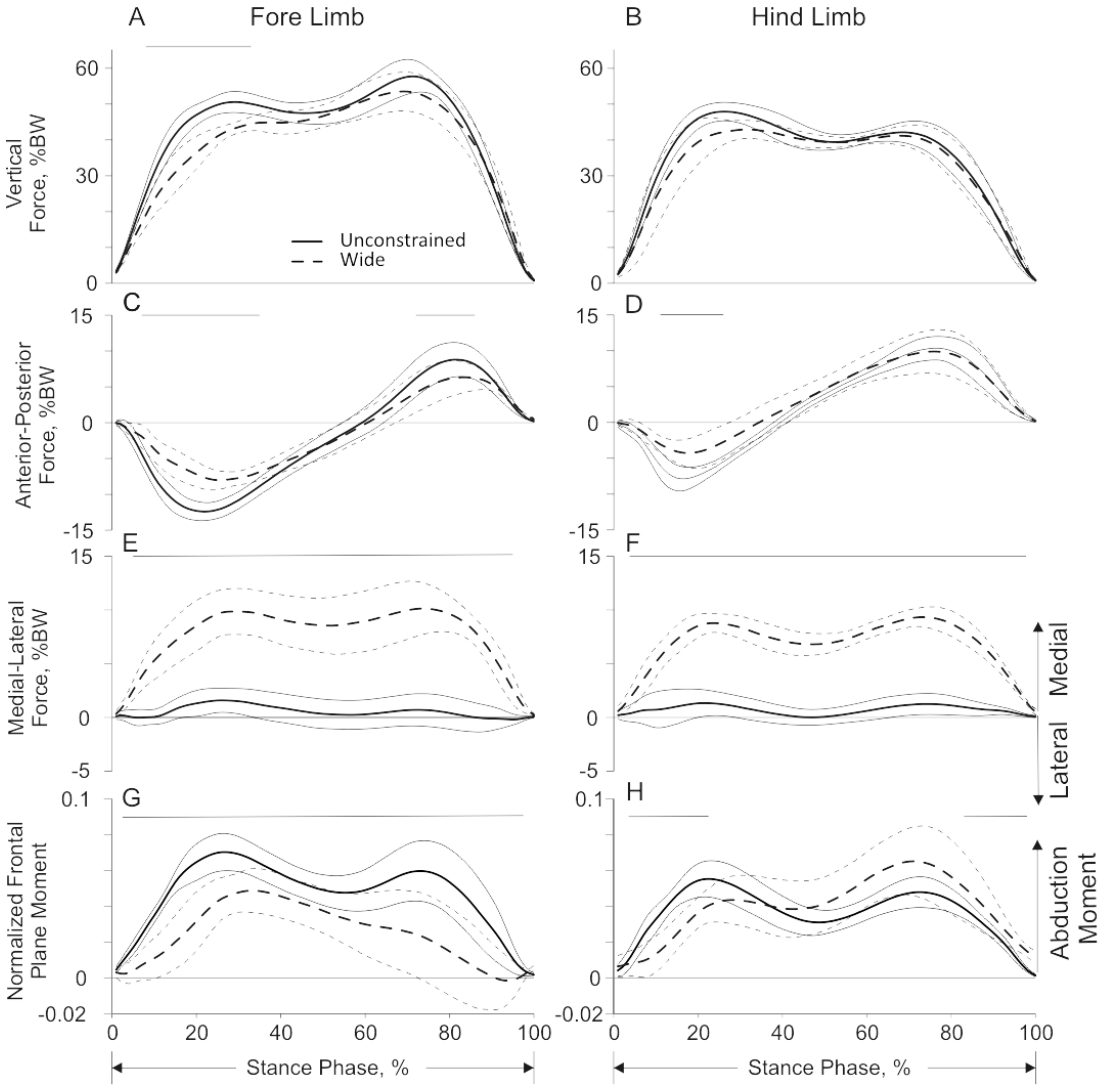

Figure 2.6 Selected kinetics variables during wide and unconstrained walking (mean ± SD). A, B) Vertical force (mean + SD) applied to the fore- and hindlimbs during stance, respectively. C, D) Anterior-posterior force applied to the fore- and hindlimbs during stance phase, respectively. E, F) Medial-lateral force applied to the fore and hind limbs during stance phase, respectively. G, H) Normalized frontal plane moment for the fore- and hindlimb, respectively. Horizontal bars indicate significant differences ($p < 0.05$) between unconstrained and wide walking.

Frontal plane joint moments at the shoulder and hip were calculated using a quasi-static approach (See 2.2 METHODS and 2.4 DISCUSSION for explanations). During wide walking, the frontal plane muscle moment acting at the shoulder tended to abduct the forelimb, but its magnitude was reduced compared to the abduction moment during unconstrained walking ($p<0.05$, Fig. 2.6). The moment acting about the hip during wide

walking followed a similar pattern to unconstrained walking with a decreased abduction moment in early stance and increased moment in the second half of the stance phase ($p<0.05$, Fig. 2.6).

Other mechanical characteristics

During swing phase, the peak of paw vertical displacement (swing height) was significantly higher for wide walking compared to unconstrained walking (Fig. 2.7A, B; Table 2.2) in all limbs. During wide walking, the fore- and hindlimbs underwent medial circumduction evident from medial displacements of the paws, whereas during unconstrained walking, the cats performed lateral circumduction (Fig. 2.7C, D). The hip and shoulder joints were significantly abducted during wide walking, i.e. their frontal angles were greater than 90^{o} (Fig. 2.7E, F). During unconstrained walking, on the other hand, the frontal shoulder and hip angles were adducted in stance and most of swing (Fig. 2.7E, F).

The vertical position of the head-neck segment was approximately 1 cm lower during wide walking compared to unconstrained walking. The head-neck was also, rotated approximately 10 degrees more toward the ground during wide walking (Fig 2.5C, D). Both the head-neck vertical position and orientation during wide walking were significantly different from those of unconstrained walking for most of the walking cycle duration.

2.3.2 EMG of Wide Walking

EMG activity was recorded from 11 hindlimb and 3 forelimb muscles in several cats during wide and unconstrained walking (for example recordings see Fig. 2.2 A, B). The mean EMG activity of the two hindlimb extensors (medial gastrocnemius,

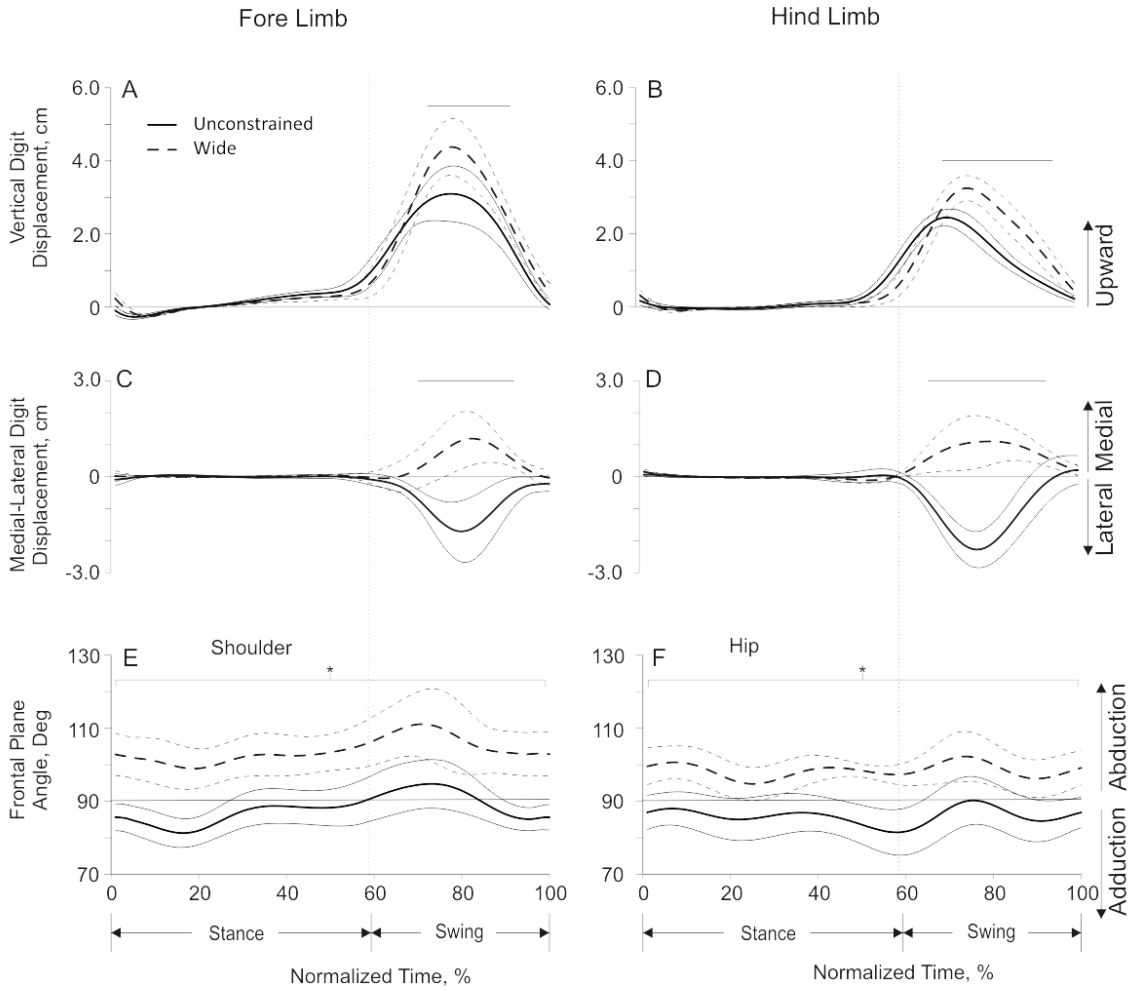

Figure 2.7 Selected limb kinematic variables during wide and unconstrained walking (mean ± SD). A, B) Vertical displacement of the paw center of mass for the fore- and hind-digits, respectively. C, D) Medial-lateral displacement of the paw center of mass for the fore- and hind-digits, respectively. E, F) Frontal plane angles (as defined in Fig 2.1) of the shoulder and hip, respectively. Horizontal bars indicate significant differences between wide and unconstrained walking ($p<0.05$).

MG) and biceps femoris anterior (BFA), as well as the majority of hindlimb flexors (tibialis anterior, TA), sartorius medial (SAM), iliopsoas (IL), and biceps femoris posterior (BFP1 and BFP2) was greater during wide than unconstrained walking. The activity of some muscles (soleus, SO; lateral gastrocnemius (LG); vastii (VM, VL); and rectus femoris (RF)) was lower during wide than in unconstrained walking. The triceps surae (SO, LG and MG) showed differing changes in activity and timing between the walking conditions. The SO and LG had significantly lower the mean activity during

wide walking compared to unconstrained, whereas the MG mean activity was higher in wide than in narrow walking (Fig 2.8A). The burst duration of the SO and MG was also longer during wide walking. The greater activity of hindlimb flexor muscles during wide walking (TA, SAM, IP, and two bursts of BFP) was consistent with the higher vertical displacements of the hind paw in this walking condition (Fig 2.7A,B). The RF activity was indistinguishable between the two walking conditions, however this muscle had significantly longer burst duration during wide walking ($p<0.05$; Fig 2.8B). Both bursts of BFP (one at the stance-swing transition and another at the swing-stance transition) showed a significantly larger mean activity during wide walking, but no difference in burst duration between wide and unconstrained conditions.

2.3.4 Cortical Activity of Wide Walking

The activity of 61 neurons (of those 52 were PTNs) in the forelimb representation of the primary motor cortex of 2 cats (Table 2.1) was recorded during unconstrained and wide walking. During wide walking the activity of 85% (52/61) of neurons was different from unconstrained walking. The average discharge rate of 26% of neurons was higher (by 7±1 imp/s), while in another 25% of them it was lower (by 6±2 imp/sec) in wide walking than in unconstrained. The activity of 93% (57/61) of neurons was stride related (i.e. the activity was dependent on the phase of gait). The depth of frequency modulation was different from unconstrained walking in 55% (34/61) of neurons: it was higher in

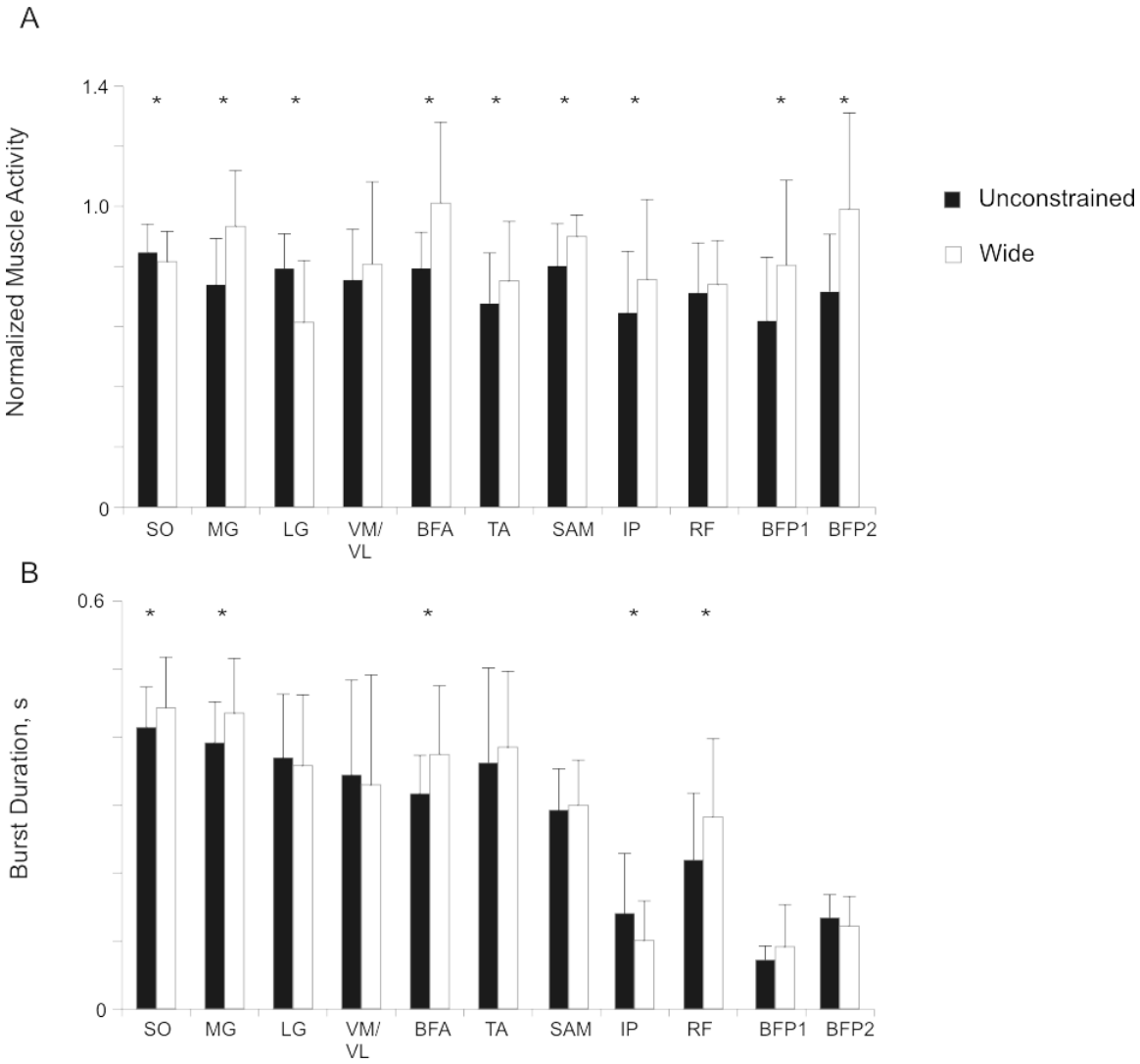

Figure 2.8 Mean (± SD) EMG activity (A) and burst duration (B) during wide and unconstrained walking. A) Mean EMG activity normalized to the peak value seen during unconstrained walking (see METHODS for details). B) Mean EMG burst duration. Unconstrained activity is shown in filled bars and wide activity is shown in unfilled bars. * Indicates significant difference between wide and unconstrained ($p < 0.05$)

34% (by 54±7%) and lower in 21% of cells (by 32±3%). In addition, 26% (16/61) of neurons discharged in a different phase of the cycle as compared to unconstrained walking, with more cells firing earlier in the cycle (by 20-30% of the cycle) wide walking. Duration of the period of elevated was different in 15% (9/61) of cells. The

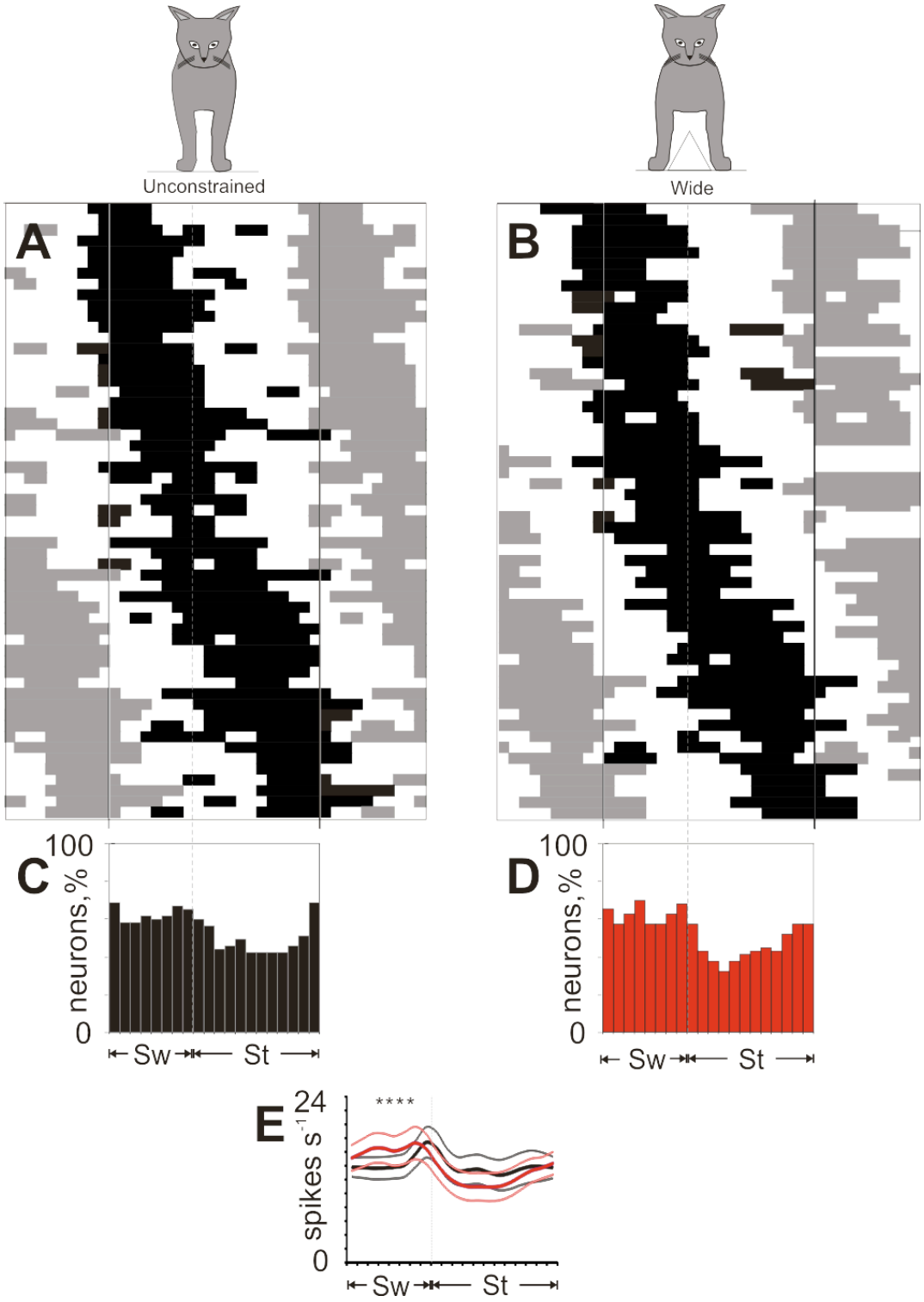

Figure 2.9 Population characteristics of neurons during locomotion with unconstrained and wide walking. A, B) Phase distribution of periods of elevated firings (PEFs). Vertical solid bars indicate beginning of swing phase. Dashed bar indicates beginning or stance. C, D) Proportion of active neurons (neurons in their PEFs) in different phases of the stride cycle during locomotion. E) Mean discharge rate (± standard error of mean) during locomotion. Sw, swing; St, stance.

overall cortical activity showed significantly increased neuronal discharge rates during bins 3,4,5 and 6 (Fig 2.9C, D; note change in cycle order). There was also a trend of decreasing firing rate during stance phase (Fig. 2.9 E), but not significantly.

2.4 Discussion

The purpose of this study was to investigate the effects of increased stance width on stability, muscle activity and cortical activity during walking. Two hypotheses were tested: (1) Margins of lateral stability would be larger for wide walking than for walking with unrestrained paws separation and (2) The activity of neurons from the right forelimb representation in the primary motor cortex will be similar in narrow and unconstrained walking. The general findings of the study indicated that wide walking had larger margins of stability in the frontal plane in some phases of walking cycle and was dynamically less stable in other phases compared to unconstrained walking (hypothesis 1 was partially supported). The study further demonstrated that overall discharge rate of neurons and its modulation in the primary motor cortex were elevated in some neurons and reduced in others, resulting in modest changes in the mean neuronal ensemble activity during wide walking (hypothesis 2 was rejected).

2.4.1 Biomechanics of Wide Gait

To my knowledge, this is the first study that describes in detail stability and the frontal plane kinematics and kinetics of whole-body during wide and unconstrained walking, which makes it difficult to compare this study to previously published reports. The whole-body kinematics and kinetics of unconstrained cat locomotion were similar to previously reported results (Prilutsky *et al.*, 2005; Beloozerova *et al.*, 2010; Prilutsky &

Klishko, 2011). The analysis of stability for wide walking indicated that static and dynamic stability depended on the area of base of support, which increased for 3-legged support phases and decreased for 2-legged support phases, as compared to unconstrained (Fig. 2.4) and narrow walking (Chapter 3). Margins of static stability increased during wide walking for 3-legged support, whereas the cat became statically unstable during 2-legged support phases of wide walking. Margins of dynamic stability on the other hand, increased during wide compared to unconstrained walking in only 2 phases (phases 1 and 5 of 3-legged support). The cats altered the duration of support phases in wide walking by making 3-legged supports with large margins of dynamic stability longer and 2-legged supports (dynamically unstable phases) shorter (Table 2.3) than during unconstrained walking. This change in pattern of limb support phases appears to increase stability of wide walking.

The resultant muscle moments in the frontal plane at the hip and shoulder during stance of wide and unconstrained walking were computed for the first time to my knowledge and thus cannot be compared with previously published data. For unconstrained walking, the moments were abduction throughout stance (Fig. 2.6) demonstrating that the resultant action of all muscles around the hip and shoulder joints was to abduct the fore- and hindlimb. The direction of the muscle moments in stance is consistent with changes in the frontal shoulder and hip angles from adduction to abduction in stance (Fig. 2.7E, F) in unconstrained walking. The shoulder and hip moments in the frontal plane were computed using eq. (2.4), which neglects linear and angular acceleration of the leg segments. This was done because frontal plane moments of inertia of the cat hindlimb segments are not known and the limb accelerations during

stance are relatively small (especially in the medial-lateral direction) judging from the CoM acceleration and ground reaction force (Fig. 2.6, see also (Manter, 1938)). To examine the validity of the assumption of small acceleration, the sagittal plane muscle moments at the ankle, knee and hip was calculated using both methods, quasi-static equations (see eq. 2.4) and dynamic equations that include inertial terms (Manter, 1938; Prilutsky *et al.*, 2005). The inertial segment parameters for the second approach were estimated using the regression equations (Hoy & Zernicke, 1985). The results of this comparison (Fig. 2.10) demonstrated that the error caused by assuming zero limb accelerations was negligibly small.

Other kinetic and kinematic changes observed during wide walking appear necessary to accommodate the increase in stance width. The increased lateral forces exerted by the limbs on the ground during wide walking (Fig. 2.6E, F) explain a larger displacement of the CoM in the medial direction (Fig. 2.5A). The increased abduction of the hip and shoulder joints allowed the cat to achieve such a large stance width during wide walking. The knee and elbow joints are typically considered a single degree of freedom joint for which the primary function is flexion and extension and does not allow for abduction and adduction.

Previous results have shown that when accuracy of paw placement is required as during walking on horizontal ladder, the head-neck segment rotates closer to the ground and its height is lowered (Beloozerova et al 2010; see also Chapter 3). It has been hypothesized that these kinematic postural adjustments facilitate acquisition of visual information about target location for paw placement.

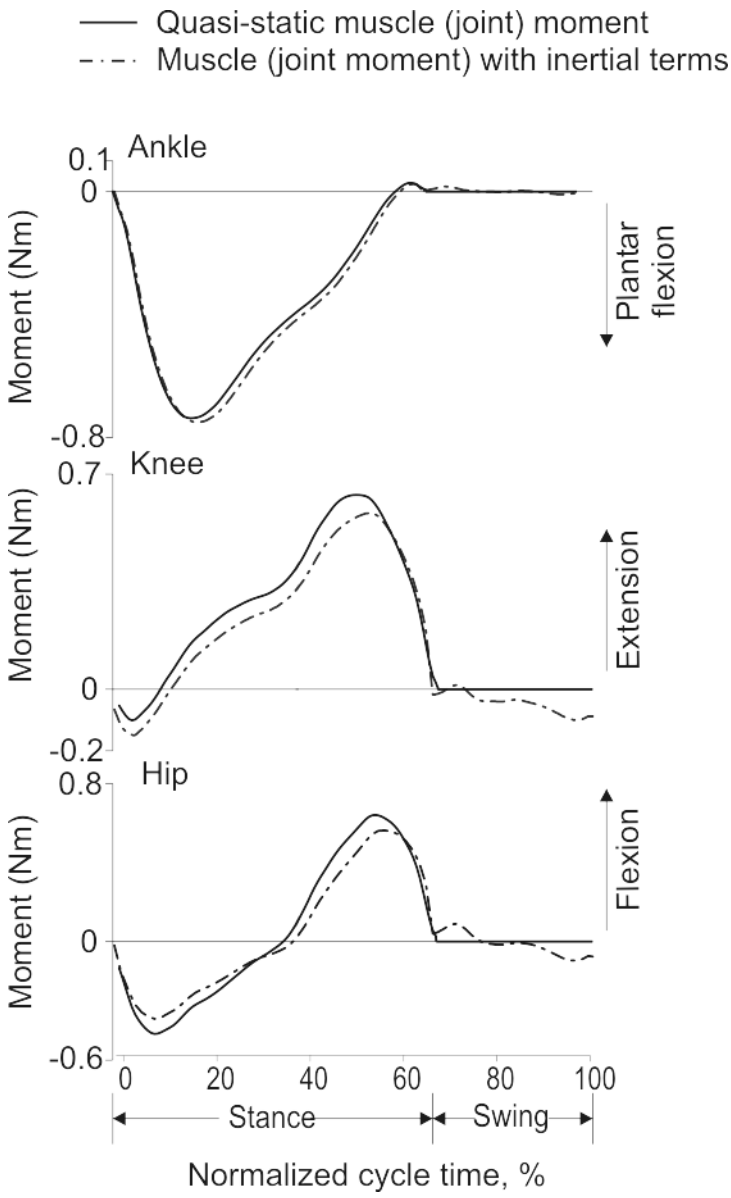

Figure 2.10 Comparisons of the resultant muscle moments at the ankle, knee and hip joints during a stride of unconstrained walking computed with (dashed lines) and without (solid lines) inertial terms.

During wide walking, similar postural adjustments take place (Fig. 2.5C, D), suggesting that the cats select location for paw placement. However, the nature of the constraints on the width of stance during wide walking restricting paw placement in just one direction

does not seem to impose stringent demands on accuracy since the cat could place the paw in any forward, backward and lateral location within reaching distance of the paw.

2.4.2 EMG activity during wide walking

EMG activity during wide walking showed changes in mean activity and burst duration in many muscles. One principle change was the increase in activity from MG and a decrease in activity from the LG and SO. The differing directions of change between the LG and MG muscles may point to the out-of-sagittal-plane secondary actions of these muscles (Lawrence *et al.*, 1993) and the contribution of MG to abduction (as in the sural nerve reflex (Nichols *et al.*, 1993)). This could result from increased tactile feedback from the lateral border of the paw pad which is experiencing increased pressure due to the increased lateral loading. Additionally, overall activity of flexor muscles (BFP, IP, and TA) was increased during wide walking. This overall increase may be due to an upregulation of the flexor half center of the central pattern generator or the flexor synergy (Markin *et al.*, 2010; Markin *et al.*, 2012). The increased activity is most likely in response to the need for increased paw clearance during swing as demonstrated by the increased paw height (Fig 2.7 B). One limitation to the EMG analysis is that EMG was not compared via phasing, which may indicate increased co-contraction or other phase related dependencies.

2.4.3 Motor cortex activity during wide walking

Cortical activity during wide walking showed somewhat limited changes in comparison to cortical activity during unconstrained walking (4 out of 20 bins; Fig 2.9), thus the hypothesis of small changes in cortical activity during wide walking due to its relatively low lateral instability and accuracy demands was only partly supported. The

elevated firing during swing of wide walking (Fig. 2.9D, E) may be attributed to an increased contribution of the primary motor cortex to control paw placement immediately after the dynamically unstable phases of contralateral 2-legged support (phases 6 and 7 for the right forelimb, Fig. 2.3), in which paw placement must be selected to stabilize body in the frontal plane, given that swing phase is the only time to control limb placement (Winter, 1995; Hof, 2008). Increased activity during swing could also be explained partially based on the increased height of the forelimbs. Though it may be expected that activity would increase prior to the need for increased height (i.e. there should be a delay) and overall cortical activity increases during late swing.

Overall activity, however, may not be the best parameter for analysis. Given the vast number of neurons, it may be unfair to group them all and suggest that overall activity should change similarly across all neurons recorded. Therefore individual neurons (or small groups of neurons) may be responsible for differing actions. Therefore, the many neurons, which increased or decreased firing rate between tasks (85% of neurons) may be responsible for regulation of different pathways. For instance, some neurons may excite the flexor half-center within the central pattern generator, while others may be used in visuomotor processing controlling paw placement. Further, the spatial location of the neurons and the phasing of activity may be important. Neurons typically did not significantly change their phase of firing only the rate, which suggests that each neuron is perhaps performing a similar function between tasks. For instance, if neuron "A" shows an increased discharge rate during wide walking, this would tend to suggest that the function of neuron A is to upregulate or downregulate activity downstream. Neurons that change phase may be more related to planning or involve in a

reorganization of the central pattern generator. These pathways could reorganize the overall muscle synergies, contribute to cortical control over endpoint trajectory, participate in integration of visuospatial processing for controlling accurate paw placement, or in setting global task goals such as maintaining stability, speed, or overall CoM height.

2.4.4 Limitations

One limitation to the dynamic stability index used is that it assumes inverted pendulum mechanics and quadrupeds might not utilize this mechanism due to the presence of multiple limbs in contact with the ground. Figure 2.11 demonstrates a representative center of mass vertical displacement and forward velocity profile over one step. It can be seen that when velocity increases, center of mass decreases in height and vise versa. Therefore, based on this data it appears that the cat CoM is, to some extent, behaving as an inverted pendulum with out-of-phase changes of CoM potential and kinetic energy.

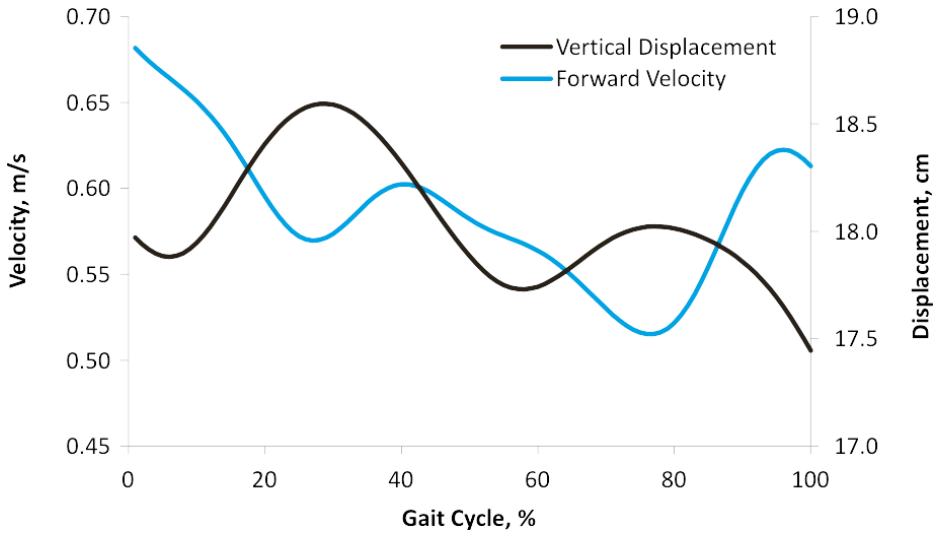

Figure 2.11 Center of mass forward velocity and vertical displacement from a representative stride.

2.4.5 Conclusions

In general, increased instability was seen during wide walking compared to unconstrained walking and it was primarily related to the frontal plane. Despite substantial changes in margins of lateral stability and mechanics during wide walking, changes in the magnitude and modulation of motor cortex activity were rather modest. I concluded that wide walking involves greater stability demands than unconstrained walking and that the activity of the motor cortex during swing phase may participate in regulation of lateral stability.

CHAPTER 3

FRONTAL PLANE MECHANICS AND MUSCLE AND MOTOR CORTEX ACTIVITY DURING WALKING ALONG A NARROW PATH: ARE REQUIREMENTS FOR FRONTAL PLANE ACCURACY AND STABILITY ADDITIVE?

3.1 Introduction

Real world locomotion involves navigation through various terrains, obstacles and paths of different widths – a complex behavioral task with many, often conflicting requirements. For example, walking on a narrow beam requires both accurate foot placement and lateral balance control. Cats, contrary to humans (e.g., (Schrager *et al.*, 2008)) seem to have the natural ability to meet these task demands as they are often seen walking on narrow fences or windowsills high above the ground without falling. How does the cat achieve locomotion when both accurate paw placement and control of balance are required? The previous research has demonstrated that such motor behaviors cannot be performed without involvement of the primary motor cortex (Burlachkova, 1979; Beloozerova & Siorta, 1993; Drew *et al.*, 2008).

It has been shown that when accuracy of paw placement is required, as during walking on a horizontal ladder, motor cortex activity is modulated as a function of accuracy demands (i.e., size of ladder rungs) indicating motor cortex involvement in this behavior (Beloozerova & Siorta, 1993; Armstrong & Marple-Horvat, 1996; Drew *et al.*, 2002; Beloozerova *et al.*, 2010). The role of the motor cortex during skilled accurate

stepping is thought to reflect visuomotor integration rather than direct control of paw trajectories since only few body mechanical and muscle activity variables change during accurate stepping compared to level (normal) walking (Beloozerova *et al.*, 2010) and motor cortex inactivation or removal of visual feedback do not change mechanics of unconstrained walking but make accurate stepping to stop (Burlachkova, 1979; Beloozerova & Siorta, 1993). The minor changes in walking mechanics associated with accurate stepping on horizontal ladders include rotation of the head and neck closer to the ground and lowering the general center of mass of the animal to presumably aid in acquiring more visual information about paw placement areas and in maintaining balance on small support surfaces, respectively (Beloozerova *et al.*, 2010).

Modulation of motor cortex activity during standing and locomotion is also related to maintenance of lateral stability of the body when it is perturbed by tilt of the support surface in the frontal plane (Beloozerova *et al.*, 2005; Karayannidou *et al.*, 2008; Karayannidou *et al.*, 2009). This postural-response related modulation of motor cortex activity has been suggested to have origin in somatosensory input from individual limbs and the trunk (Karayannidou *et al.*, 2008) as well as from vestibular (Zarzecki *et al.*, 1983; Macpherson *et al.*, 2007; Shinder & Taube, 2010) and visual inputs (Armstrong & Marple-Horvat, 1996; Drew *et al.*, 1996; Drew *et al.*, 2008). As with accurate stepping, the role of motor cortex activity modulation during postural perturbations is likely related to integration of posture related sensory information and to preparations for voluntary interventions if intrinsic musculoskeletal mechanisms (Bunderson *et al.*, 2010) and spinal and low brain reflexes (Dufosse *et al.*, 1985; Macpherson & Fung, 1999; Stapley & Drew, 2009; Honeycutt & Nichols, 2010; Musienko *et al.*, 2012) are insufficient to

recover balance and voluntary postural modifications are needed (Drew *et al.*, 1996; Jacobs & Horak, 2007).

Given that imposing requirements on either accuracy of stepping or lateral stability results in increased modulation of motor cortex activity in the cat, it is expected that walking along a narrow path only slightly wider than the paw will lead to greater involvement of motor cortex in this task. During unconstrained cat locomotion or standing on a flat surface, the distance between left and right paws on the ground, stance width is less than 10 cm, whereas the shortest distance between paws in the rostral-caudal direction is at least 20 cm (Misiaszek, 2006a; Macpherson *et al.*, 2007). Therefore the body center of mass is much closer to the boundaries of support in the frontal than in the sagittal plane and thus the cat body is less stable in lateral than rostral-caudal directions. Walking on a narrow path of 5-cm width makes lateral stability even more challenging. This task also imposes accuracy demands on paw placement. Although this walking task is a part of every-day behavioral repertoire of animals and people, little is known about the role of the primary motor cortex in control of this behavior and motor control strategies employed.

The goal of this study was to compare full-body mechanics, muscle electromyographic (EMG) activity and activity of neurons from the right forelimb representation of the primary motor cortex between unconstrained walking and walking on a narrow path of 5 cm in the cat. The hypothesis that activity of the primary motor cortex will be much greater during narrow walking because of imposed additional requirements on lateral stability and accurate paw placement was tested. Lateral and rostral-caudal dynamic stability derived from the extrapolated center of mass position

with respect to the boundaries of support (Hof *et al.*, 2005; Hof, 2008) in cats performing unconstrained and narrow walking was measured. Contrary to expectations lateral dynamic stability of the body was similar between unconstrained and narrow walking. Generally similar frontal and sagittal plane mechanics of the two locomotion tasks were consistent with small differences in myoelectric activity of major hindlimb muscles. The activity of 116 neurons from the right forelimb representation of the motor cortex, recorded during narrow and unconstrained walking, was in most cases higher during narrow than unconstrained walking, but lower than during ladder walking as reported previously. I concluded that narrow walking imposes additional demands on accuracy of stepping in frontal plane but not on lateral stability. Thus, the elevated motor cortex activity is likely related to the role of motor cortex in visuomotor integration. Preliminary results of this work have been published in abstract form (Farell *et al.*, 2008; Farrell *et al.*, 2011).

3.2 Methods

3.2.1 Ethical approval

All animal procedures were approved by the Institutional Animal Care and Use Committees of Georgia Institute of Technology and Barrow Neurological Institute and in agreement with the US Public Health Service Policy on Humane Care and Use of Laboratory Animals and

3.2.2 Animal characteristics and locomotion tasks

Nine cats (mass = 3.5 $\pm$ 0.5 kg; Table 3.1) were trained to walk on a walkway (3.0 m long and 0.25 m wide) with Plexiglas walls with unconstrained stance width

(unconstrained walking) and a narrowed stance width (<5cm, narrow walking) using positive reinforcement (food). The narrow path was created by placing two small triangular prisms with 2-cm sides on either side of the walkway or treadmill, creating a path 5 cm in width (Fig. 3.1A). Cats undergoing cortical recordings were fitted with a light backpack containing connectors and an electro-mechanical sensor on the right fore paw for determining paw contact and lift-off (Beloozerova & Siorta, 1993; Beloozerova *et al.*, 2010).

Table 3.1 Animal characteristics and analyses conducted

Cat	Gender	Mass, kg	Forelimb Length, cm	Hindlimb length, cm	Full-Body Mechanics	EMG	Motor Cortex
Az	Female	4.2	21.1	24.4	x	x	
In	Female	3.2	19.1	25.8	x	x	
Kr	Female	3.0	19.4	25.1	x	x	
Ma	Female	2.8	21.4	27.6	x	x	
Sv	Female	3.8	19.5	26.0	x	x	
1	Male	3.9					x
3	Male	3.0				x	x
4	Female	3.8					x
11	Female	3.7				x	x

Note: Hindlimb length is defined as the sum of tarsals, shank and thigh lengths; forelimb length is defined as the sum of carpals, forearm, and arm lengths.

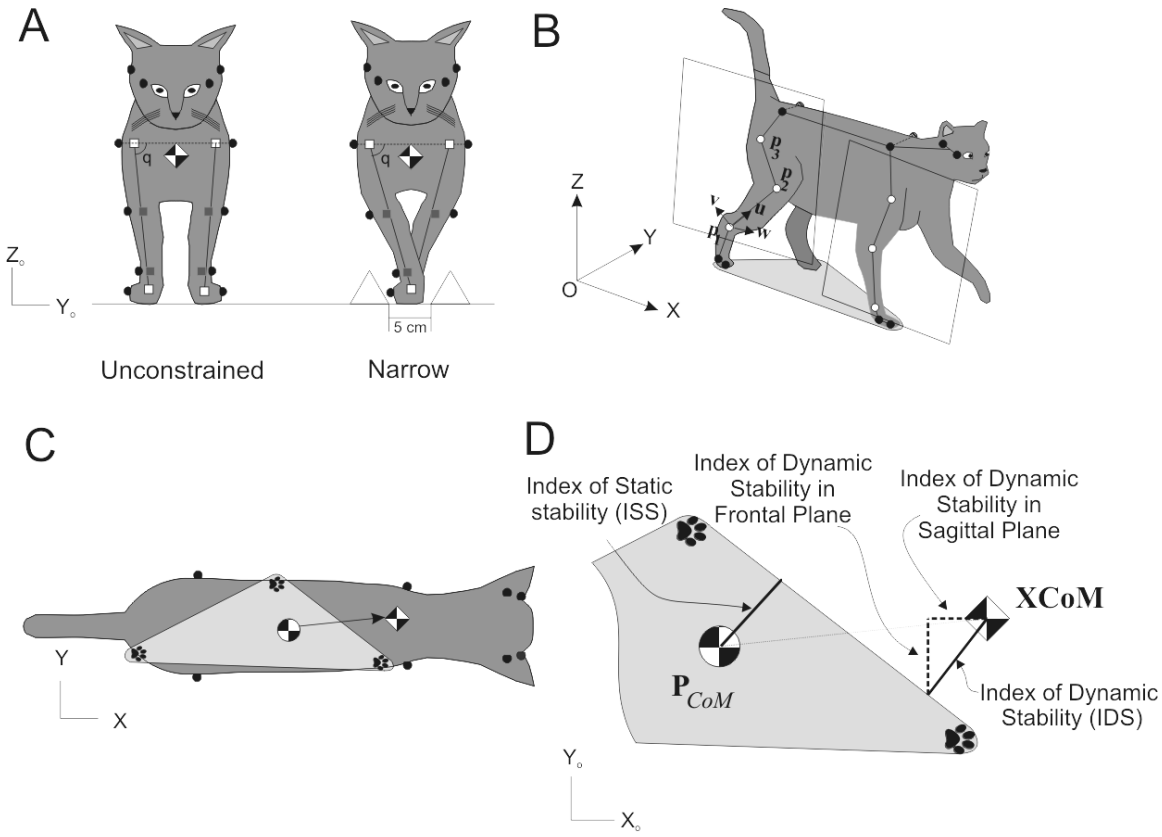

Figure 3.1 Determining static and dynamic stability of locomotion. A) Frontal view of the cat demonstrating walking conditions with narrow and unconstrained paw separation. Gray and open squares indicate estimated centers of the joints or paw. Angle q is the hip and shoulder angle in the frontal plane. B) Perspective view of the cat during walking showing how the hindlimb plane was defined (the forelimb plane was defined in the same way). Three open markers on each limb were used to define unit vectors v, u and w and the limb plane (see text for further explanations). C) Dorsal view of the cat during walking: ◔, center of mass (CoM) and ✦, extrapolated center of mass (XCoM). Paw prints indicate paws on the ground, which form the base of support (lighter gray area). Filled circles are markers on iliac crests and scapulars, and at the corner of each eye and ear. D) Definitions of the base of support, index of static stability (ISS), index of dynamic stability (IDS, panel indicates unstable IDS) and its components, i.e. index of dynamic stability in the frontal plane (IDS_f) and index of dynamic stability in the sagittal plane (IDS_s) (see text for further explanations).

3.2.3 Experimental procedures

Surgical procedures

The 5 cats undergoing full-body assessment of biomechanics for unconstrained and narrow walking were implanted with EMG electrodes after initial locomotor training (for details see (Prilutsky *et al.*, 2011); Chapter 2). Fine wire EMG electrodes were implanted in the following muscles: soleus, ankle extensor, SO; medial, MG and lateral, LG gastrocnemii, ankle extensors and knee flexors; tibialis anterior, ankle flexor, TA; vastus medialis, knee extensor, VM; rectus femoris, knee extensor and hip flexor, RF; sartorius medial, knee and hip flexor, SAM; iliopsoas, hip flexor, IP; biceps femoris anterior, hip extensor, BFA; biceps femoris posterior, hip extensor and knee flexor, BFP; adductor magnus, hip adductor, AM; and semimembranosus posterior, hip extensor and knee flexor, SMP, . Electrode location was confirmed using electrical stimulation. After implantation the segment lengths for each limb and the width of each joint were measured.

Four separate cats (Table 3.1) underwent surgery to allow for cortical activity recordings (for detailed methods see (Beloozerova & Siorta, 1993; Prilutsky *et al.*, 2005; Beloozerova *et al.*, 2010) and are only briefly discussed here. The skull and dura mater above the motor cortex were removed for and replaced with a 1-mm thick acrylic plate. Identification of pyramidal tract neurons (PTNs) was achieved by inserting two hypodermic guide tubes above the medullary pyramids until the tips were located at the Horsley-Clarke coordinates (P7.5, L0.5) and (P7.5, L1.5) with a depth of H0. A plastic cap covered and provided protection for all implants. During the terminal experiment, after all cortical recording experiments, the cats were anaesthetized and euthanized with

pentobarbital sodium. Histological sections were made to verify the placement and position of the electrodes.

Cell recording and identification

Extracellular recordings of motor cortex activity were made using electrodes inserted into the right forelimb projection on the motor cortex. Recordings were made using tungsten varnish-insulated microelectrodes (120 μm OD; Frederick Haer & Co, USA) or platinum-tungsten quartz insulated microelectrodes (40 μm OD) each with a resistance of 1-3 MΩ at 1000 Hz. Electrode depth into the cortex as controlled using a custom micro-drive (2.5 g) attached on the head cap. Cortical recordings were pre-amplified, further amplified (CyberAmp 380, Axon Instruments, USA), and filtered (0.3-10 kHz band pass). Signals were then displayed on a screen and sent to an audio monitor and before being saved on the hard drive of a PC at 30 kHz using a data acquisition system (Power-1401/Spike-2 System, Cambridge Electronic Design, UK). Exemplar cortical recordings during unconstrained and narrow walking are shown in Fig 3.2 C,D for a pyramidal tract neuron. Neurons were evaluated for antidromic activation before, during and after recording session. The receptive fields of the PTNs were determined using audible changes of the cortical recording elicited through palpation and passive joint movement.

Biomechanical and electromyographic recordings

Full-body mechanical recordings during unconstrained walking have been described previously in Chapter 2 (see also (Prilutsky *et al.*, 2005; Beloozerova *et al.*, 2010)) and are only briefly described here. In summary, the three-dimensional positions of 28 markers representing major the limb joints and body segments were recorded at 120

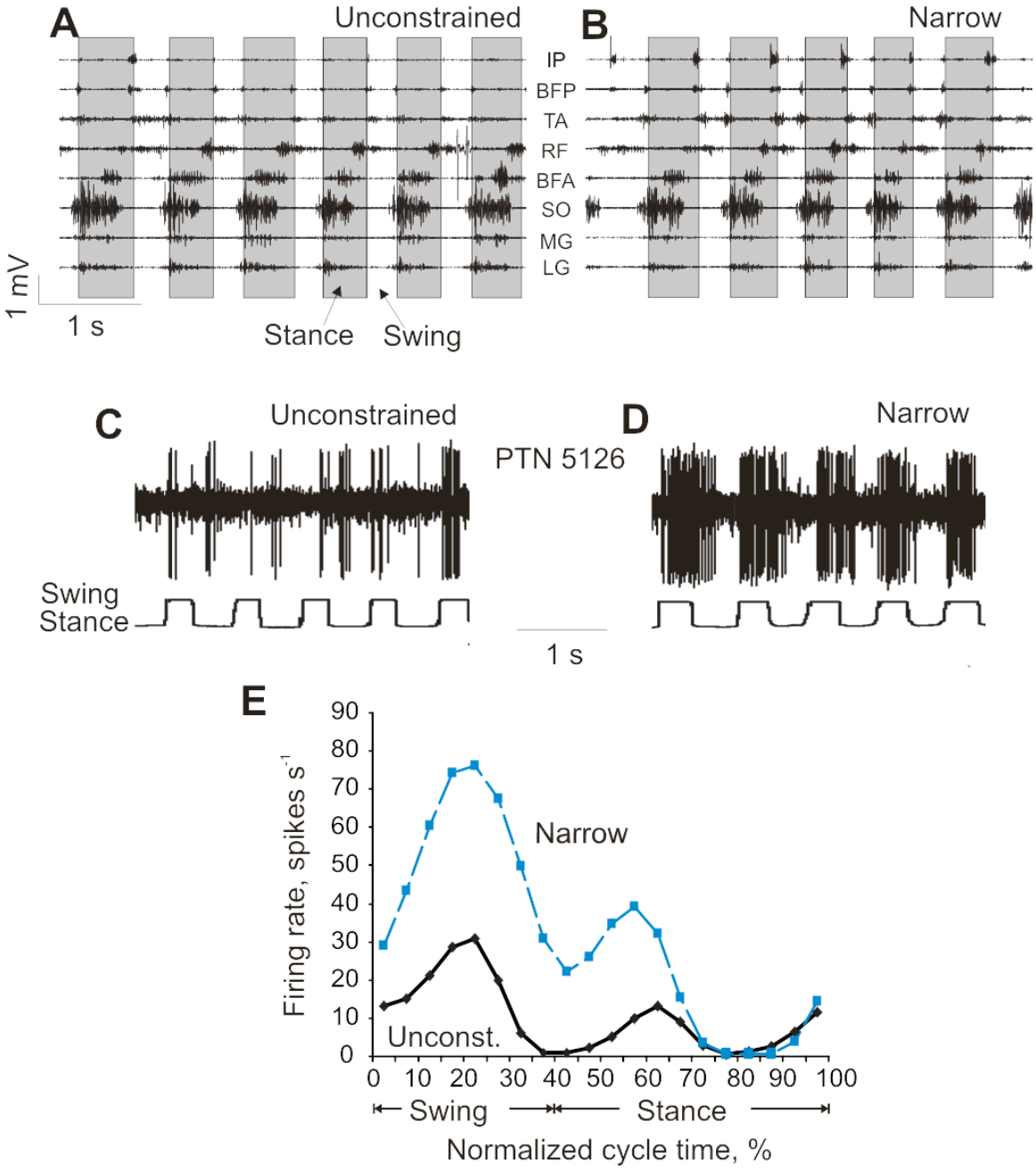

Figure 3.2 Examples of typical EMG hindlimb muscle activity and cortical activity of during walking with unconstrained and narrow paws separation. A, B) EMG activity of hindlimb muscles during unconstrained and narrow walking, respectively. IP, iliopsoas; BFP, biceps femoris posterior; TA, tibialis anterior; RF, rectus femoris; BFA, biceps femoris anterior; SO, soleus; MG, medial gastrocnemius; and LG, lateral gastrocnemius. C, D) Activity of a PTN during unconstrained and narrow walking (the lower trace shows Swing- deflection up and Stance - deflection down phase of the stride). E) Activity of the same neuron is presented as a histogram during locomotion with unconstrained vs. narrow paws separation.

frames/s (Vicon Motion Systems, UK). (Figure 3.1A, B, C; for further details see CHAPTER 2 and (Prilutsky *et al.*, 2005)). The ground reaction force and center of pressure were recorded at 360 Hz using 3 embedded force platforms (0.16 x 0.11 m (2) and 0.11 x 0.07 m; Bertec Corporation, USA).

During each experimental session, both unconstrained and narrow walking tasks were recorded without changing markers or the EMG cable attached to the head-mounted connectors (for details see Chapter 2). EMG recordings were synchronized with the motion capture recordings and sampled at 3000 Hz. Examples of raw EMG signals recorded during unconstrained and narrow walking are shown in Fig. 3.2 A, B. Walking tasks were randomized between sessions and animals.

3.2.4 Data analysis

Kinematic and kinetic analysis

The full-body mechanical analysis has been described in detail (Chapter 2) and only a brief description is presented here. Good trials were identified as trials where the cats maintained a steady forward walking speed and were not included if the cats exhibited an atypical walking pattern. Markers positions were low pass filtered (4^{th} order, zero-lag Butterworth filter, cut-off frequency 6-7 Hz). A limb plane for each frame of the gait cycle was determined (Fig. 3.1B, white filled circles indicate markers used to define limb plane; Eq. 2.1). Within this plane, the knee and elbow marker positions were recalculated and the location of the distal limb joint centers (MTP, ankle, knee, MCP, wrist, elbow) and location of digit/paw centers were estimated using the joint width and the orthogonal vector (Fig. 3.1A, B). The hip and shoulder joint centers were estimated by shifting the marker position medially along the line connecting the two hip and two

shoulder markers, respectively (Fig. 3.1A). The displacement of the center of mass (CoM; Fig. 3.1C, D) was determined using an 18-segment model (Eq. 2.2 and 2.3), the measured mass (Table 3.1), segment lengths and the previously reported regression equations (Hoy & Zernicke, 1985).

Additional stride related kinematic parameters were calculated. These include: stride length, stance width, forward velocity of the CoM, stance duration, swing duration and duty factor (the ratio of stance duration over stride duration). Stance width was calculated as the paw center to paw center distance for the forelimbs and for the hindlimbs. Stance, swing and stride durations were determined based on initial paw contact with the ground and paw lift-off. The contact and lift-off times were determined using either the force plate contact and lift-off times or the forward velocity of the paw (for details see (Pantall *et al.*, 2012), Method 2).

Frontal plane angles and moments were calculated at the shoulder and hip. Shoulder ab/adduction angles were defined using the shoulder joint centers and the line from the shoulder center to the MCP joint center (Fig 3.1 A; see also (Misiaszek, 2006a)). Hip ab/adduction angles were calculated similarly using the hip joint centers. The ab/adduction resultant muscle moments for the hip and shoulder joints were calculated using Eq. 2.4.

Analysis of body stability

Static and dynamic stability indices were determined for each frame of the gait cycle. Static stability was defined using the projection of the CoM onto the ground (Fig 3.1D). The cat was considered statically stable during that frame if the projection fell within the support area or statically unstable if the projection was outside the support

area. To calculate dynamic stability, the extrapolated center of mass (XCoM) was calculated based on the previously published equations (Hof *et al.*, 2005). Using XCoM, the index of dynamic stability, *IDS*, was computed as the shortest (perpendicular) distance between the projection of the XCoM onto the ground and the edge of support area (Fig. 3.1D). The cat was determined to be dynamically stable if XCoM fell inside support area (IDS>0), and dynamically unstable if XCoM fell outside the support area (IDS<0). The IDS was further broken down into two components representing indices of dynamic stability in the frontal and sagittal planes, respectively (Fig. 3.1D).

EMG analysis

Raw EMG recordings were band-pass filtered (30-1000 Hz) rectified. EMG activity onset and offset times were determined when the activity reached a threshold value defined as the mean value during a silent period plus 2 SD ((Gregor *et al.*, 2006; Prilutsky *et al.*, 2011). The mean EMG activity and duration was calculated for all analyzed strides. EMG activity was normalized by the maximum mean EMG value seen in all strides of unconstrained walking.

Analysis of cortical activity

Each stride was divided into 20 equal bins based on the stride duration of the right forelimb detected with the electro-mechanical sensor (Fig. 3.2C, D). The binned spike activity for each cortical neuron during walking was calculated for each condition (e.g. Fig. 3.2E). Using the binned data for each neuron, the subsequent variables were computed (for details see (Beloozerova & Siorta, 1993; Beloozerova *et al.*, 2010): mean discharge frequency, coefficient of frequency modulation (dM), preferred cycle phase, and duration of the period of elevated firing (PEF). The mean discharge frequency over

walking cycle, range of coefficients of modulation, and widths of the PEFs were calculated for the population of all neurons and were compared between unconstrained and narrow walking.

Statistical analysis

All mechanical variables for individual limbs were time normalized to 100% of the limb stride duration. Comprehensive mechanical variables describing center of mass and stability measures were time normalized to the right forelimb stride duration. The mechanical variables from averaged within each cat and then between cats for unconstrained and narrow walking conditions. Student's t-test was to test for differences between conditions. Mechanical variables were compared at each percent of walking cycle. Stride parameters, mean EMG burst activity, and parameters of PTN activity were compared between unconstrained and narrow walking. The significance level was set at 0.05.

3.3 Results

In total, 227 strides from 5 cats were used for mechanical analysis of unconstrained and narrow walking, 194 strides from 5 cats were used for analysis of EMG, and 116 neurons from the right forelimb representation of the primary motor cortex in 4 cats were recorded and analyzed.

3.3.1 Mechanics of narrow walking

General stride characteristics of narrow walking

The mean speed of narrow overground walking (mean ± SD: 0.55 ± 0.13 m/s) was similar to mean speed of unconstrained walking (0.61 ± 0.05; $p>0.05$, Table 3.2).

Kinematic stride parameters of fore- and hindlimbs during narrow walking – stride length (0.436 ± 0.032 m and 0.443 ± 0.031 m, respectively), stride duration (0.842 ± 0.141 s and 0.844 ± 0.149 s), stance duration (0.549 ± 0.115 s and 0.518 ± 0.106 s), swing duration (0.293 ± 0.029 s and 0.326 ± 0.045 s), and duty factor (0.65 ± 0.03 and 0.61 ± 0.02) – were likewise indistinguishable from those of unconstrained walking ($p>0.05$, Table 3.2). The average stance width (the distance between left and right paw centers in the frontal plane when legs were in stance) for the forelimbs (1.67 $\pm$ 0.55 cm) and hindlimbs (0.99 $\pm$ 0.57 cm) during narrow walking was smaller than during unconstrained walking (2.68 $\pm$ 1.32 cm and 2.50 $\pm$1.06 cm, respectively; $p<0.05$, Table 3.2).

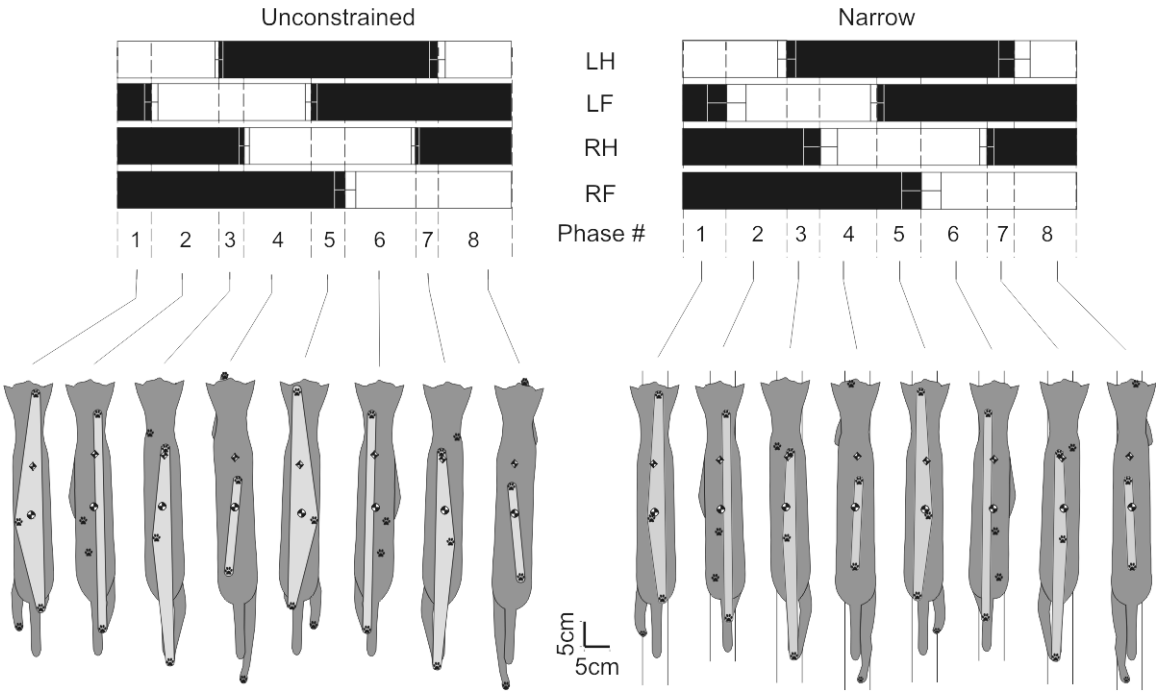

Figure 3.3 Limb support pattern (sequence of phases with different number of limbs on the ground; top panels) and the corresponding cat postures (bottom panels) during walking with unconstrained and narrow paws separation. Top panel: Stance phase is shown by black bars and swing phase by white bars. Thin horizontal bars indicate standard deviation for the phase onset and offset normalized time. Phases follow the 3-2-3-2-3-2-3-2 pattern; each phase is indicated by numbers 1-8. Bottom panel: The base of support area (in light gray), paw prints, center of mass (◓) and extrapolated center of mass (◓) are overlayed on the cat postures.

Table 3.2 Stride characteristics (mean ± SD) of unconstrained and narrow walking.

Stride parameter	Limb	Unconstrained	Narrow	p-value
Stance time (s)	Fore	0.47 ± 0.03	0.55 ± 0.12	0.185
	Hind	0.44 ± 0.03	0.52 ± 0.11	0.157
Swing time (s)	Fore	0.26 ± 0.02	0.29 ± 0.03	0.063
	Hind	0.30 ± 0.03	0.33 ± 0.04	0.173
Cycle time (s)	Fore	0.73 ± 0.05	0.84 ± 0.14	0.147
	Hind	0.74 ± 0.05	0.84 ± 0.15	0.159
Duty factor	Fore	0.64 ± 0.01	0.65 ± 0.03	0.542
	Hind	0.60 ± 0.01	0.61 ± 0.02	0.177
Stride length (cm)	Fore	43.72 ± 3.27	43.56 ± 3.24	0.719
	Hind	44.73± 2.90	44.25 ± 3.11	0.424
Stance width (cm)	Fore	2.73 ± 1.23	1.67 ± 0.55	0.043*
	Hind	2.50 ± 1.06	0.99 ± 0.57	0.015*
Swing height (cm)	Fore	3.91 ± 0.89	5.11 ± 1.11	0.001*
	Hind	3.66 ± 0.28	5.44 ± 0.83	0.006*
Speed (ms^{-1})		0.61 ± 0.05	0.55 ± 0.13	0.162
Maximal IDS (cm)		1.63 ± 0.30	1.37 ± 0.25	0.115
Minimal IDS (cm)		-6.53 ± 1.50	-5.13 ± 3.49	0.207
Peak lateral CoM acceleration (cms^{-2})		-59.80 ± 14.62	-54.92 ± 9.91	0.152
Max BoS Area (cm^2)		146.5 ± 23.5	116. 7 ± 12.1	0.009*
Min BoS Area (cm^2)		31.7 ± 1.5	31.2 ± 2.8	0.564

* Significant differences between unconstrained and narrow walking.

Similar to walking with unconstrained stance width, narrow walking had support pattern (sequence of phases with different number of limbs on the ground) typical for tetrapod walking with intermediate speeds (e.g., (Gray, 1968)): 3-2-3-2-3-2-3-2 (Fig. 3.3)). The number of limbs in contact with the ground at a given time determined the area of support and body static stability (see below). The area of support during narrow and

unconstrained walking was the smallest for cycle phases with 2 limbs on the ground (phases 2, 4, 6 and 8, Figs. 3.3 and 3.4, Table 3.3). The support area during the double support phase provided by contralateral fore- and hindlimbs (phases 4 and 8) was statistically smaller that during the double support phase provided by ipsilateral fore- and hindlimbs (phases 2 and 6, $p<0.05$; Figs. 3.3 and 3.4, Table 3.3). The minimum support area during the stride of narrow walking (31.2 ± 2.8 cm^2) was similar to that of unconstrained walking (31.7 ± 1.5 cm^2; $p>0.05$, Figs. 3 and 4, Table 3.2), whereas the maximum support area during narrow walking (116.7 ± 12.1 cm^2) was statistically smaller than during unconstrained walking (146.5 ± 23.5; $p<0.05$; Figs. 3.3 and 3.4, Table 3.2).

Stability of narrow walking

Indices of static (ISS) and dynamic stability (IDS) fluctuated during the walking cycle in accordance with the limb support pattern and the support area discussed above (see Figs. 3.3 and 3.4). In 3-legged support phases (phases 1, 3, 5 and 7), the ISS and IDS with its frontal (IDS_f) and sagittal (IDS_s) components were either positive or indistinguishable from zero for both narrow and unconstrained walking, i.e. the cat was statically and dynamically stable (Fig. 3.4). In double support phases of both narrow and unconstrained walking (phases 2, 4, 6 and 8), the static stability (ISS) and dynamic frontal stability (IDS_f) were likewise non-negative, and there was no difference in the ISS and IDS_f between narrow and unconstrained walking ($p>0.05$, Fig. 3.4). Thus, both narrow and unconstrained walking were found to be statically and dynamically stable in the frontal plane. The cat was dynamically unstable in the sagittal plane during the double

Table 3.3 Base of Support Area (mean ± SD) during unconstrained and narrow walking

Support phase #	Unconstrained	Narrow	p-value
1	131.9 ± 28.4	104.6 ± 14.7	p< 0.05*
2	72.1 ± 2.6	71.7 ± 4.2	0.75
3	125.1 ± 16.4	94.4 ± 8.9	p< 0.05*
4	35.0 ± 2.5	34.3 ± 1.2	0.43
5	128.6 ± 21.7	104.1 ± 11.7	p< 0.05*
6	74.7 ± 5.3	72.4 ± 3.1	0.15
7	124.0 ± 31.5	98.4 ± 17.1	p< 0.05*
8	35.8 ± 2.6	34.3 ± 3.2	0.18

* Significant differences between unconstrained and narrow. Support phases correspond to those in Fig 3.3.

support phases by contralateral fore- and hindlimbs (phases 4 and 8) – the peak shift of the extrapolated center of mass beyond the boundaries of support was -5.1 ± 3.5 cm for narrow walking and -6.5 ± 1.5 cm for unconstrained walking, and there was no difference in the IDS and IDSs between narrow and unconstrained walking ($p>0.05$, Table 3.2, Fig. 3.4).

Given the definitions of static and dynamic stability (see Methods), the results presented in Fig. 3.4 are a consequence of motion of the CoM with respect to paws on the ground. Although there was no substantial difference in static and dynamic frontal stability between narrow and unconstrained walking, the range of CoM displacement toward the left and right sides of the cat had a tendency to be larger during narrow walking (up to 0.4 cm) than during unconstrained walking (close to 0.2 cm, Fig. 3.5 A),

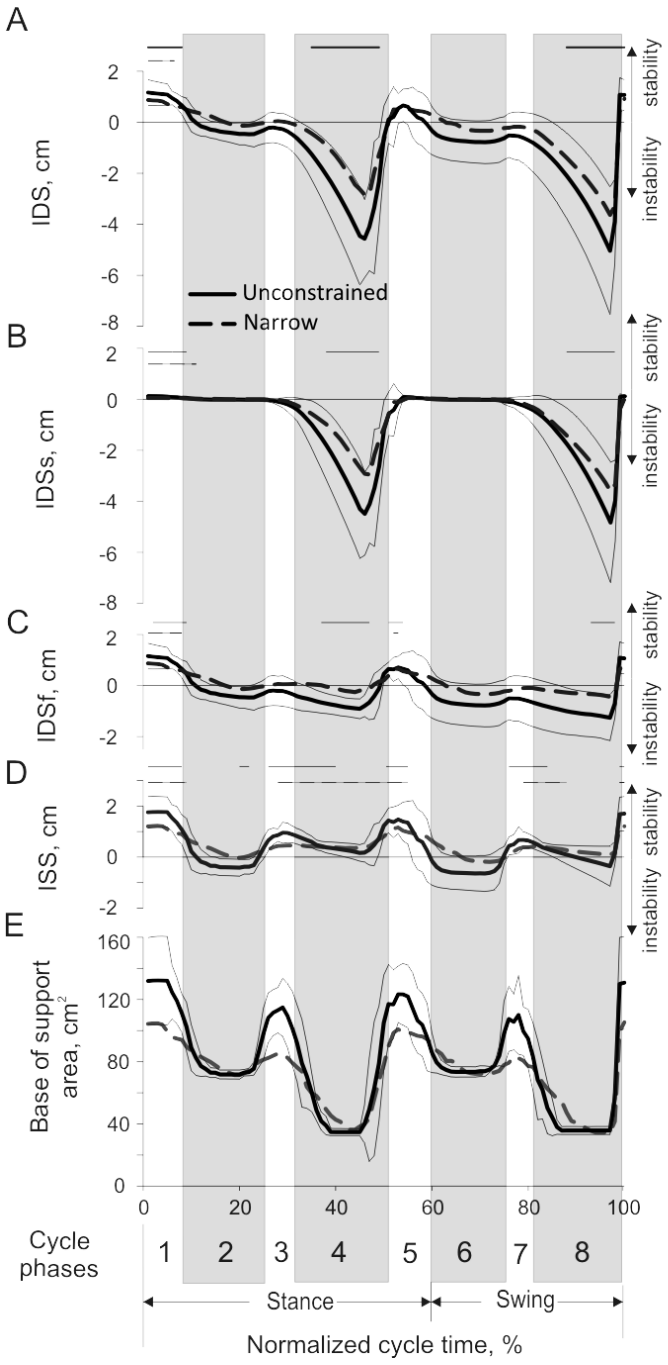

Figure 3.4 Index of dynamic stability during walking with unconstrained and narrow paws separation. Thick continuous lines, the mean for unconstrained walking; thick dashed lines, narrow walking; and thin continuous line, SD for the mean of the unconstrained condition. A) Index of dynamic stability (IDS, see Fig. 3.1 and text for explanations) averaged across studied strides and cats. Solid and dashed lines indicate walking with unconstrained and narrow paws separation, respectively. Thin lines indicate ±SDs for the walking with unconstrained paws separation. Solid and dashed horizontal bars indicate phases in which the IDS for unconstrained and narrow walking is significantly different from zero. Negative values indicate instability. B) Index of dynamic stability in the sagittal plane (IDS_s). C) Index of dynamic stability in the frontal plane (IDS_f). D) Index of static stability (ISS). No significant differences were found between the two walking conditions. E) Base of support area.

however this difference did not reach the significance level of 0.05. This difference appears to be related to a more variable pattern of CoM motion in the left-right direction during unconstrained walking – the peaks of displacement in different cats did not coincide in time (not shown), which caused the smaller mean values and larger SDs compared to narrow walking. The peak CoM displacement in the left and right directions occurred at 10-25% and 60-75% of the right forelimb stride during double support phases by the right fore- and hindlimb and the left fore- and hindlimb, respectively (see Figs. 3.3, 3.4 and 3.5A, phases 2 and 6). This pattern of CoM left-right displacements away from the area of support may, however, be a deliberate strategy to improve dynamic lateral stability. The CoM and XCoM lateral positions were closest to the midline of the cat body during the transition from a double-support by diagonal fore- and hindlimbs (phases 4 and 8) to a 3-legged support provided by two forelimbs and one hindlimb (phases 1 and 5; Figs. 3.3 and 3.5A). Vertical displacement of the CoM was synchronized with left-right CoM displacement in both narrow and unconstrained walking (Fig. 3.5B) – the CoM reached peak vertical positions during the phases of maximum CoM deviations from the body midline (phases 2 and 6), whereas the CoM lowest position occurred during the phases with the minimum CoM deviation from the body midline. Interestingly, just prior to reaching the lowest CoM position at 50% and 100% of cycle time, the body was most dynamically unstable in the anterior direction (IDS peaks were -5.1 ± 3.5 cm and -6.5 ± 1.5 cm for narrow and unconstrained walking; Fig. 3.4, IDS, IDS_s) due to relatively high forward CoM velocity (not shown) and a small support area (Fig. 3.4). The recovery of dynamic stability was achieved by a forelimb that contacted the ground rostral to the XCoM and 'caught' the CoM moving forward and downward.

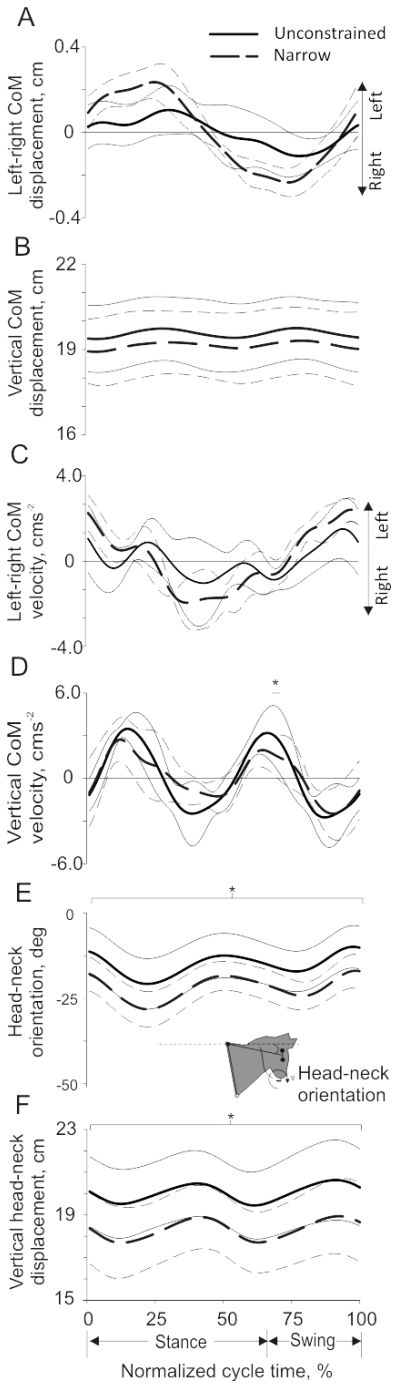

Figure 3.5 Selected mechanical variables of walking with narrow and unconstrained paw separation as a function of the normalized stride cycle of the right forelimb (see Fig. 3.4 for definition of lines and the horizontal axis). Mean data of 5 cats (Table 3.1). A) Displacement of the CoM in the left and right direction; left direction corresponds to the left side of the body. B) Vertical displacement of the CoM. C) Velocity of the CoM in the left and right direction; left direction corresponds to the left side of the body. D) Vertical velocity of the CoM. E) Head-neck segment orientation; clockwise segment rotation from the horizontal is defined as negative. F) Vertical displacement of the head-neck segment.

There was a small trend for the CoM vertical position to be lower during narrow walking, however this trend was insignificant ($p>0.05$). The vertical position of one part of the body, the head-neck segment, was significantly lower for narrow walking than for unconstrained walking by about 1 cm throughout the stride (Fig. 3.5D). The pattern of vertical displacement of this segment was similar to that of the CoM (both had two peaks and two nadirs) but was slightly advanced forward in time. This segment was also more rotated from the horizontal to the ground throughout the whole stride of narrow walking ($p<0.05$, Fig. 3.5C). These two features of head-neck movements were described previously for precise stepping on the horizontal ladder and have been explained by the need to improve conditions for acquiring visual information about paw placement areas (Beloozerova *et al.*, 2010).

Other characteristics of narrow walking in frontal and sagittal plane

The ground reaction forces acting on the cat's body determined motion of the CoM. The three orthogonal components of the ground reaction force vectors applied to the fore- and hindlimbs were similar between narrow and unconstrained walking ($p>0.05$; Fig. 3.6) and their values and patterns qualitatively corresponded to previous studies of cat unconstrained level walking (Manter, 1938; Beloozerova *et al.*, 2010; Prilutsky & Klishko, 2011). For example, the forces applied to the forelimbs were greater than those of hindlimbs in the vertical, upward direction (55% of body weight versus 47%) and posterior direction (deceleration phase, 11% versus 8%); the forces in anterior direction (acceleration phase) were greater on the hindlimbs than forelimbs (11% versus 9%; Fig. 3.6). No difference in the peak vertical and anterior-posterior forces were found between

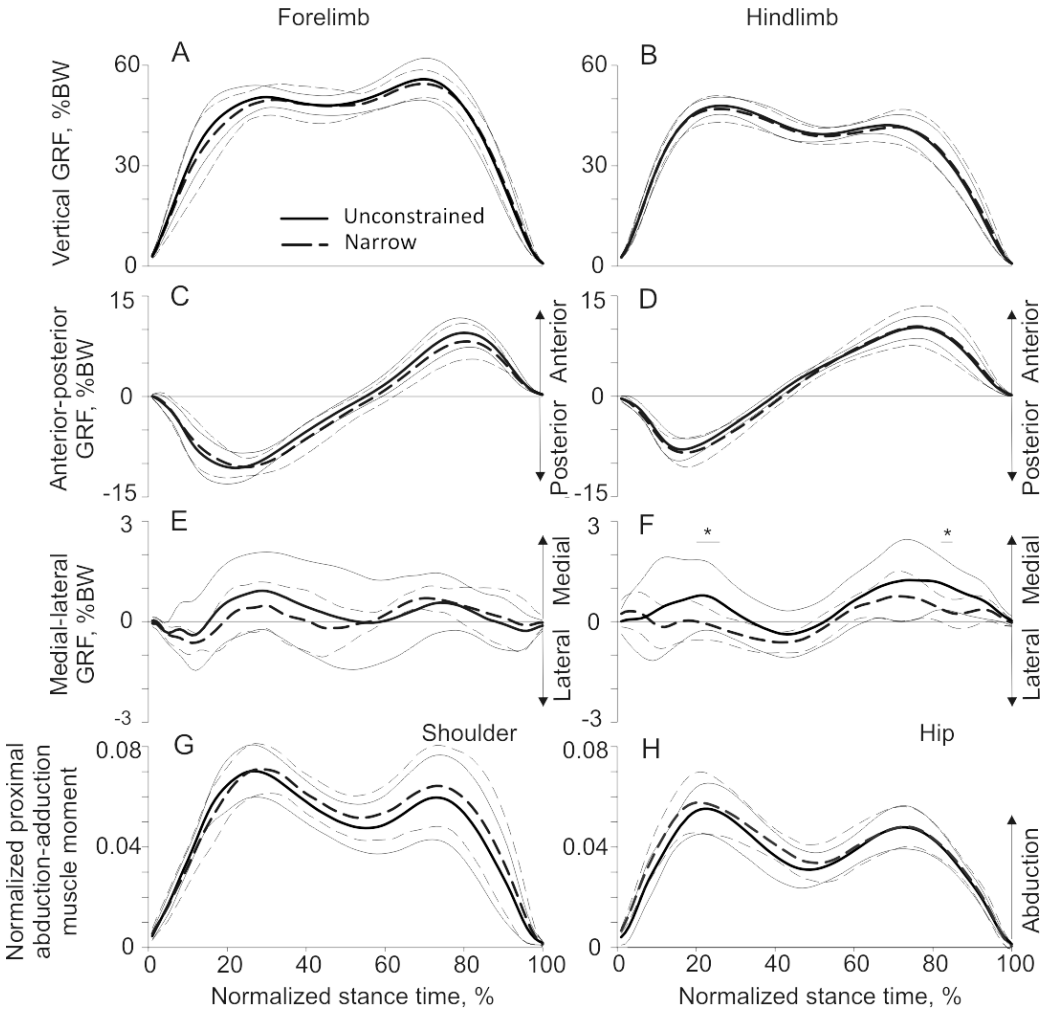

Figure 3.6 Selected kinetic variables (mean ± SD) of walking with narrow and unconstrained paw separation as a function of the normalized stance time (see Fig. 3.4 for definition of lines). Mean data of 5 cats (Table 3.1). Thin horizontal bars with symbol * indicate statistically significant differences ($p<0.05$) between narrow and unconstrained walking. A, B) Vertical ground reaction force applied to the fore- and hindlimbs, respectively. C, D) Anterior-posterior ground reaction force applied to the fore- and hindlimbs. E, F) Medial-lateral ground reaction force applied to the fore- and hindlimbs. G, H) Normalized frontal plane moment for the shoulder and hip joints, respectively. The moment in Nm is normalized to the cat's body mass and limb length.

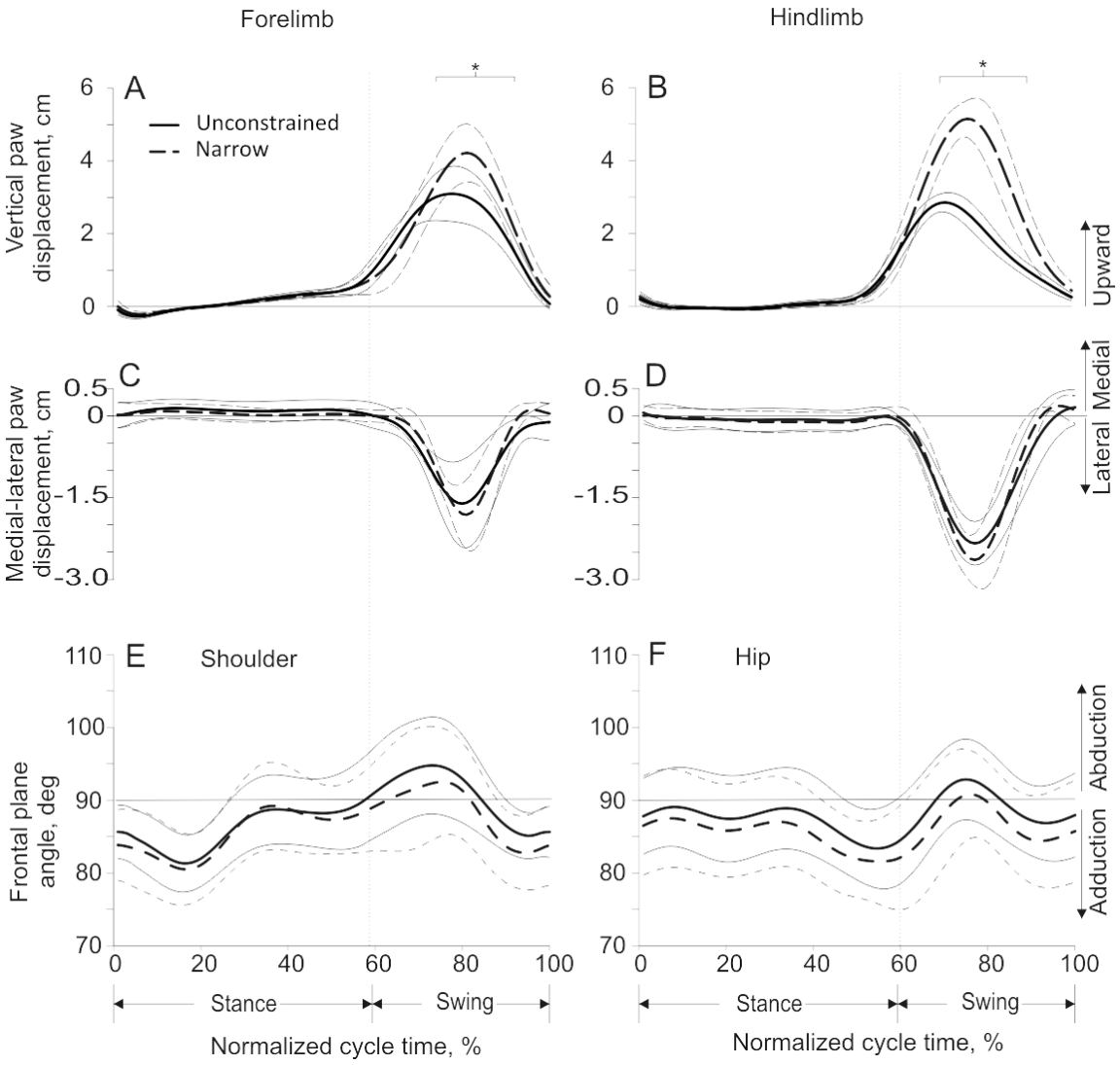

Figure 3.7 Limb Kinematics. A, B) Vertical displacement of the digit center of mass for the fore and hind digits, respectively. C, D) Medial-lateral displacement of the digit center of mass for the fore and hind digits, respectively. E, F) Frontal plane angles (as defined in figure-1) of the shoulder and hip, respectively. All values shown are means (bold line) $\pm$ 1 standard deviation. Unconstrained is solid line and narrow dashed line.

narrow and unconstrained walking ($p>0.05$). The medial-lateral forces applied to fore- and hindlimbs during both narrow and unconstrained walking were relatively small (typically below 1% of body weight). Throughout most of the stance, this force was directed medially, which corresponded to exerting force by the limb on the ground in the lateral direction. The values of these forces were similar between narrow and unconstrained walking except during two short periods of the hindlimb stance ($p<0.05$; Fig. 3.6).

The patterns of shoulder and hip muscle moments in the frontal plane resembled the patterns of the vertical ground reaction forces (Fig. 3.6). Throughout the stance phase the moment direction was in abduction, which means that the resultant action of all muscles around the shoulder and the hip tended to abduct the limb in contact with the ground and thus move the body medially. No difference in the muscle moment magnitude was found between narrow and unconstrained walking ($p>0.05$, Fig. 3.6).

The shoulder and hip joints in the frontal plane fluctuated around 90 deg during the stride and did not have a large range of motion– the ranges were between 10 and 15 deg for both narrow and unconstrained walking ($p>0.05$, Fig. 3.7E, F). During most of stance of narrow and unconstrained walking, the hindlimbs were slightly adducted, and in the first half of swing the hindlimb was abducted. This pattern of frontal angles is consistent with hindlimb circumduction during swing which resulted in lateral displacement of hind paws up to about 2 cm (see Fig. 3.7D and (Misiaszek, 2006a)). Lateral displacements of forelimbs were slightly smaller (Fig. 3.7C). The later displacements of paws during swing seem necessary to avoid collisions with the contralateral limbs being in stance. Vertical paw displacements were higher in mid swing

during narrow compared to unconstrained walking, which was especially apparent for the hindlimbs ($p<0.05$; Fig. 3.7A, B). The higher lift of paws (especially hind paws) may have been related to the way stance width was constrained using triangular prisms (Fig. 3.1D) – in order to perform circumduction of the limb in this situation, the cat had to elevate the limb first to avoid collision with the prism. A higher elevation of hind paws compared to fore paws could have been needed to increase safety margin since hindlimbs are not under visual control.

3.3.2 Muscle activity during narrow walking

EMG activity from 11 hindlimb and 3 forelimb muscles was recorded in several cats during narrow and unconstrained walking. Hindlimb EMG patterns of narrow walking were qualitatively similar to those of unconstrained walking (see representative examples in Fig. 3.2A, B and references (Yakovenko *et al.*, 2002; Krouchev *et al.*, 2006; Markin *et al.*, 2012)). Specifically, muscles with stance related activity (SO, MG, LG, VM/VL, BFA, AM) were active during stance; two-joint rectus femoris (RF) and biceps femoris (BFP) muscles demonstrated their typical activity at the transition from swing to stance (burst BFP1, Figs. 3.2A, B; 3.8 A, B) and from stance to swing (RF had a much longer period of activity than the corresponding burst of BFP, BFP2, Fig. 3.2 A, B; 3.8 A, B); and swing related EMG activity occurred in flexors (TA, IP, SAM; Fig. 3.2, A, B). The EMG magnitude in many muscles was generally similar between narrow and unconstrained walking which may be expected given that most of the major hindlimb muscles has their primary functions, i.e. flexion-extension, in the sagittal plane. Some of the recorded muscles have however a substantial secondary function in the frontal plane,

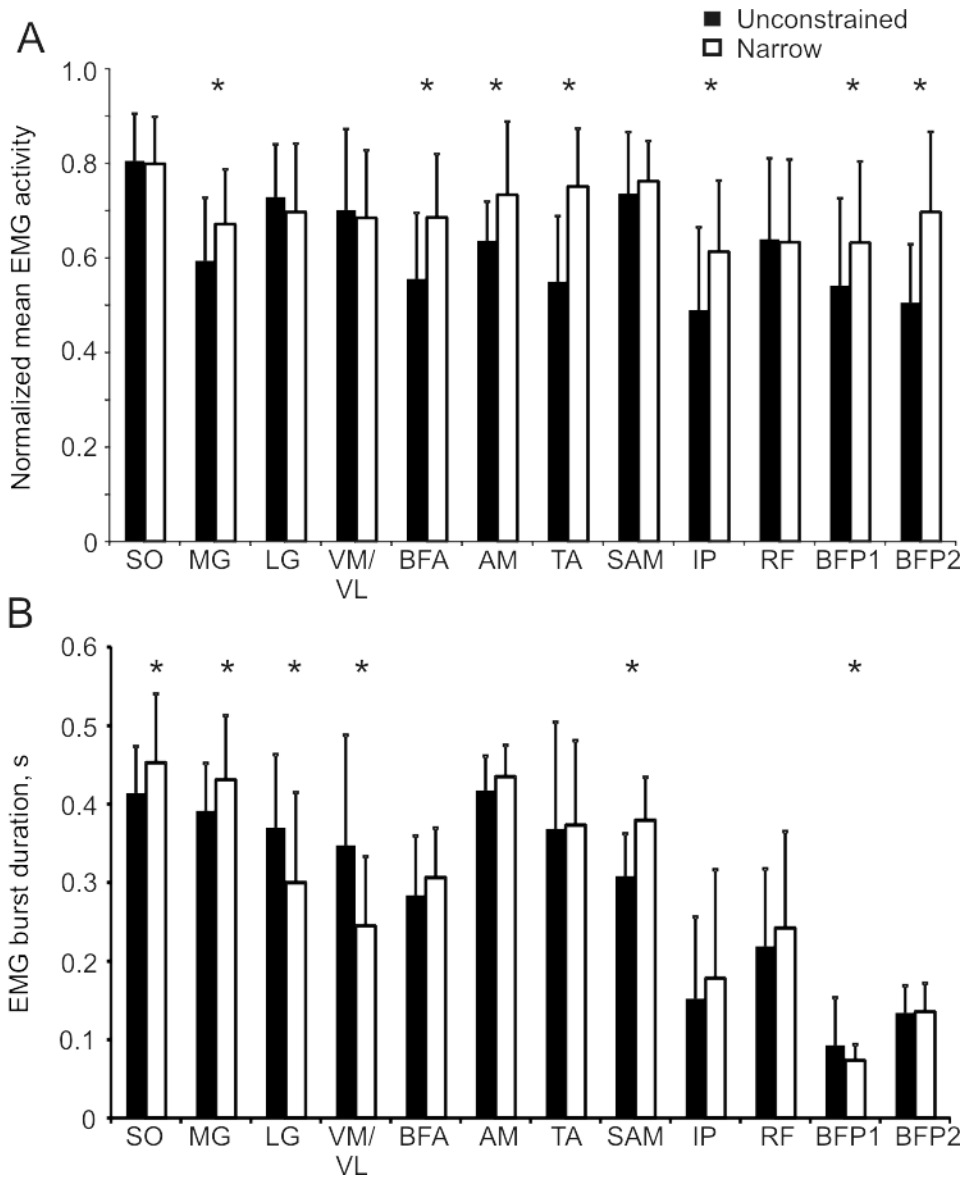

Figure 3.8 Normalized mean (±SD) EMG burst activity (A) and burst duration (B) for walking with unconstrained and narrow paws separation. Symbol * indicates statistically significant difference ($p<0.05$) between the two types of walking tasks. Data of 5 cats. Muscles: SO, soleus; MG, medial gastrocnemius; LG, lateral gastrocnemius; VM/VL, medial and lateral vastii; BFA, biceps femoris anterior; AM, adductor magnus; TA, tibialis anterior; SAM, sartorius medial; IP, iliopsoas; RF, rectus femoris; BFP1; burst of biceps femoris posterior at the swing to stance transition; BFP2, burst of biceps femoris posterior at the stance to swing transition.

i.e. adduction and abduction. The AM, for example, is a hip extensor and adductor; it was active during stance and its mean EMG activity was higher during narrow than unconstrained walking ($p<0.05$, Fig. 3.8A). The MG, ankle extensor and abductor, had produced higher activity during narrow walking and had a significant increase in EMG duration (Fig. 3.8A, B). The SO, ankle extensor, demonstrated longer burst duration during narrow walking ($p<0.05$, Fig. 3.8B). The SO is a postural muscle, which is highly active during standing and walking (Walmsley *et al.*, 1978; Hodgson, 1983). The LG, ankle extensor, had a significant decrease in burst duration ($p<0.05$; Fig 3.8 B). The flexors TA and IP and two bursts of BFP (BF1 and BFP2) had a greater activity during narrow walking ($p<0.05$; Fig. 3.8 A) with BFP1 having a significant decrease in duration ($p<0.05$, Fig 3.8 B). The burst duration of the extensors VM/VL was shorter in narrow than in unconstrained walking ($p<0.05$, Fig. 3.8 B) and the burst activity of BFA, hip extensor, had an increase in activity ($p < 0.05$; Fig 3.8 A). The burst duration of SAM, hip and knee flexor, was significantly longer during narrow walking ($p<0.5$; Fig 3.8 B).

3.3.3 Cortical activity

The activity of 116 neurons (including 85 PTNs) recorded from the forelimb representation in the motor cortex of 4 cats (2 males and 2 females, Table 3.1) was recorded during narrow and unconstrained locomotion. The activity of 84% (97/116) of neurons was different between the two tasks. In 36% of cells the average discharge rate was higher on the narrow pathway (by 11±2 imp/s, mean ± SEM; $p<0.05$, t-test), whereas in the other 25% of them it was lower (by 7±1 imp/sec). The activity of 92% (107/116) of neurons was stride-related during both tasks: it was higher in one phase of the stride and

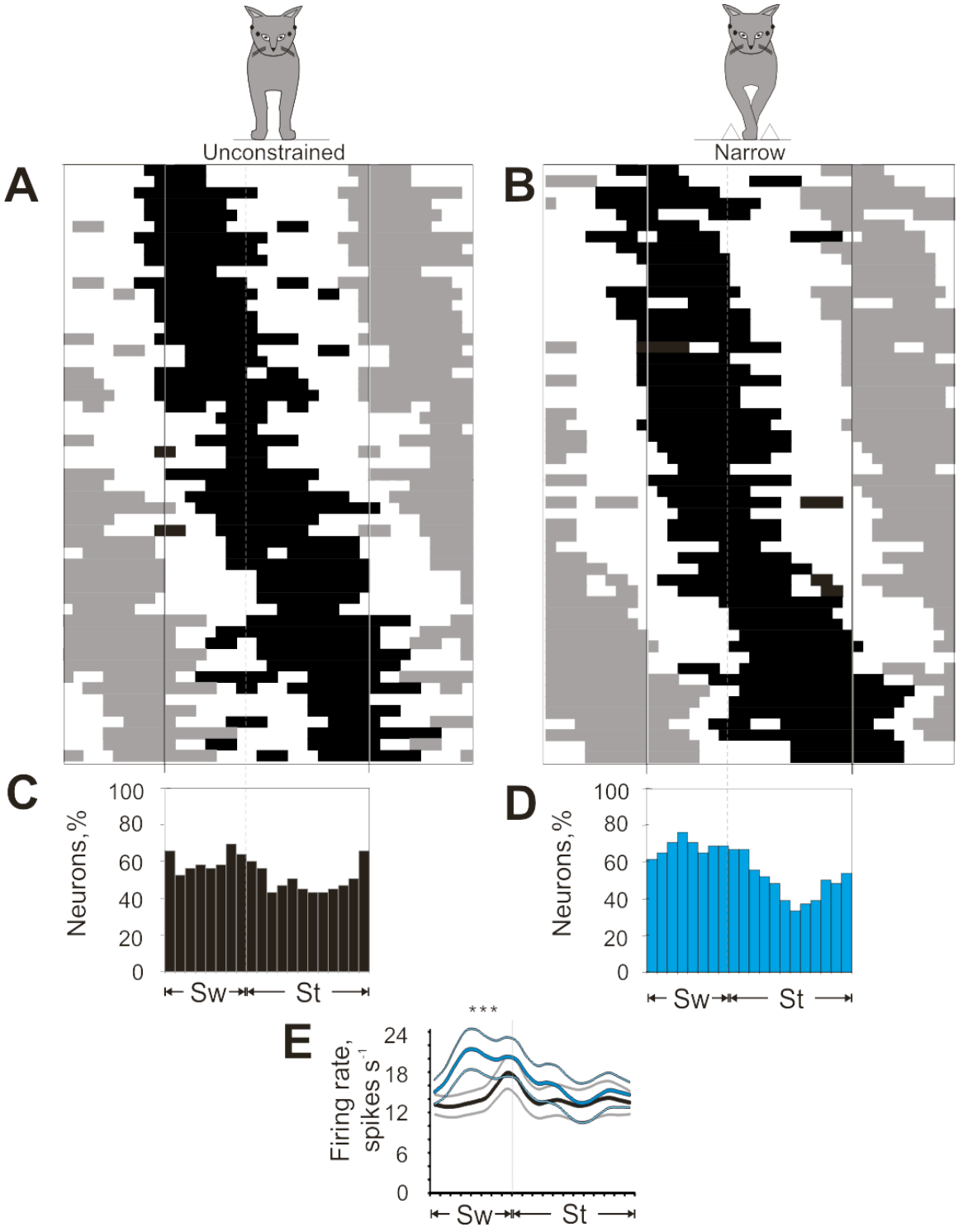

Figure 3.9 Population characteristics of neurons during locomotion with unconstrained (A, C) and narrow (D, D) paw separation from a representative cat. A) and B) Phase distribution of periods of elevated firings (PEFs). C, D) Proportion of active neurons (neurons in their PEFs) in different phases of the stride cycle during locomotion. E) Mean discharge rate (± standard error of mean) during locomotion. Sw, swing; St, stance.

lower in the other phase. The depth of frequency modulation, however, was different between the two tasks in 45% of neurons: on the narrow pathway, it was higher in 20% of cells (by 81±14%) and lower in 25% of other cells (by 35±3%). In addition, in 23% of neurons duration of firing was different and more often longer (by ~30% of the cycle) on the narrow pathway. Also, 15% (17/116) of neurons discharged in different phases during the tasks, with more cells firing later in the cycle (by 20-30% of the cycle) on the narrow pathway compared to unconstrained walking. Overall the average discharge rate in bins 4, 5, and 6 of were statistically higher for narrow walking compared to unconstrained walking (Fig 3.9C, D).

3.4 Discussion

The goal of this study was to compare full-body mechanics, hindlimb muscle activity and activity of neurons from the right forelimb representation in the primary motor cortex between unconstrained walking and walking on a narrow path in the cat. Simultaneously imposing accuracy and stability demands in the frontal plane by reducing width of walking path to 5 cm was expected to lead to a greater modulation of motor cortex activity indicating the greater involvement of the primary motor cortex. Although the observed modulation of cortical activity in a large number of cells during narrow walking was greater than in walking with unconstrained separation of paws, it was relatively modest compared with accurate stepping (Beloozerova & Siorta, 1993; Armstrong & Marple-Horvat, 1996; Drew *et al.*, 2002; Beloozerova *et al.*, 2010) and my expectations. Before proposing possible explanations for these results, I will first discuss the validity and limitations of the experimental procedures.

3.4.1 Frontal and sagittal plane mechanics and muscle activity during narrow and unconstrained cat locomotion

Overall, the stride kinematic parameters; linear displacements of paws, head and CoM; frontal plane hip angles; and ground reaction forces during unconstrained walking and walking on a narrow path obtained in this study (Table 3.2, Figs. 3.5-3.7) were consistent with the previous reports (Manter, 1938; Griffin *et al.*, 2004; Prilutsky *et al.*, 2005; Misiaszek, 2006a; Beloozerova *et al.*, 2010; Galvez-Lopez *et al.*, 2011; Prilutsky & Klishko, 2011), Specifically, fore and hind paw vertical displacements during swing were higher during narrow walking (Fig. 3.7 A, B); the shoulder and hip frontal plane angles changed from being adducted in early stance to being abducted in early swing (Fig. 3.7 E, F); and fore- and hindlimbs underwent lateral circumduction in swing (Fig. 3.7 C, D; see also (Misiaszek, 2006a)). The CoM displacement, velocity (Fig. 3.5) and acceleration (not shown; see ground reaction forces Fig 3.6) during unconstrained and narrow walking demonstrated patterns typical for quadrupedal gait (Manter, 1938; Griffin *et al.*, 2004; Prilutsky *et al.*, 2005). The fore- and hindlimbs applied force to ground laterally during stance, so the ground reaction force applied to the paws was directed medially (Fig. 3.6, see also (Manter, 1938; Griffin *et al.*, 2004)). Forelimb forces were larger than hindlimb forces (Fig. 3.6; see also (Manter, 1938; Griffin *et al.*, 2004; Prilutsky *et al.*, 2005; Prilutsky & Klishko, 2011) because the CoM is shifted more rostral due to the head and neck segments (Gray, 1968) and possibly because the forelimbs have to stop downward movement of the CoM during stride phases 1 and 5 to prevent fall of the cat forward when it dynamically unstable in phases 4 and 8 (see below and Figs. 3.3, 3.4, 3.5D, 3.6). The directions and distribution of ground reaction forces between fore- and hindlimbs

during stance of walking was similar to those during quiet standing in the cat (Fung & Macpherson, 1995).

The majority of studied kinematic and kinetic variables did not differ significantly between narrow and unconstrained walking except hindlimb stance width and fore- and hindlimb swing height (Table 3.2, Fig. 3.7A, B), as well as orientation and vertical position of the head and neck (Fig. 3.5E, F). In agreement with the previous report on head position during precise stepping (Beloozerova *et al.*, 2010), the head and neck were rotated toward ground more during narrow walking than during walking with unconstrained separation of paws (by 6-8^{o}, Fig. 3.5 E); as a result the vertical position of the head-neck segment was lower by about 1.5 cm during narrow walking (Fig. 3.5F). On the other hand, there was no difference in the vertical position of the CoM between narrow and unconstrained walking (Fig. 3.5B), whereas the CoM vertical position is lower during horizontal ladder walking (Beloozerova *et al.*, 2010). The partial similarity of these results with the previous report on horizontal ladder walking (i.e., lowering the head presumably for improving visibility of target for foot placement) suggests that narrow walking imposes certain demands on accuracy of paw placement. However, narrow walking seems less demanding in terms of accuracy than horizontal 5-cm ladder walking given that the vertical position of the CoM is the same for both narrow and unconstrained walking. Another difference in kinematics between narrow and unconstrained walking was the swing height (Fig. 3.7A, B). The greater swing height in narrow walking is likely related to the way in which the narrow path was constrained by triangular prisms (Fig. 3.1D). In order to circumduct the limb laterally during swing without touching the prisms, the cat must raise the paw above the prism height (1.7 cm)

before moving paw laterally (Fig. 3.7A, B). The hind paws were raised higher than fore paws (Fig. 3.7B) possibly because the animal could rely only on proprioception and motor memory to determine position of the hind paws with respect to the prism, and raising them higher could provide a greater safety margin for clearing the prism.

The ab/adduction muscle moments in the frontal plane at the hip and shoulder during stance of narrow walking were calculated for the first time to my knowledge and thus cannot be compared with previously published data. Both narrow and unconstrained moments indicated abduction throughout stance (Fig. 3.6) demonstrating that the resultant action of all muscles around the hip and shoulder joints was to abduct the fore- and hindlimb. The muscle moment directions during stance phase were in agreement with changes in the frontal shoulder and hip angles from adduction to abduction in stance (Fig. 3.7E, F).

The action of major hindlimb muscles is mostly constrained to the sagittal plane (Bunderson *et al.*, 2010) except small ankle everters and inverters (Young *et al.*, 1993; Bunderson *et al.*, 2010). Nevertheless, several large muscles such as BFA (Figs. 3.2A, B; 3.8A, B), gluteus maximus, medius and minimus and tensor fascia lata (Misiaszek, 2006a; Bolton & Misiaszek, 2009) are active during stance and produce the abduction moment at the hip and the lateral hindlimb endpoint force (Bunderson *et al.*, 2010). Several adductors such as AM (Fig. 3.8A, B), adductor femoris are gracilis (Misiaszek, 2006a) and anterior semimembranosus (Smith *et al.*, 1998) are co-active with abductors during stance, but their contribution to the moment in the frontal plane is smaller than that of the abductors (Fig. 3.6). The mean magnitude and duration of EMG bursts of hindlimb muscles had several differences between narrow and unconstrained walking

(Fig. 3.8A, B). EMG of flexors typically had a higher mean EMG (see BFP1, BFP2, IP, TA; Fig 3.8A) with some changes in burst duration during narrow walking (see BFP1, SAM; Fig. 3.8B), which was consistent with the higher paw trajectory during this task (Fig. 3.7A, B). Therefore the increased flexor activity may suggest that there is increased excitability in the flexor synergy.

3.4.2 Static and dynamic stability during narrow and unconstrained walking

The mechanical analysis of narrow and unconstrained walking revealed that walking on a narrow path 5-cm in width was in many respects similar to unconstrained walking. Despite the smaller distances between left and right paws in stance of narrow walking (Table 3.2), other mechanical variables and stride parameters were similar (see previous section and Figs. 3.3, 3.5, 3.6, 3.7C-F, Table 3.2). This was also true for the maximum and minimum values of the IDS characterizing dynamic stability (Table 3.2) and for patterns and values of static stability (ISS) and frontal (IDS_f) and sagittal (IDS_s) components of dynamic stability (Fig. 3.4). During both types of walking the CoM was either inside the base of support (the ISS was positive while 3 limbs were supporting the body in cycle phases 1, 3, 5, 7; Figs. 3.3 and 3.4) or on the border of the base of support (ISS was not different from zero during double support phases 2, 4, 6 and 8; Figs 3.3 and 3.4). As expected the index of static stability was closely related to the base of support area, the latter being larger when 3 legs were supporting the body (Fig. 3.4). Although there was no statistically significant difference in static and dynamic stability indices between narrow and unconstrained walking, there was a trend of greater static and dynamic stability during unconstrained walking as demonstrated in Fig. 3.4 and Results section 3.3. Overall, the two investigated walking tasks appear to have similar frontal

stability demands, which might explain why decreases in vertical position of the CoM were not observed during narrow walking (Fig. 3.5B) (a compensatory motor strategy to increase body stability (Bolton & Misiaszek, 2009; Beloozerova *et al.*, 2010; Galvez-Lopez *et al.*, 2011)).

Although in both tasks, the CoM was inside or on the border of the base of support and the cats were dynamically stable in the frontal plane, the cats demonstrated substantial dynamic instability in the direction of propulsion (during fore- and hindlimb double support phases 4 and 8, Fig. 3.4) due to influence of forward velocity of the CoM $\mathbf{v}_{CoM}$ (see eq. 2.5). To prevent fall forward, the cat makes a forward step by the forelimb being in swing (see phases 5 and 1, Fig. 3.3). If the animal is suddenly pushed forward during this phase of dynamic instability, corrective postural responses are expected to be much more vigorous compared to perturbations in other directions. If a perturbation is such that the extrapolated CoM position (XCoM) is beyond the reach of the paw placement, the animal will lose balance (Hof, 2008) and be forced to take additional steps. Human experiments seem to support this conclusion (e.g. (Bolton *et al.*, 2012)).

3.4.3 Contribution of the primary motor cortex in control of walking on narrow paths

My hypothesis was that walking on narrow paths would require a greater involvement of the primary motor cortex than during precise stepping on horizontal ladder (Beloozerova *et al.*, 2010) or postural corrections after perturbations in the frontal plane (Beloozerova *et al.*, 2006; Karayannidou *et al.*, 2008) due to anticipated additive influences of accuracy and stability demands in the frontal plane. The hypothesis was not supported, as changes in the modulation of neuronal activity during narrow walking were

small (3 out of 20 bins) compared to unconstrained walking. As evident from the previous discussion, this result can be explained by the fact that narrow walking does not significantly alter stability demands in the frontal plane, and stepping on a narrow 5-cm path in the sagittal plane appears to be less demanding an accuracy task than stepping on a horizontal ladder with 5-cm rungs in the frontal plane (Beloozerova *et al.*, 2010). The ability of cats to walk on narrow paths is superior to that of other terrestrial animals like rats (Schmidt & Fischer, 2010), dogs (Galvez-Lopez *et al.*, 2011) or humans (Shkuratova & Taylor, 2008; Dunlap *et al.*, 2012) and close to arboreal animals (Lammers & Biknevicius, 2004; Stevens, 2006) and therefore challenging cats in the frontal plane may require a further decreased base of support.

The activity changes in opposite directions seen across neurons (some increase, some decrease) do substantiate the fact that not all neurons are responsible for control of one mechanical variable, and individual neurons or groups of neurons may coordinate different tasks. For instance, some neurons may be responsible for the increase swing height (due to activation of flexor synergy), while some may be responsible for inhibition of an extensor synergy or for visuomotor coordination. One limitation to this study is that the ability to determine exactly what the activity of a single cortical neuron or a group of neurons is encoding is not currently available, thus only speculative suggestions can be made.

3.4.4 Conclusion

The goal of this study was to compare full-body mechanics, muscle electromyographic (EMG) activity and activity of neurons from the right forelimb representation of the primary motor cortex between unconstrained walking and walking

on a narrow path of 5 cm in the cat. The hypothesis that activity of the primary motor cortex would be much greater during narrow walking because of imposed requirements on lateral stability and accurate paw placement was tested. Dynamic stability was measured in the lateral and rostral-caudal directions using the extrapolated center of mass position with respect to the boundaries of support (Hof *et al.*, 2005; Hof, 2008) in cats performing unconstrained and narrow walking. Contrary to expectations, lateral dynamic stability of the body was similar between unconstrained and narrow walking. Generally similar frontal and sagittal plane mechanics of the two locomotion tasks were consistent with small differences in myoelectric activity of major hindlimb muscles. The activity of 116 neurons from the right forelimb representation of the motor cortex, recorded during narrow and unconstrained walking, was in most cases higher during narrow compared to unconstrained walking, thus narrow walking may impose additional demands on accuracy of stepping in frontal plane and not on lateral stability.

CHAPTER 4

PORE SIZE, IMPLANTATION TIME AND NANO-SURFACE PROPERTIES INFLUENCE RAT SKIN INGROWTH INTO PERCUTANEOUS POROUS TITANIUM IMPLANTS

4.1 Introduction

Percutaneous devices allowing access into the body's internal environment for drug delivery, internal monitoring, and external prosthesis attachment have one main problem: the skin-implant interface does not completely isolate the internal environment and permits external pathogens inside the body. At present there is no known artificial material with which skin will readily integrate and effectively seal the exit site of protruding devices. Lack of complete skin integration with the device permits various pathogens inside the body, which may cause infection (von Recum & Park, 1981; Donlan, 2001; Peramo & Marcelo, 2010). Infection can occur in all types of percutaneous devices including central venous catheters, endotracheal tubes, external fixators and bone-anchored external prostheses. The severity of infection for percutaneous devices depends on the amount of infectious agent present at the interface and time since implantation (von Recum, 1984; Donlan, 2001).

Many biomaterials have been evaluated for skin integration using histological analyses. Previous results on the use of polymers (Feldman & von Recum, 1985; Krouskop *et al.*, 1988; Schreuders *et al.*, 1988; Jansen *et al.*, 1990; Knowles *et al.*, 2005; Fukano *et al.*, 2010; Underwood *et al.*, 2011), tantalum (Stynes *et al.*, 2008; Chou *et al.*, 2010), titanium (Jansen *et al.*, 1990; Pitkin *et al.*, 2006; Pitkin *et al.*, 2007b; Perry *et al.*,

2009; Pitkin *et al.*, 2009), ceramics (Davis *et al.*, 1972) and other materials have not demonstrated sufficient integration with the skin to prevent bacterial penetration. Of the biomaterials available, titanium has excellent biocompatibility, readily integrates with bony structures and is frequently used in percutaneous applications (Brånemark & Albrektsson, 1982; Branemark, 1983; Tjellström *et al.*, 1983; Jansen *et al.*, 1990; Jansen *et al.*, 1994; Bonding, 2000; Snik *et al.*, 2005; Pitkin *et al.*, 2006; Pitkin *et al.*, 2007b; Hagberg & Brånemark, 2009; Perry *et al.*, 2009; Pitkin *et al.*, 2009; Jeyapalina *et al.*, 2012).

Titanium implant internal structure and surface treatments may influence skin attachment, ingrowth and overall integration of the implant. Previous research using porous titanium implants has demonstrated the potential for the skin cells to distribute throughout the porous titanium and maintain sustainable metabolism inside the implant (Pitkin *et al.*, 2006; Pitkin *et al.*, 2007b; Pitkin *et al.*, 2009; Isackson *et al.*, 2011; Jeyapalina *et al.*, 2012). Quality of skin integration with porous titanium depends on such factors as pore size, nano scale implant surface topography, and duration of implantation. Porosity influences transportation of nutrients and removal of cellular debris and toxins (Winter, 1974; von Recum & Park, 1981). Nano-textured titanium surface can improve cellular adhesion and increase keratinocyte proliferation and cell spreading compared to machine finished surfaces (Chehroudi & Brunette, 2002; Puckett *et al.*, 2010). The decrease in implant surface hardness by the nanotubular surface treatment may also make the nanotube surface layer a promising intermediate structure for the implant-skin interface. Investigations of skin interface with percutaneous porous titanium implants

have started only recently and therefore there is insufficient information about the effects of the factors discussed above on the quality of skin-implant integration.

The goal of this study was to investigate the effects of pore size, nanotubular surface treatment and duration of implantation on skin ingrowth into porous titanium. I hypothesized that (1) implants with larger pores (100 – 160 mm) would demonstrate more skin ingrowth compared to implants with smaller pores (40-100 μm), (2) nanotubular treatment would increase ingrowth over non-treated implants and (3) a longer time period before implant removal would result in greater skin ingrowth. Preliminary results of this study have been published in abstract form (Farrell *et al.*, 2012b).

4.2 Materials and Methods

4.2.1. Implants

Porous titanium rods (0.3 cm diameter x 2 cm length; Poly-Ortho International, MA, USA; Ti-6Al-4V) with and without nanotubular surface modifications (see below for description; Fig. 4.1A, B) were used in the experiments. The manufacturing process for the skin and bone integrated pylon of cylindrical shape (SBIP-2) has been described in detail elsewhere (Pitkin *et al.*, 2009; Pitkin & Raykhtsaum, 2012). Briefly, commercially available pure titanium (Ti) sponge powder was filled and compacted on a vibrating table inside a graphite mold with a 3-mm-round channel. Three thin (0.5-mm diameter) titanium wires were inserted inside the graphite mold before the 4-hour sintering cycle performed in a Vacuum Industries Super VII furnace (Centorr Vacuum Industries Inc; Nashua, NH, USA) under vacuum and high temperature. The sintered rods were examined for desired porosity using a scanning microscope and then cut into 2-cm

long pylons. Figure 4.1A demonstrates a porous titanium rod used in the study and a diagram of a rod cross-section with 3 thin titanium wires. Porous titanium rods of two pore sizes were studied: Small, 40-100 μm, and Large, 100-160μm, with porosity ranging from 35% - 50% (Pitkin *et al.*, 2009). Nanotubular surface treatment was performed on a select group of small pore implants (Fig. 4.1 C-D). Nanotubular surfacing was accomplished through electron beam evaporation where the nano-tube size is predominately determined by the anodization voltage, electrolyte composition, and pH (Ruckh *et al.*, 2009). The fabricated nanotubular

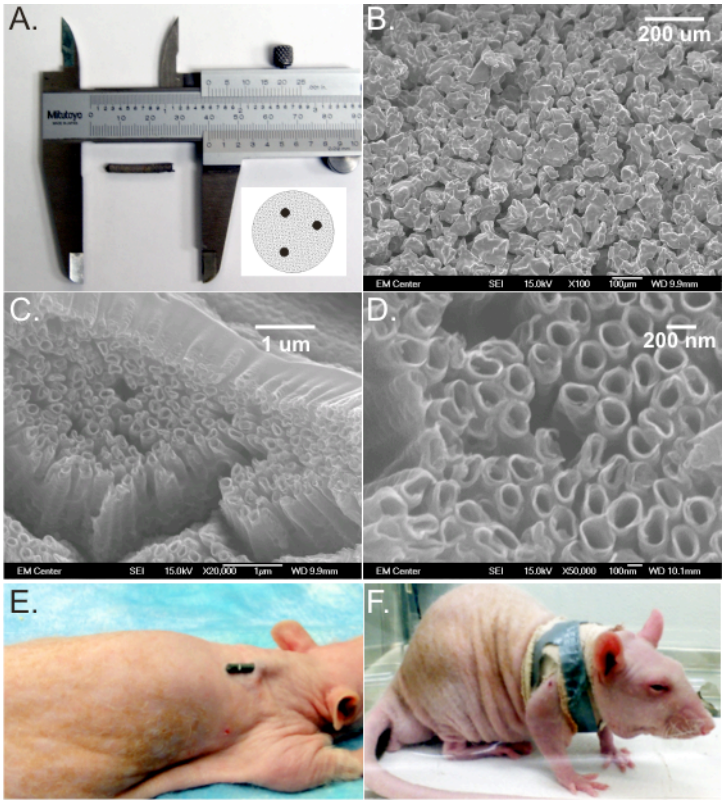

Figure 4.1 Implants and implantation method. A) An example of implant used in experiments; the insert shows a diagram of an implant cross-section with 3 thin titanium reinforcing wires. B) Scanning electron micrograph (SEM) of small pore implant without nanotube addition (100x Magnification). C) SEM of small pore implant with nanotube addition (20,000x Magnification). D) Detailed SEM of nanotube surface structures (50,000x Magnification). E, F) Illustration of implant location and orientation in the back of an anesthetized rat and how implant was secured.

surfaces had pore diameters ranging from 50 to 250 nm. Mechanical tests revealed the hardness of the nanotube layer to be in the range of 1.5-2.0 GPa compared to 2.0-2.5 GPa for solid titanium.

Several 0.3 cm diameter x 2.5 cm length solid titanium implants were used for comparison.

4.2.2 Animals and study design

Two groups of adult rats (at least 6 weeks old, (mass 210 -- 519 g) were used for implantations of porous implants: 25 CD Hairless rats and 10 Sprague Dawley (SD) rats (Charles River, Wilmington, MA, USA). (The two different rat species were used in the study due to the inability of the supplier to provide the sufficient number of CD hairless rats at the time of the study; see description of rat-difference related results and discussion in sections 3.2.4 and 4.3.) The CD Hairless rats were randomly assigned into groups corresponding to 3 types of implanted pylons (Small, implanted with small pore pylons; Large, implanted with larger pore pylons; and Nano, implanted with small pore pylons with nanotubular surface treatment) and 2 periods of implantation (3 or 6 weeks). The Sprague Dawley rats were randomly assigned into 2 groups: Small and Nano; these groups of rats were implanted for 6 weeks. Five Sprague Dawley rats were also implanted with solid titanium implants as a control group, as solid implants are currently used for attachment of osseointegrated prostheses (Hagberg & Brånemark, 2009). Table 4.1 summarizes study design. All animal procedures were in accordance with the US Public Health Service Policy on Humane Care and Use of Laboratory Animals and approved by the Institutional Animal Care and Use Committee of Georgia Institute of Technology.

Table 4.1 Study design and experimental groups. Small group designates animals implanted with pylons of small pore size (40-100 μm). Large group, animals implanted with pylons of large pore size (100 – 160 μm). Nano group, animals implanted with small pore implants containing a nanotubular surface treatment.

Groups	Rat type	3 Weeks	6 Weeks	Total
Solid	SD	5		5
Small	CD Hairless	5	5	10
Small	SD		5	5
Large	CD Hairless	5	5	10
Nano	CD Hairless	5		5
Nano	SD		5	5

4.2.3 Implantation Surgery

Implants were thoroughly washed and autoclaved prior to surgery. Rats were sedated and maintained throughout surgery using isoflurane, 1-3%. The surgical skin area was shaved and scrubbed 3 times with chlrohexidine followed by gauze soaked in isopropyl alcohol. After preparation of the skin surgical area, the rat was moved to a heated surgical table and covered with a sterile drape with an opening over the area of device implantation on the rat back. A skin incision was made in the midline between the scapulae using an appropriate sized biopsy punch. A sterile implant was then inserted into the incision parallel to skin surface leaving approximately 3-5 mm of implant exposed (Fig. 4.1E). The initial exposed length was measured using calipers. The incision and implant was then secured with several drops of 3M Vetbond tissue adhesive (n-butyl cyanoacrylate; 3M, St. Paul, MN, USA). After allowing time for the adhesive to setup, a

sterile piece of gauze was placed over the implant for bandaging. The bandage consisted of a single layer of 2.54 cm wide elastic tape (Elastikon, Johnson & Johnson, New Brunswick, NJ, USA) wrapped in "X" pattern around the forelimbs and chest as shown in Fig. 4.1F followed by a reinforcing strip of cloth-backed tape (Polyken, Evansville, IN, USA). The rats were then moved to a separate warm cage for recovery and monitoring and maintained in a 12/12 light/dark cycle with *ad libitum* access to food and water.

Bandages were changed at least weekly during measurements of external implant length and rat mass while the animal was anaesthetized with isoflurane, 1-3%. The criteria for terminating the experiment were either the animal reaching the specified implantation time (i.e., 3 or 6 weeks, Table 4.1) or implant exposed length exceeded 1.5 cm, which corresponded to less than 5 mm of implant beneath the skin. At the terminal experiment, rats were euthanized by carbon dioxide asphyxiation and the implant with skin surrounding the skin-implant interface (at least 1-cm in diameter) was carefully removed with a sharp scalpel. The implant with skin was placed in 10% buffered formalin for subsequent histological analysis.

4.2.4. Histological analysis

After fixation in formalin, samples were infiltrated and embedded in methylmethacrylate blocks, sectioned along the long axis of implant as shown in Fig. 4.2A using the Exakt System (EXAKT Technologies, Inc., Oklahoma City, OK), and polished. Sections were stained with either haematoxylin and eosin or haematoxylin and basic fuchsin. The entire slide was scanned at high resolution (40x magnification) for image analysis (Nanozoomer, Hamamatsu Corporation, Japan).

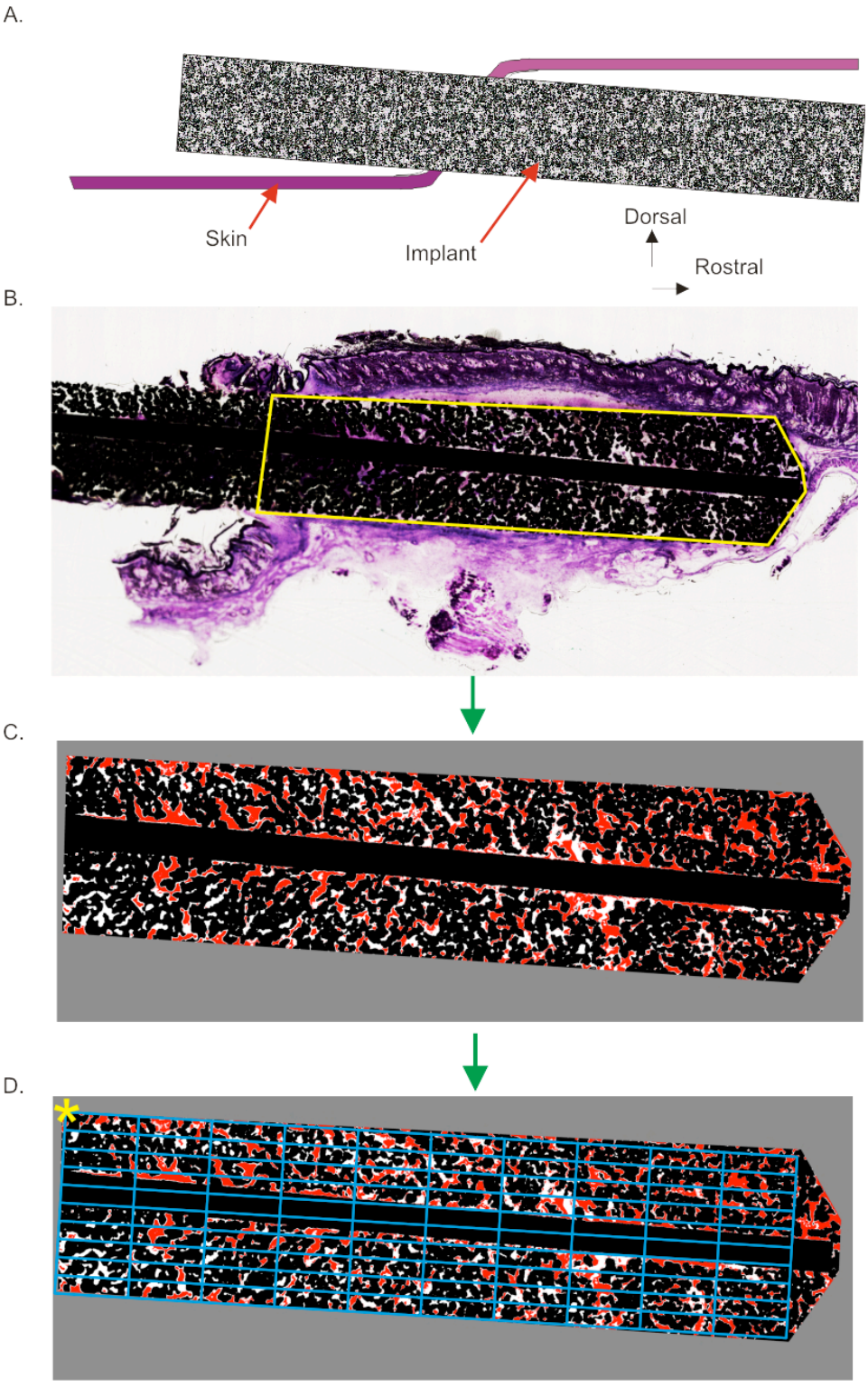

Figure 4.2 Implant image analysis steps. A) Cartoon illustrating a longitudinal cross-section through the skin and implant. B-D) Image processing steps. B) Implant outline identified for histomorphometry. C) Resulting image after thresholding. Black regions are implant metal, red tissue and white empty space. D) Area bin definition for binned implant area. Asterisk indicates corner of bin1,1

4.2.5. Image analyses

Skin ingrowth area and fraction of implant pores filled with skin tissue were determined using a custom Matlab (MathWorks, Natick, MA, USA) program. The region of interest (e.g., the subdermal implant from the outer edge of the epidermis to the deepest portion of the implant, Fig. 4.2B) was extracted from the larger scanned image at full resolution. The gross edges of the implant were identified. The line separating the internal and external portions of the implant was determined using the outer edges of the epidermis as reference (Fig. 4.2B, area marked by yellow line). The tissue, implant metal and empty pore areas in the image were determined via brightness thresholds. The threshold values were determined using the program ImageJ (Schneider *et al.*, 2012) based on visual inspection of regions from several different implants. Pixels were identified as implant metal if all the red, green, and blue (RGB) values of the RGB color model were less than 30/255 (< 12%). The image was then converted to hue, saturation, and value (HSV) components to identify the tissue regions. Pixels were determined to be tissue if: hue, H > 190/255 (75%); saturation, S > 28/255 (11%); and value, V > 70/255 (27%). The remaining areas of the image were set to be empty space (Fig. 4.2C). Using the identified threshold values, a custom image analysis algorithm was written to process the image in blocks of 1000x1000 pixels. The image was then binned into regions for each 10% of the implant subdermal length and width (Fig. 4.2D) by creating an appropriately sized rectangle to fill the region. The calculated metrics of skin-implant integration included: total area of subdermal implant, metal area, area of empty pores, area of pores filled with skin tissue, and the percentage of pore area filled with skin tissue. The latter was determined as:

$$PoreFill\,[\%] = \frac{TissueArea}{(TissueArea + EmptyArea)} \cdot 100 \qquad \text{(eq. 4.1).}$$

If an image bin contained only implant metal (e.g., if the bin covered only a reinforcing wire), that bin was excluded from the analysis.

4.2.6. Statistical analysis

Statistical analysis was performed using STATISTICA 7.0 (StatSoft, Inc., Tulsa, OK). The effects of implant type and time duration after implantation on weekly extrusion length, total implant area beneath skin (Fig. 4.2C), binned implant areas, the area of skin ingrowth, and the fraction of pores filled with skin were determined using a two-way ANOVA (Implant: 3 levels and Duration: 2 levels) with Tukey post-hoc tests if significant effects were found. The effect of 3 implant types on the mean implant extrusion rate (total distance extruded divided by implantation time) was determined using a one-way ANOVA. The effect of skin hair (or rat species: CD Hairless rats vs. Sprague Dawley (SD) haired rats) on extrusion length and rate and on skin ingrowth was tested using t-Student tests for independent variables. For all analyses significance level was set to $p < 0.05$.

4.3 Results

Survival times for implants are shown in Table 4.2. Several implants were removed before the set time points because the extruded length reached the endpoint criterion. A single solid implant survived implantation for 3 weeks; the other solid implants were ether extruded by skin or removed by the rat. Only 1 of the 35 rats implanted with porous implants (2.9%) had to be removed from the study due to clinical signs of infection (e.g. (Torralba & Quismorio, 2009)). This rat was implanted with a

Table 4.2 Implant survival times. Total number of implants surviving through each week of the study

Implant type	1 Weeks	2 Weeks	3 Weeks	4 Weeks	5 Weeks	6 Weeks
Solid	1	1	1			
Small	15	15	15	10	9	9
Large	10	10	10	5	2	1
Nano	10	10	10	5	5	5

small pore size implant and was removed from the study at 4.5 weeks; initial signs of infection were first noted at 2 weeks (the cause of infection is unknown).

4.3.1 Qualitative analyses

All porous implants regardless of pore size or surface modification demonstrated signs of tissue ingrowth into the implant pores (Fig. 4.3). Formation of a fibrous capsule surrounding the subdermal part of the implant was noticed (Fig. 4.2B); it comprised of connective tissue, small vessels and fibroblasts. A serocellular crust composed of degenerated neutrophils and inflammatory debris was observed at the exit point of implant from skin (Fig. 4.3 and 4.4A). In many instances bacteria were found present in the external crust and surrounding external pores of the implant (Fig. 4.4A). Bacterial cultures were taken from the exterior surface surrounding 4 implants. The cultures noted *staph spp.* of varying resistance present on the skin. However no bacteria, except in one rat in which infection was noted (see above), were observed beneath skin (See Discussion 4.4.2). In general the epidermis appeared to be in close apposition to the implant. There was typically epidermal downgrowth that stopped a few millimeters below the level of the epidermis seen at the skin-implant interface, which was perhaps more exaggerated on

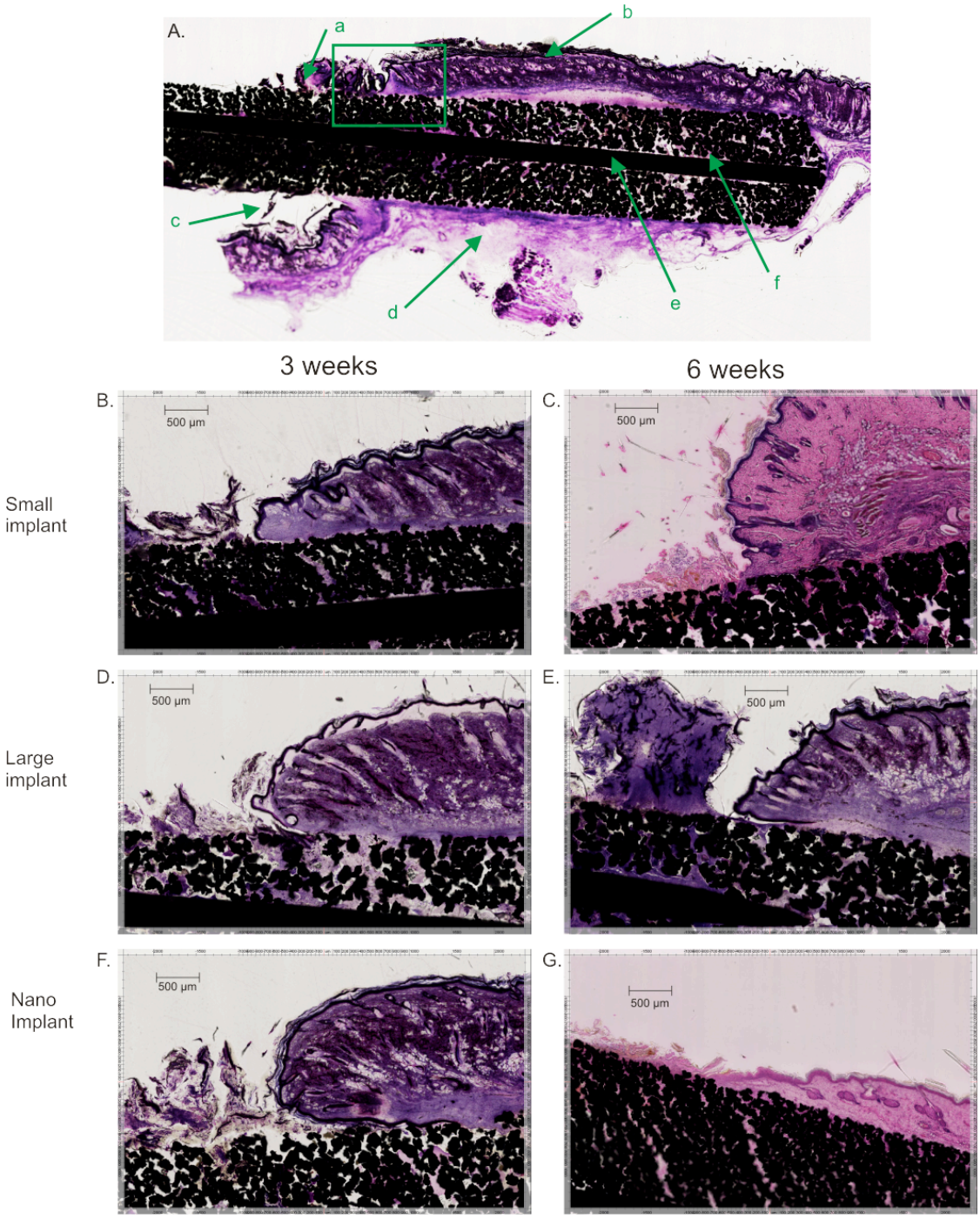

Figure 4.3 Examples of implant sections stained with haematoxylin and basic fuchsin. Top: Representative stained section through a porous implant. a) Serocellular crust on exterior side of implant. b) Skin on upper edge of implant. c) Pocket created by implantation method. d) Fibrous capsule surrounding implant. e) Central reinforcing wire. f) deep skin ingrowth into pores of implant. B-G) Examples of tissue ingrowth at the skin implant interface into representative implants and across different implantation durations (All magnifications are 2x).

the ventral side (underside) of the implant as a result of the implanted position (Fig 4.3A). This skin under the implant tended to form a pocket for tissue debris.

The implant pores were typically filled with fine fibrovascular tissue (Fig 4.3, 4.4B-D) that extended deep into the implant. Small caliber vessels were recognizable in only a few of the small pore implants, but were more pronounced in the large pore implants with survival times over 4 weeks (Fig. 4.4B). Inflammation was noted along the edges of the implants which when present tended to extend into the pores of the implant (Fig. 4.4C).

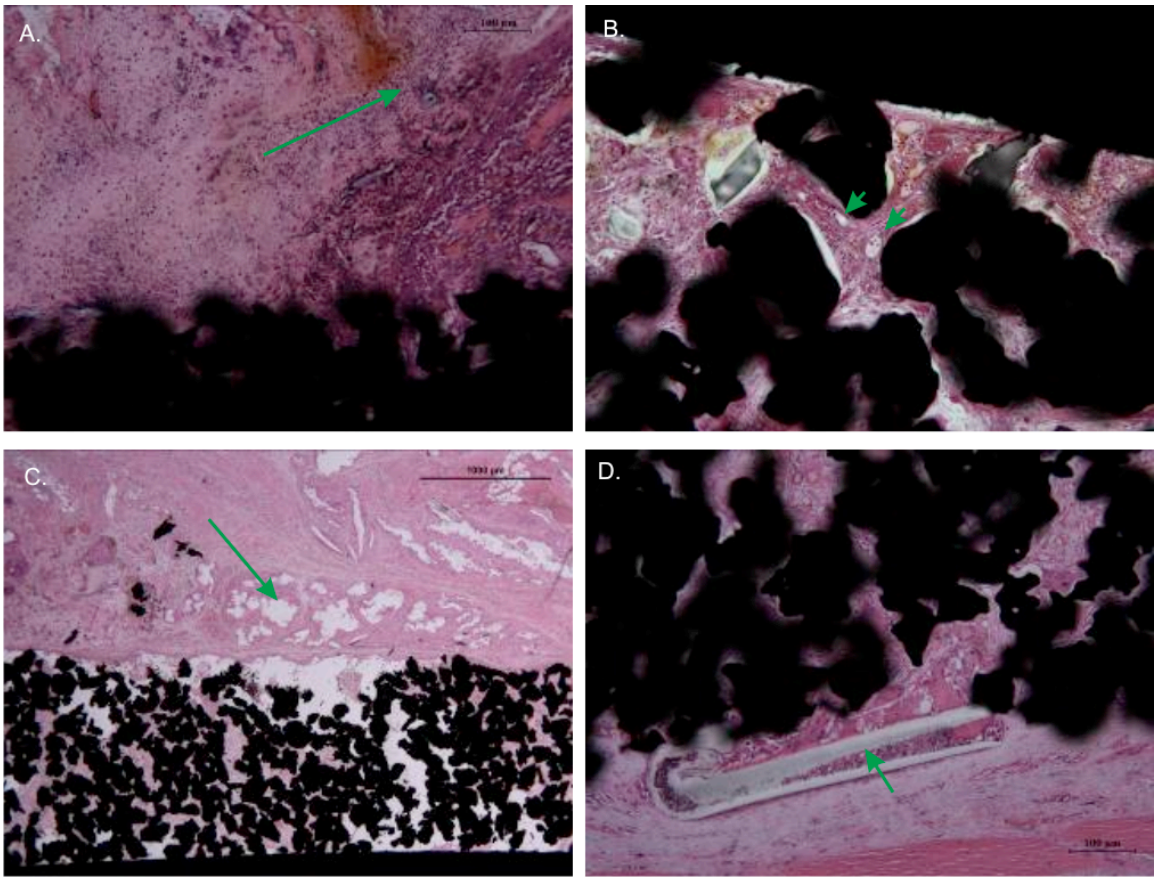

Figure 4.4 Representative histology sections. A) Serocellular crust on exterior implant (200x H-BF). Arrow indicates pocket of bacteria. B) Small caliber vessels in a large pore implant 4 weeks after implantation (200x H-BF). Arrows indicate vessels. C) Pockets of inflammation along edge of inflammation indicate by arrow (200x H-BF). D) Hair shaft near edge of implant indicated by arrow (200x H-BF).

4.3.2. Quantitative analysis

4.3.2.1. Implant extrusion length and rate

Mean implant extrusion length for small, large, and nano implant groups are shown in Fig. 4.5A. Extrusion length of a single solid implant over the course of 3 weeks is also shown for comparison. The Small, Large and Nano implants had similar extrusion lengths at week 3, after that time point the extrusion length of Small and Nano implants did not change substantially and remained below 4 mm, whereas the mean extrusion length of the large implant reached almost 1 cm by week 5 and then decreased to about 5 mm. Statistically, extrusion length was higher in the large implants at weeks 4 and 5 compared to the small implants ($F(10,132) = 4.5501$, $p < 0.05$). The mean extrusion rate for the large pore implants was also statistically higher ($F(2, 32) = 5.25$, $p< 0.05$) than that of the Small implants (Table 4.3). Extrusion rate showed no differences between Small and Nano or Large and Nano implant groups.

4.3.2.2 Percentage of implant pore area filled with skin tissue

The percentage of pore area filled with skin tissue for different implants and duration of implantation is shown in Fig. 4.5B. Statistical analysis revealed that implantation time was a significant factor for pore fill percentage (Fig. 4.5B, $F(1,31) = 23.16$, $p <0.05$). There was no significant difference in percentage of filled pore area between implant types. At 3 weeks in all types of implants at least 30% of pore area was filled with skin tissue; at 6 weeks, over 50%.

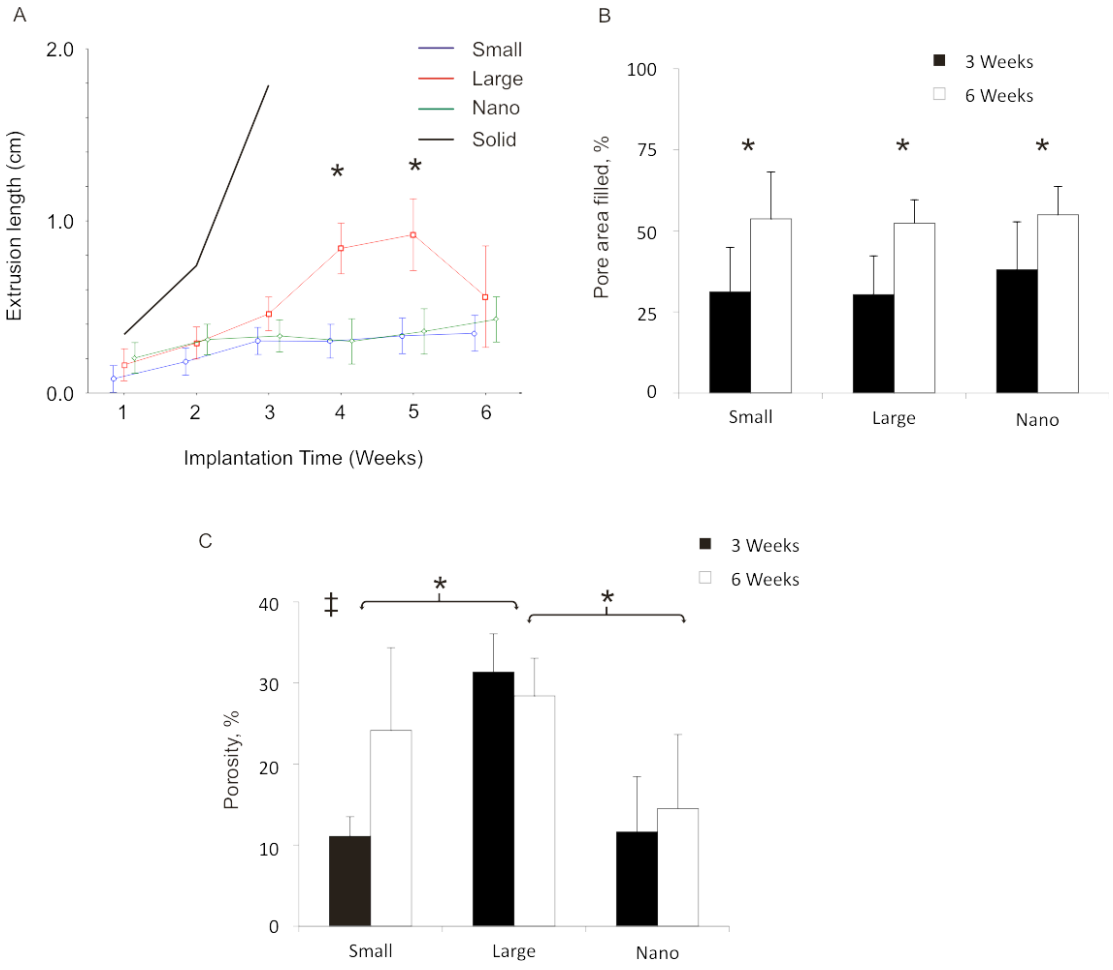

Figure 4.5 Quantitative analysis results. A) Extrusion length for each implant type over the course of the study. B) Percentage of total pore area filled with stained tissue. * Indicates a significant ($p < 0.05$) difference between 3 week and 6 week conditions. No differences were found between implants. C) Calculated porosity of the implants from the cross-section images. * indicate significant differences between large and small and large and nano groups ($p < 0.05$). ‡ indicates significant differences between small 3 week and 6 week implants. All panels show mean+SD.

Table 4.3 Mean extrusion rate for each group (in mm/week). * Significant difference between small and large groups ($p < 0.05$).

Implant type	Mean Extrusion Rate (mm/week)
Small	0.080 ± 0.050*
Large	0.161 ± 0.068
Nano	0.128 ± 0.067

4.3.2.3 Porosity of histological sections

The measured porosity of the implants in the histological sections is shown in Fig 5C. Measured porosity was variable and in many instances differed from the mathematical predicted porosity. For instance, the theoretical porosity was 30-50% yet the mean porosity for the small pore implants was 19.8 $\pm$ 10.5 %. As expected, porosity was significantly higher in the larger implants compared to the small pore and nano pore implants ($F(2, 28) = 12.790$ $p < 0.05$) (Fig 4.5C). However porosity of the small implants at 6 weeks tended to be greater than the porosity of the implants at 3 weeks. (See Discussion for details). The actual pore diameters were not measured in the histological sections.

4.3.2.4. Distribution of skin ingrowth within implant

The distribution of skin tissue inside porous implants of different types and implanted for different duration is presented in Fig. 4.6. The top row of bins in each panel represents pore area at the dorsal edge of implant right under the dermis. The left most column represents the bins that would line along the implant exit site; * indicates $bin_{1,1}$ (see Fig 4.2 D diagram for further details). Qualitatively, more skin ingrowth can be seen at the implant end opposite to the exit site irrespective of duration of implantation. On average, implantation of 6 weeks resulted in a greater percentage of skin ingrowth compared to 3 weeks in all types of implants. Statistical analysis showed that implantation time was the only significant factor affecting skin ingrowth ($F(1,3252) = 1093.5$, $p < 0.05$) and there was no significant effect of bin or implant.

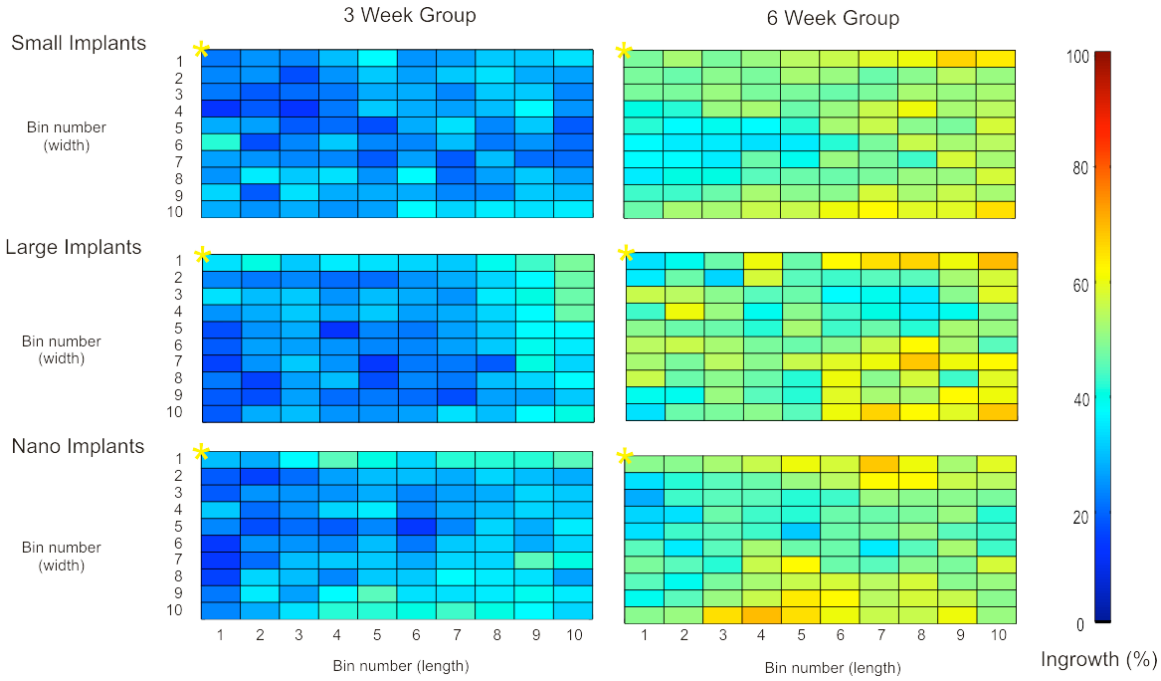

Figure 4.6 Distribution of skin ingrowth within different porous implants. Each panel represents normalized pore area of implant under the skin. The area is divided into 100 bins. The top row of bins in each panel indicates the pore area at the dorsal edge of implant right under the dermis. The left most column represents the bins that would line along the implant exit site; * indicates bin1,1 (see Fig 2 D for further details). Percentage pore area filed with skin tissue is shown for each bin by color.

4.3.2.5 Influence of skin hair on extrusion length and skin ingrowth

The effect of hair (or rat species: CD Hairless rats vs. Sprague Dawley (SD) haired rats) was examined by comparing extrusion rate and skin ingrowth of the 5 CD rats with 5 SD rats implanted with small pore size implants (Table 4.1). Extrusion length and rate tended to be higher in CD hairless rats (mean $\pm$ SD: 0.43 $\pm$ 0.30 cm and 0.08 $\pm$ 0.05 cm/week, respectively) compared to SD rats (0.26 $\pm$ 0.11 cm and 0.04 $\pm$ 0.02 cm/week, respectively), but showed no significant differences ($p > 0.05$, Student's t-test). Skin ingrowth also tended to be higher for SD rats 53.4 $\pm$ 13.2% whereas CD hairless rats had 41.8 $\pm$ 6.0 %, but had no significant difference ($p > 0.05$, Student's t-test).

4.4. Discussion

4.4.1. Hypotheses of the study

The goal of this study was to investigate the effects of pore size, nanotubular surface treatment and duration of implantation on skin ingrowth into porous titanium. It was found that all three types of porous titanium pylons demonstrated skin tissue ingrowth at both 3 and 6 weeks of implantation. Pylons with small pore size (40-100 μm) showed fewer signs of extrusion compared to implants with large pores (100-160 μm), which was in apparent contradiction to hypothesis 1, that larger pores would demonstrate better skin ingrowth. Neither pore size nor nanotubular surface treatment significantly affected the area of skin ingrowth; thus, hypotheses 1 and 2 were not supported. Duration of implantation was shown to be a significant factor for the area of skin ingrowth – the longer implant was in contact with skin, the better was skin integration in all 3 types of implants. Thus, hypothesis 3 was supported.

4.4.2. Skin-implant integration

There is an apparent contradiction between the lower extrusion length (Fig. 4.5A) and extrusion rate (Tables 4.2 and 4.3) of implants with smaller pores, on the one hand, and the similar amount of skin ingrowth in implants with small and large pores (Figs. 4.5B and 4.6), on the other hand. Larger pores would seem to allow easier tissue migration into the deep pores. This trend could be noticed in Fig. 4.6, although it did not reach statistical significance. It has been postulated that the quicker the skin can migrate through the implant (permigration (von Recum, 1984)) and regain some type of epidermal continuity, the faster the percutaneous implant will be extruded. This is because increasing pore size increases the strength of skin attachment (Bobyn *et al.*,

1982). Most likely this was the reason the implants with larger pores were extruded faster in this study. When pore size is smaller, it is more difficult for the tissue to migrate through the pores and thus the implant might be extruded slower. These considerations suggest that there may be an optimum pore size that permits sufficient skin ingrowth and does not lead to fast implant extrusions. It is important to note that in this study implants were not anchored to bone; nevertheless, the extrusion length of Small and Nano implants appear to reach a plateau after week 3 and maintained a nearly constant extrusion length until week 6 (Fig. 4.5A). This could be an indication that pore size 40-100 μm may be close to optimum.

Tissue ingrowth was evident throughout the entire width of implant at 3 and 6 weeks of implantation as green-colored area bins (at least 40% of implant pore area filled with tissue) were present in central width bins 4 through 7 (Fig. 4.6). The maximum skin ingrowth distance in many cases may have been limited by the reinforcing wires in the central region of implants. Thus, the maximum depth of skin ingrowth was 2.75 mm, i.e. the implant radius (3 mm) minus the wire radius (0.25 mm) (2.75 mm = 3.00 - 0.25) assuming a wire was placed in the center of the implant. A previous study on skin ingrowth into porous poly(2-hydroxyethyl methacrylate) implants (pore size 40 μm and 60 μm) (Underwood *et al.*, 2011) reported a much lower maximal ingrowth distance of about 90 μm over 3 to 14 days. This difference suggests that skin has better affinity to titanium than to poly(2-hydroxyethyl methacrylate). Implants with porous-coated titanium anchored in bone in the sheep for 5 to 9 months have also demonstrated good integration of skin with porous coating (Perry *et al.*, 2009; Jeyapalina *et al.*, 2012).

While only one case of infection out of 35 porous implants (infection rate 2.9%)

was observed, there is no guarantee that a skin barrier was formed inside the implants. Nevertheless, low infection rate in this and other studies (Perry *et al.*, 2009; Jeyapalina *et al.*, 2012) suggests that skin interface with porous titanium percutaneous implants limits bacterial penetration, however additional studies are needed to confirm these results. It should also be noted that the pores may also provide a site for potential infection as bacterial colonies were observed in the exterior pores and serocellular crust (Fig. 4.4A).

4.4.3. Study limitations

There are several limitations of the present study. First, it is unclear what role the bandaging played in the amount of extrusion of the implants. The bandaging was used to prevent self-removal of the implants by the rats; however, it likely reduced the implant extrusion rate. Still, since this type of pylon is designed for attachment of bone-anchored external prostheses (Pitkin *et al.*, 2009), no extrusion and thus better skin integration with osseointegrated percutaneous implants can be expected (Jansen *et al.*, 1990; Perry *et al.*, 2009; Jeyapalina *et al.*, 2012).

The second limitation of the study was a relatively short duration of implantation (3 and 6 weeks). This duration was selected because of the concern that pylons implanted for periods longer than 6 weeks would be extruded and no histological analysis would be possible. This is a limitation typical for studies of percutaneous implants that are not anchored to bone. Despite this limitation a significant effect of time on skin ingrowth was established.

Presently it is difficult to discern the role of hair on skin integration with a porous percutaneous device. Hair might, in the long term, enhance protection of the implants as it provides a loose barrier and has been shown to decrease transdermal drug delivery for

some substances (Lauer *et al.*, 1997). Presumably, it might also reduce the bacterial penetration rate. However, the presence of hair around the surgical site during the implantation may prevent proper sterilization and result in a contaminated wound. Hair fragments may also interfere with skin ingrowth by mechanically blocking access to pores of the device (Fig 4.4D). In histological cross-sections some hair fragments observed to be in direct apposition to the implant. Therefore a more in-depth study may be needed if animals with extensive body hair will be implanted with percutaneous devices.

4.4.4 Conclusions

The main problem of percutaneous osseointegrated implants is poor skin-implant integration, which may cause infection. The goal of this study was to investigate the effects of pore size Small (40-100 μm) and Large (100-160 μm), nanotubular surface treatment (Nano), and duration of implantation (3 and 6 weeks) on skin ingrowth into porous titanium. It was found that all 3 types of implants demonstrated skin tissue ingrowth of over 30% of total implant available area under the skin at 3 and 6 weeks of implantation; longer implantation resulted in greater skin ingrowth in all 3 types of implants ($p<0.05$). Only one case of infection was observed (infection rate 2.9%). The Small group showed lower implant extrusion rate than Large group (0.08±0.05 and 0.16 ± 0.07 mm/week, respectively; $p<0.05$). Neither pore size nor implant nanotubular surface treatment significantly affected the area of skin ingrowth. I concluded that percutaneous porous titanium implants can provide skin integration.

CHAPTER 5

AN ANIMAL MODEL TO STUDY SKIN-IMPLANT-BONE INTEGRATION AND PROSTHETIC GAIT WITH LIMB PROSTHESES DIRECTLY ATTACHED TO THE RESIDUAL LIMB

5.1 Introduction

Bone-anchored (or osseointegrated) limb prostheses have been developed and evaluated in human amputees in several countries (Brånemark *et al.*, 2001; Sullivan *et al.*, 2003; Hagberg & Brånemark, 2009; Aschoff *et al.*, 2010). These prostheses are rigidly attached to the bone via a solid titanium implant in the marrow cavity protruding through the skin (Branemark, 1983). Prostheses with a direct skeletal attachment (DSA) eliminate the limitations seen in traditional socket prostheses. These limitations include difficulties of precise fitting of the socket onto the residual limb, occasional discomfort and pain due to skin irritation, the development of pressure sores, sitting discomfort, limited range of motion due to the socket, and transmission of external loads to the limb via soft tissues (Pezzin, 2004; Hagberg *et al.*, 2005). In addition, the conventional socket prostheses provide little to no proprioceptive feedback to the residual limb thus, visual feedback with a relatively long delay becomes critical for successful performance of complex motor tasks (Glencross, 1977; Barnett *et al.*, 2012). The lack of sensory feedback from the prosthesis influences the control of balance and placement of the sound and prosthetic foot during standing and locomotion particularly on complex terrains (Buckley *et al.*, 2002; Hof *et al.*, 2007; Curtze *et al.*, 2010; Segal *et al.*, 2010; Curtze *et al.*, 2012). Thus, DSA prostheses might have certain advantages over traditional

socket prostheses in balance control: (i) ground reaction forces are transmitted directly to the bone of the residual limb compared to indirect force transmission through soft tissues and (ii) the amputee have a better sense of load on and position of the prosthesis due to osseoperception (Jacobs *et al.*, 2000).

Despite the number of advantages of DSA prostheses, their use in many countries, including the US, is limited or prohibited due to the lack of complete skin-implant integration. As a result amputees with DSA prostheses have the rather high skin infection rate (18%), which can lead to implant loosening, revision and/or removal (Hagberg & Brånemark, 2009; Tillander *et al.*, 2010). The majority of current DSA prostheses utilize intramedullary titanium implants with smooth surface (Hagberg & Brånemark, 2009; Aschoff *et al.*, 2010; Jonsson *et al.*, 2011). Since these implants do not completely eliminate skin infection problems, researchers have tried to improve the skin-implant integration by using porous implants imitating natural percutaneous structures as deer antlers (Pendegrass *et al.*, 2006b). Recent *in vitro* and *in vivo* studies of porous implants has demonstrated the potential for a better skin-implant integration and possibility of developing a robust skin barrier to bacteria and other pathogens from the outside environment (Pendegrass *et al.*, 2006a; Pitkin *et al.*, 2006; Pitkin *et al.*, 2007b; Pendegrass *et al.*, 2008; Pitkin *et al.*, 2009; Chou *et al.*, 2010; Shelton *et al.*, 2011; Jeyapalina *et al.*, 2012).

The effects of porous implant properties on skin and bone integration have been studied in various animal models: rats (Ysander *et al.*, 2001; Pitkin *et al.*, 2006), guinea pigs, rabbits (Jansen & de Groot, 1988; Jansen *et al.*, 1994), cats (Pitkin *et al.*, 2009), dogs (Murphy, 1973; Drygas *et al.*, 2008) and sheep (Williams *et al.*, 2010; Shelton *et al.*,

2011). Some of these studies involved limited gait analysis. For example, dogs have been shown to walk on a DSA prosthesis, however the detailed gait mechanics were not reported (Drygas *et al.*, 2008). A recent study in sheep has shown that loading on the implanted limb decreased to approximately 74% of the pre-implantation load 12 months after implantation of a percutaneous osseointegrated prosthesis with a porous skin-implant interface into third metacarpal bone (Shelton *et al.*, 2011). The limited data on gait with DSA prostheses suggest incomplete functional recovery, which warrants further investigation and the development of an animal model that permits detailed histological investigations of skin and bone integration with porous implants, as well as detailed biomechanical analysis of gait with DSA prostheses.

A feline model appears to be well suited for this purpose. It has been the model of choice in studies of the neural control and biomechanics of posture and locomotion (Sherrington, 1910; Brown, 1914; Shik *et al.*, 1966; Rossignol, 2006; Beloozerova *et al.*, 2010; Honeycutt & Nichols, 2010; Musienko *et al.*, 2012). The advantage of the cat model compared to a rodent model is that the cat has highly developed locomotor abilities, it maintains the upright posture, and the loads experienced by the hindlimbs during locomotion are larger than those in rodents and match patterns of human ground reaction forces during walking. Loading on the implant is important because osseointegration is load dependent (Torcasio *et al.*, 2008). Furthermore, cat limb inertial properties have been determined (Hoy & Zernicke, 1985), which permits calculations of forces and moments at the joints and the prosthesis interface with the residual limb by means of inverse dynamics analysis (Manter, 1938; Hoy & Zernicke, 1985; Prilutsky *et al.*, 2005; Gregor *et al.*, 2006). Larger animal models (e.g., large dogs, sheep) have also

been used to study DSA prostheses (Drygas *et al.*, 2008; Shelton *et al.*, 2011), however lab settings for a detailed biomechanical analysis of prosthetic gaits in these models are not readily available.

The objective of the present study was to develop a feline model for evaluating gait with the DSA prostheses attached through porous titanium implants (Pitkin *et al.*, 2009) and for testing skin-implant-bone integration of these implants. This model would permit both a detailed histological analysis of the skin-implant-bone interface after physiological loading of the implant and investigations of prosthetic gait adaptations. Based on data available in the literature (Pitkin *et al.*, 2007b; Pitkin *et al.*, 2009; Shelton *et al.*, 2011; Jeyapalina *et al.*, 2012) I hypothesized that (1) skin and bone tissue will be present inside the porous titanium implants after physiological loading of implant and (2) the animals will modify gait to accommodate the prosthesis, however locomotion will be stable (margins of stability will not be compromised). The preliminary results of the study have been published in abstract form (Farrell *et al.*, 2012a).

5.2. Methods

5.2.1. Animal model and study design

All experimental procedures in this study were in agreement with the US Public Health Service Policy on Humane Care and Use of Laboratory Animals and were approved by the Institutional Animal Care and Use Committees of Georgia Institute of Technology and Saint Joseph's Translational Research Institute. Two adult purpose bred cats (mass 3.2 and 3.0 kg; Table 5.1) were selected for this study. They were trained daily for two weeks to walk across an enclosed walkway with embedded force platforms for food reward. After completion of training, full body walking mechanics were recorded

(see section 5.2.8) for another two weeks (Fig. 5.1A). X-ray images were taken prior to surgery to measure the dimensions and geometry of the tibia marrow cavity; X-ray images taken again after implantation were to monitor healing and bone lysis or fracture (Fig. 5.1B). After implantation of the implant into the tibia medullary cavity (see below), a cast was placed on the residual limb to prevent loading of the implant (Fig. 5.1B,C). Starting at week 8, the protruding end of implant was loaded to promote bone integration (Frossard *et al.*, 2008; Torcasio *et al.*, 2008). At the end of week 10 the cast was removed and a standing prosthesis (Fig. 5.2A) was attached to the protruding implant several times a day to train the animal to use the prosthesis for standing. After initial training of approximately a week, the animals started wearing the standing prosthesis continuously.

Table 5.1 Cat and prosthesis characteristics

	Animal 1	Animal 2
Pre Mass, kg	3.2	3.0
Post Mass, kg	4.0	4.0
Thigh, cm	9.8	9.8
Shank, cm	10.5	10.4
Tarsals, cm	5.6	6.2
Hind Paw, cm	3.2	3.8
Arm, cm	8.4	9.0
Forearm, cm	7.6	8.3
Carpals, cm	2.4	2.2
Fore Paw, cm	3.4	3.2
Residual Limb, cm	8.5	8.8
Standing prosthesis mass, g	14.0	14.0
Standing prosthesis MOI, gcm^2	48.0	48.0
Walking prosthesis Mass, g	18.4	15.5
Walking Prosthesis MOI, gcm^2	156.5	172.1

Leg length was determined as the sum of thigh, shank and tarsals for the hindlimb and arm, forearm and carpals for the forelimb.

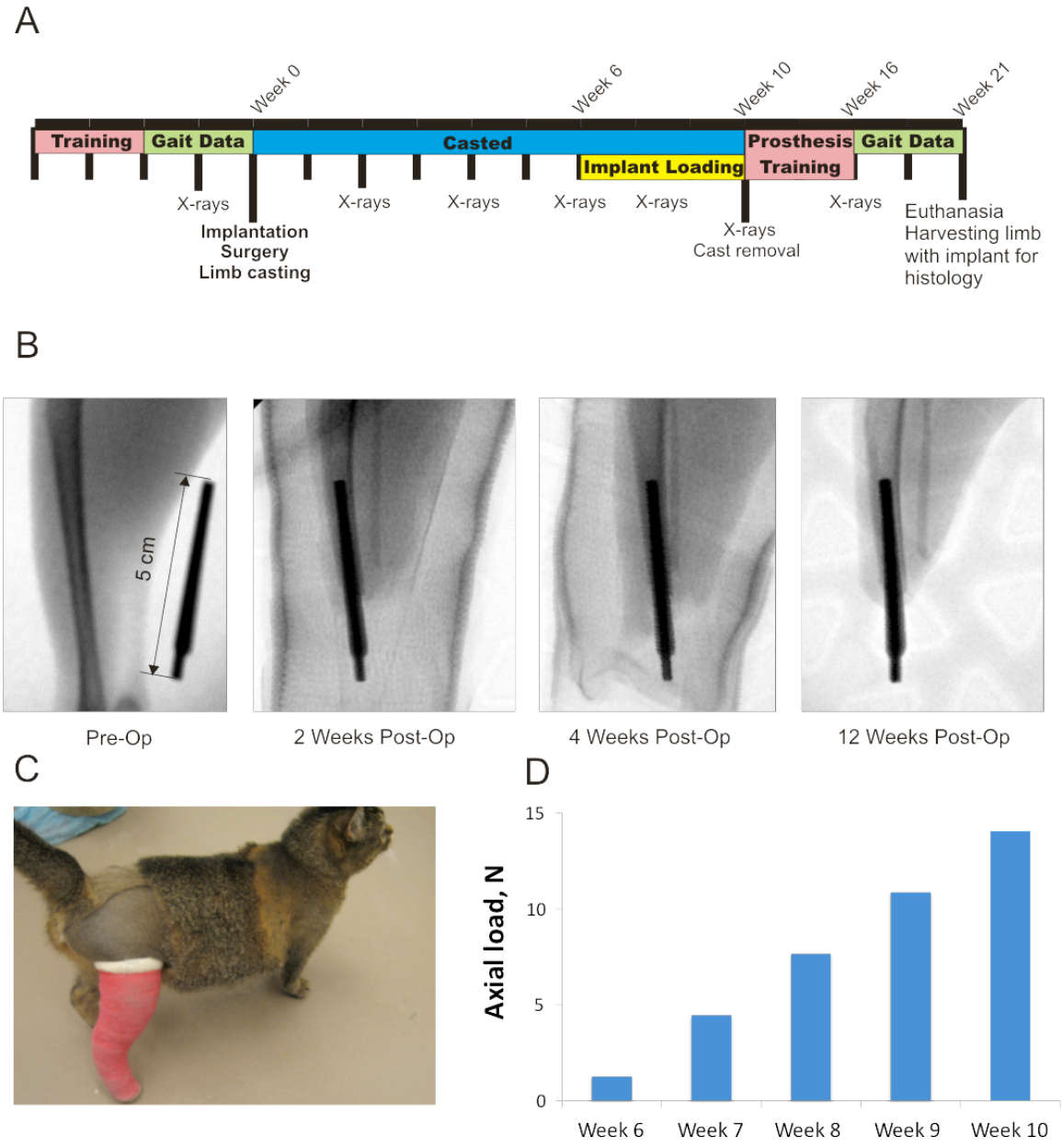

Figure 5.1 Major stages of the study. A) Study timeline. Week 0 corresponds to the implantation surgery; the study ended with euthanasia and bone-skin-implant removal for histology. B) X-ray pictures taken before surgery, and 2, 4 and 12 weeks after implantation. C) Casting to prevent premature loading of implant. D) Loads applied to implant using a handheld dynamometer from 6 to 10 weeks after implantation.

Starting at week 13-14, a J-shape walking prosthesis was attached (Fig. 5.2B, C), and the animals were retrained to walk along the walkway using food reward. Training lasted for 4-6 weeks until the animals reached stable walking performance. Walking mechanics were recorded for several weeks. At week 21 the animals were euthanized using deep anesthesia and the limb with implant was harvested for histological analysis (see section 2.9).

5.2.2. Implants

Porous titanium implants were obtained from Poly-Ortho International (Sharon, MA). The manufacturing technology for these implants has been described elsewhere (e.g. (Pitkin *et al.*, 2009)). Implants were tapered to fit the tibia marrow cavity (0.3 cm diameter at proximal end, 0.5 cm diameter at distal end, and 5 cm in length; Fig. 5.1B). Implants had a central 0.3 x 0.3 cm cross-shaped rod. Pore size in the implant ranged from 40-100 μm (porosity of 30-50%). The distal 0.7 cm of the implant had no porous coating and served as the prosthesis attachment interface.

5.2.3. Implantation surgery

After cats were trained and intact gait mechanics were recorded (see section 5.2.8), each cat underwent an amputation and implantation surgery using standard aseptic surgical procedures. Animals were sedated using a combination of drugs (Dexmedetomidine, SC, 60-80 μg/kg, Antipamezole, SC, 60-80 μg/kg, Ketamine, SC 10 mg/kg, and Xylazine, SC, 10 mg/kg) and anesthesia was maintained using isoflurane inhalation, 1-3%). The right hindlimb was shaved and scrubbed. A circumferential incision was made at the level of the distal $^{1}/_{3}$ of the tibia. In making this incision, a posterior skin flap was incorporated to allow for tension-free closure. The muscles and

tendons at this level were transected using electrocautery. The periosteum was reflected from the exposed tibia proximal to the level of the skin incision and a transverse osteotomy was performed at the juncture of the middle and distal thirds of the tibia using an oscillating saw. The edges of the tibia were rasped to eliminate any sharp edges. A fibular osteotomy was performed approximately 2 cm proximal to the level of the tibial osteotomy. Any remaining soft tissue was transected using cautery thereby completing the amputation. The medullary canal of the tibia was broached using a curette and carefully widened with a reamer that had the same diameter and taper as of the implant. Prior to closure, the fat and subcutaneous tissue of the posterior skin flap was sharply excised to the level of the dermis. A small stab incision was placed with a 15 blade through the posterior skin flap. The sterile implant was inserted through the stab incision and into the medullary canal of the tibia to a depth of approximately 2-3 cm. The wound was copiously irrigated with normal saline and closed with nylon suture so that the dermis of the posterior skin flap made direct contact with the distal end of the tibia. These procedures allowed for a tight interface between the skin and the implant as well as the skin and bone and bone and implant. A sterile gauze dressing was applied over the pylon through a hole placed in the gauze in order to further secure the skin- implant-bone interface. Additional gauze dressing was applied around the pin with sufficient bulk to protect and pad the implant.

The limb was then casted from the proximal thigh to just past the distal end of the implant using a modified Robert Jones Bandage (Brodell *et al.*, 1986) (Fig. 5.1C) to protect the implant and prevent premature loading. In summary, tape stirrups running down the medial and lateral aspects of the limb were used to secure the cast. A nylon

stocking was placed over the leg for casting followed by layers of cast padding and roll gauze. Fiberglass casting tape (Scotchcast, 3M) was applied to the limb. The distal portion of the cast was covered with a small plastic jar and a screw cap that allowed access to the implant. The jar and screw cap were secured to the cast using vet-wrap (3M). The animal recovered for 1–2 weeks with the pain medication administered for at least 3 days and antibiotics for at least 10 days. Blood samples were taken once before surgery and then one week after the surgery to monitor white blood cells counts and infection. Body temperature was measured for several weeks after surgery.

5.2.4. X-rays

Prior to the implantation surgery sagittal and frontal plane X-ray images of the right tibia were taken (Fig. 5.1B). The images aided in determining geometry and dimensions of the tibia marrow cavity, surgical planning and implant selection. After implantation surgery, X-ray images were taken every two weeks (or as needed) to monitor healing and possible bone lysis, fracture and implant loosening.

5.2.5. Implant loading

Six weeks after implantation, each cat was gently restrained, fed and petted by a researcher while another researcher removed the distal cast cover. An axial force of 1.2 N was applied to the distal end of the implant (for 15 minutes a day, 3 days a week) using the digital dynamometer. Each week the load was increased by 3.1 N to reach in 4 weeks 13.8 N (Fig. 5.1D), i.e., the load close to the peak vertical force exerted by the hindlimb during walking or 40-50% of animal body weight. The above implant loading procedure is a scaled version of the procedure used to promote osseointegration of implant in human amputees (Frossard *et al.*, 2008; Hagberg & Brånemark, 2009; Aschoff *et al.*, 2010) .

5.2.6. Prostheses

Once the loading of the implant achieved 40-50% of body weight (approximately 10 weeks after implantation), the restraining cast was removed and a prosthesis was attached to the skin-protruding part of the implant (approximately 2 cm in length) through a female receptacle and setscrews (Fig. 5.2A, B). The first prosthesis attached was a standing prosthesis made of an aluminum rod (9 mm diameter x 6.5 cm length)

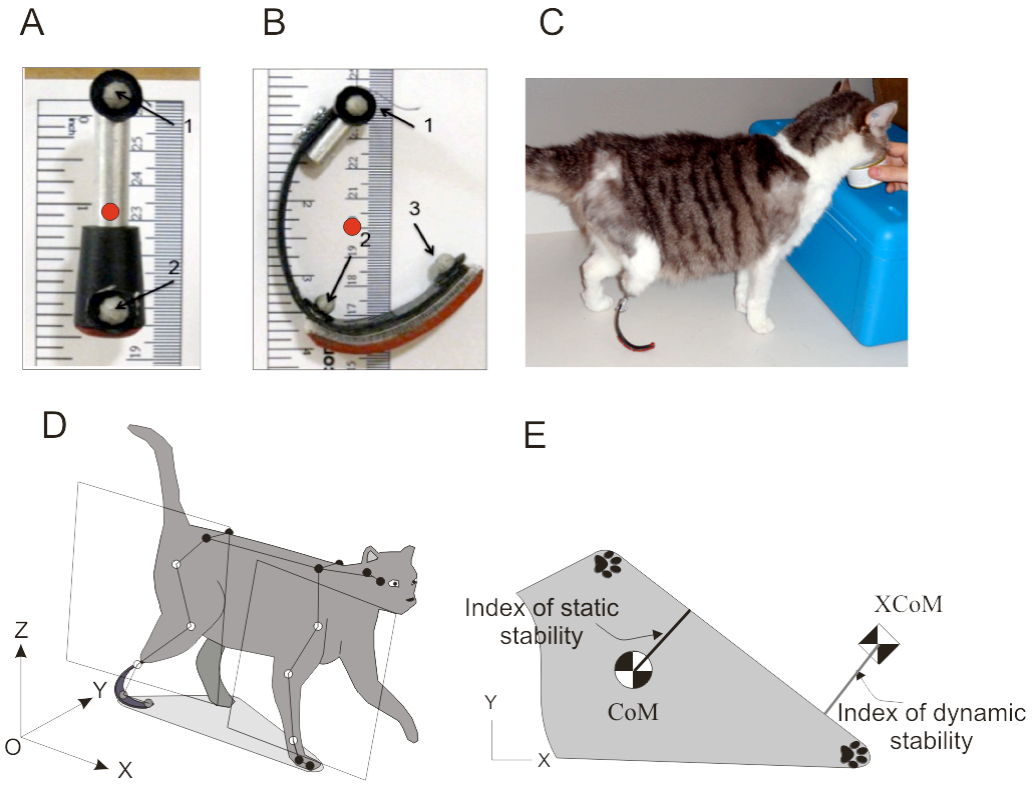

Figure 5.2 Determining stability of prosthetic gait. A, B) Standing and walking prosthesis, respectively. Gray circles indicate marker placement on prostheses (marker 1 approximates location of the ankle center in the intact leg; marker 2, MTP joint; and marker 3, tip of the 5th digit). Red circles indicate center of mass of prosthesis. C) Standing on a walking prosthesis. D) Perspective view of the cat during prosthetic walking and definition of instantaneous area of support. The shaded area between paws (or prosthetic foot) on the ground is defined as area of support. The limb plane was defined for hind- and forelimbs using 3 markers on each limb (open markers; see text for further explanations). E) Definitions of index of static stability and index of dynamic stability (see text for further explanations).

milled to fit a non-slip rubber tread mounted to the bottom (Fig. 5.2A). The animals were adapted to standing on this prosthesis for several weeks before a walking prosthesis was attached.

The walking, J-shape prosthesis incorporated a rocker bottom (Fig. 5.2B, C) to simulate foot function during walking. The curved portion of the prosthesis was fabricated using molded carbon fiber. A hook and loop strip were attached to the bottom of the foot so that treads with different thickness and friction coefficient could be exchanged easily without changing the prosthesis. The initial prosthesis design (length and curvature) was selected to match intact hindlimb length at touch down, mid-stance and lift-off assuming that hip and knee angles would remain unchanged. Prosthesis curvature and length were adjusted as needed to improve symmetry of prosthesis loading and gait speed.

The inertial parameters of each prosthesis were determined for subsequent prosthetic gait analysis (Table 5.1). The mass was measured using a digital scale, the location of the center of mass in the sagittal plane (Fig. 5.2A, B; red dots) was determined using a suspension method (e.g., (Drillis *et al.*, 1964)), and the moment of inertia (MOI) with respect to the frontal axis through the center of mass was calculated using measured elemental volumes of the prosthesis form its high resolution image and known material density of each elemental volume and compared to a computer generated moment of inertia (Solidworks, MA, USA).

5.2.7. Gait rehabilitation

Initial wearing time for the standing prosthesis began with 20 minutes, twice a day and the wear time increased moderately so that the cats could continuously wear the

prosthesis by the end of the first 1-2 weeks after cast removal. Cats were initially trained to stand on the prosthesis using food reward. During training cats were fed when they successfully stood on the prosthetic limb. If the cats raised the limb off the ground food was removed until the cat placed the prosthesis back on the ground. Standing training continued daily for 2-3 weeks.

After adequate standing was achieved, cats were transitioned to the walking, J-shape prosthesis. They were trained for several weeks to walk and stand on the new prosthesis. Positive reinforcement (petting and food) was used when the cats would demonstrate loading of the prosthesis during walking. Once the researchers deemed the cat reached consistent walking performance on the prosthesis, gait recording commenced.

5.2.8. Gait recordings and analysis

Full-body mechanical characteristics of intact and prosthetic gait were recorded before and after surgery and gait rehabilitation. In each experimental session, 28 small reflective markers (6-9-mm in diameter) were attached to major joints and body segments on the cat and/or prosthesis using double-sided adhesive tape (Fig. 5.2A-B, D). Three-dimensional marker positions and the three components of the ground reaction force were recorded using a high-speed motion capture system (120 Hz; Vicon, UK) and 3 force plates embedded in the walkway (360 Hz; Bertec, USA). Food reward was given each time the cat successfully walked across the walkway. Gait mechanics were recorded daily for approximately 3-5 weeks.

Gait mechanics were analyzed using a full-body inverse dynamics cat model (see Fig. 5.2D, Chapter 2 and (Prilutsky *et al.*, 2005; Beloozerova *et al.*, 2010)). In summary, recorded trials were examined for consistent walking with constant velocity. The marker

positions were low-pass filtered (Butterworth, 4th order, 6-7Hz). For each trial, kinematics of each body segment and the general center of mass (CoM) were calculated. To compute positions of the joint centers, a limb plane was established using the hip, knee and ankle marker positions for hindlimbs or the shoulder, elbow and wrist marker positions for forelimbs (see Fig. 5.2D; also see Chapter 2). Within this plane, the knee and elbow marker positions were recalculated using measures of limb segment lengths (Miller *et al.*, 1975). The estimated joint centers for the knee, ankle, elbow and wrist joints were calculated by shifting the marker positions medially half the width of the joint along the orthogonal vector to the limb plane. The hip and shoulder joint centers were estimated by shifting the marker position medially along the line defined by the left and right hip or shoulder markers half the width of the joint. The centers of mass location for each segment was calculated using the computed joint centers, the mass of the cat and the measured length of each segment (Hoy & Zernicke, 1985). The CoM displacement for each cat was determined based on the locations of each segment center of mass (e.g., (Drillis *et al.*, 1964)). The velocity and acceleration of the CoM was calculated as the first and second time derivative of its position, respectively.

A measure of dynamic body stability was calculated for each walking trial. The animal was considered to be statically stable if the projection of the CoM onto the ground was within the base of support (Fig. 5.2E) (Ting *et al.*, 1994). Dynamic stability was calculated using the position of the extrapolated center of mass (XCoM), which accounts for CoM velocity (Hof *et al.*, 2005): XCoM = CoM + VCoM/w_o, where XCoM, CoM and VCoM are extrapolated position, position and velocity of the general center of mass of the body, respectively; and $\omega = \sqrt{g/l}$ is eigen (natural) frequency of the (inverted)

pendulum with mass equaled cat mass balancing on a massless stick of length *l* equaled leg length (Table 5.1), and g is acceleration of gravity. If the projection of XCoM onto the ground fell outside the base of support the cat was considered dynamically unstable, otherwise, it was dynamically stable (Fig. 5.2E). The stability index (margin of stability) was calculated as the minimum distance from the base of support to either the CoM or XCoM.

Stride kinematic parameters were calculated for each analyzed stride. Stride length was defined for all limbs as the distance between two consecutive paw positions at the paw-contact instance. Stance width was determined for fore- and hindlimbs as the lateral distance from left fore paw to right fore paw centers, left hind paw to right hind paw center, or from left hind paw to prosthesis center. Forward velocity was calculated as the mean velocity of the CoM over the gait cycle. Stance, swing and cycle times were determined based on the paw contact and lift-off times. Measured ground reaction forces and computed resultant joint moments were time normalized and averaged across fore- or hindlimbs for each animal.

5.2.9. Histology

At the end of the study, animals were euthanized and the residual shank with implant was carefully removed by knee disarticulation. Samples were fixed in 10% formalin, embedded in methlymethacrylate, sectioned and ground to thickness (approximately 100 μm) using the Exakt system (EXAKT Technologies, Inc., Oklahoma City, OK), then polished and stained with haemotoxylin and eosin. The samples were sectioned at the level of proximal half of implant (4 transverse sections with a step of approximately 2 mm) and at the distal end (one longitudinal section) as shown in Fig.

5.3A). A veterinary pathologist evaluated the slides for tissue response and bone and skin ingrowth into implant in each section. For the purpose of scoring the degree of bone ingrowth into the porous implant at each sectioned level of the pylon, a grade 1 through 4 was assigned if bone ingrowth was observed in one, two, three or four quadrants of the porous coating, respectively. Furthermore, bone ingrowth was characterized as "superficial" when it was restricted to the outer layers or the porous spheres, and "deep" when the growth extended to the interface of the central rod and the inner porous coating.

5.2.10. Statistical Analysis

All mechanical time-dependent variables were time normalized to 100% of either stance time or cycle time and averaged across all strides for each animal. Gait parameters before and after surgery for each animal were compared using a Student t-test for dependent variables. The same test was used to determine differences in time dependent variables at each percent of gait cycle between pre and post surgery gait. Significance level was set at $p<0.05$ for all variables in the study.

5.3 Results

The two animals implanted with porous titanium implants did not have clinical signs of skin infection, distress or pain, had normal temperature (range: 35.6 to 37.8 ^{o}C), white blood cells count (range: 9.5 to 11 x $10^{3}/\mu L$) and appetite (body mass increased after surgery from 3.2 kg to 4.0 kg and from 3.0 to 4.0 kg in cats 1 and 2, respectively). No indications of bone lysis, fracture or implant loosening could be found in X-ray images of the residual limb (Fig. 5.1B) for the duration of the study (20 weeks). The animals adopted the cast for standing and walking within several days after surgery (Fig.

5.1C); subsequently (starting with week 12), the animals successfully utilized a DSA prosthesis for standing and walking.

5.3.1 Bone and skin integration with porous titanium implant

Histological analysis of sections through the residual limb demonstrated bone ingrowth into pores of the implant in both animals, although ingrowth was not equal around the circumference of the implant and was greater in areas in closer contact to the residual tibia (Figs. 5.3 and 5.4). Bone ingrowth was typically noticed in one or three quadrants of implant sections with generally more superficial ingrowth in proximal parts of implant (ingrowth grades 1 or 3) than in distal parts (grades 0 and 1, see Table 5.2) in both animals (Fig. 5.3B-E, Fig. 5.4A-D). More deep bone ingrowth was noticed in the most proximal implant section of animal 1 (grade 3) and in two most distal sections of animal 2 (grades 3 and 4, Table 5.2). The implant-skin-bone interface can be seen in Fig. 5.3F, G and 5.4E, F. The epidermal layer enters the pores of both implants and results in skin tissue ingrowth into the deeper implant pores. Dermal ingrowth into implant could be only assessed in animal 2 for technical reasons. Skin penetrated implant to depth of approximately 0.7 mm and followed the edge of the implant.

5.3.2. General kinematics of prosthetic gait

Each cat successfully used the prosthesis for locomotion. Both cats tended to walk slower with the prosthesis than during intact locomotion, however only cat 1 showed significantly lower walking speed and longer cycle duration (Fig. 5.5). Nevertheless, speed of walking with the prosthesis was within normal ranges. Stride length was shorter in both cats (by about 9 cm or 18%; $p<0.05$), whereas stance width was much wider (over 2 times; $p<0.05$) during prosthetic gait compared to intact walking in cat 2, but was not

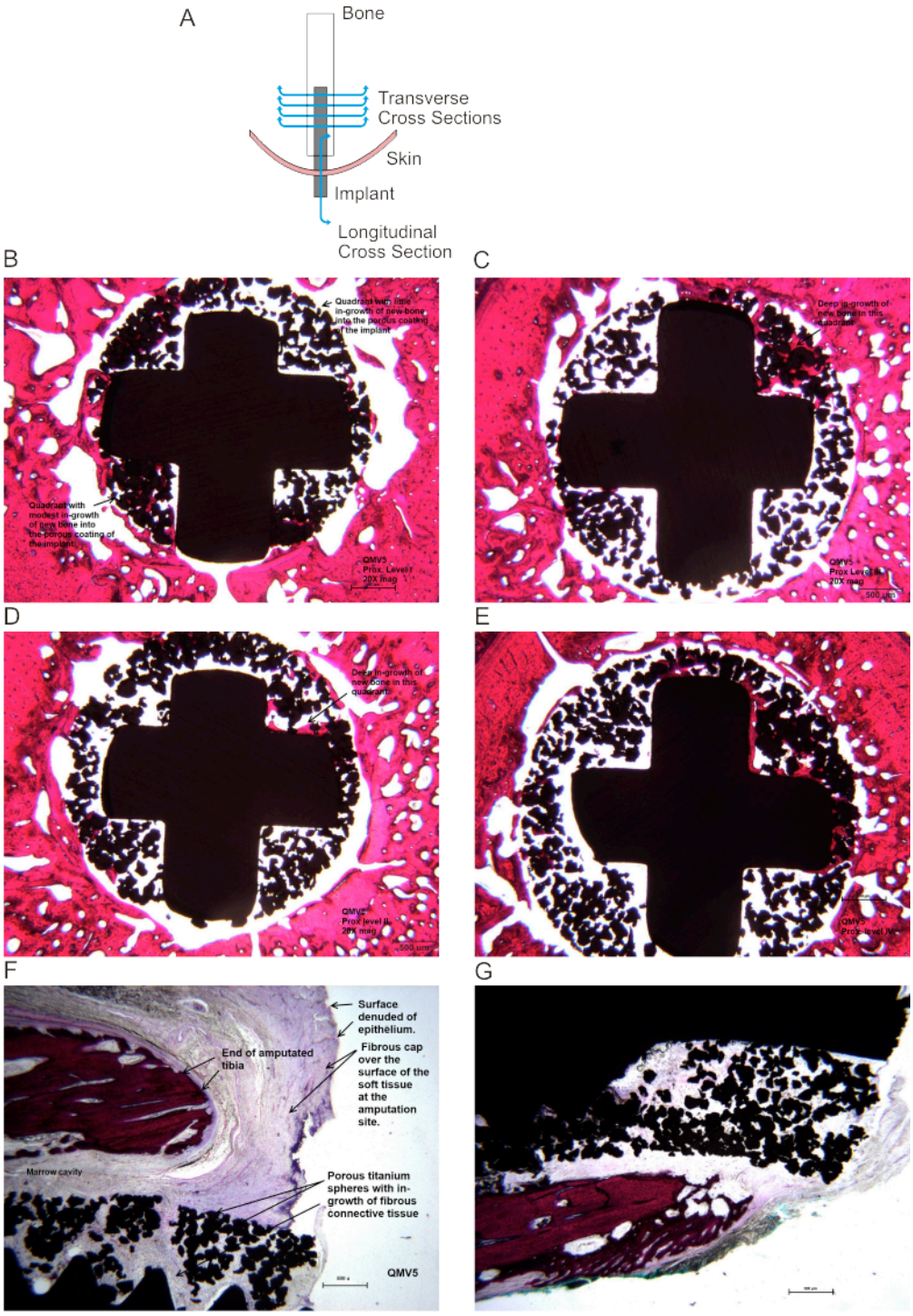

Figure 5.3 Images of sections through implant, bone and skin from cat 1. Haemotoxylin and eosin staining. A) Schematics for the transverse and longitudinal sections of the implant. B-E) Transverse cross sections through the bone and implant from proximal to distal sections, respectively (20x magnification). F, G) Left and right sides of the longitudinal section through the distal implant (20x magnification).

Figure 5.4 Images of sections through implant, bone and skin from cat 2 (haemotoxylin and eosin stain). A-D) Transverse cross-sections through the bone and implant from proximal to distal sections, respectively (20x magnification). E, F): Left and right views of the longitudinal section through the distal implant (20x magnification). See locations of sections in Fig. 5.3 A.

Table 5.2 Bone ingrowth scores

Animal 1				
Level of the tibia	**Superficial ingrowth**	**Deep ingrowth**	**Impression of endosteal bone proliferation**	**Impression of periosteal bone proliferation**
Proximal I (nearest to the knee joint)	1	3	Mild	Minimal
Proximal II	3	1	Mild	Mild
Proximal III	3	1	Mild	Mild
Proximal IV (nearest to the amputation site)	1	1	Mild	Mild
Distal	N/A		N/A	N/A
Animal 2				
Proximal I (nearest to the knee joint)	3	1	Minimal to mild	Minimal
Proximal II	3	1	Mild	Mild
Proximal III	1	3	Mild to moderate	Moderate
Proximal IV (nearest to the amputation site)	0	4	Mild to moderate	Moderate to marked
Distal	1	3	Mild	Marked

statistically different in cat 1. Stance time of the prosthetic right hindlimb increased in cat 1 and decreased in cat 2 by about 100 ms (~20%; $p<0.05$, Fig. 5.5). Duty factor during prosthetic gait tended to increase for the intact limbs, i.e. it was significantly higher incontralateral (left) limbs for both cats and in the ipsilateral (right) forelimb for cat 2; $p<0.05$). Duty factor for the right hind prosthetic limb decreased significantly in both cats.

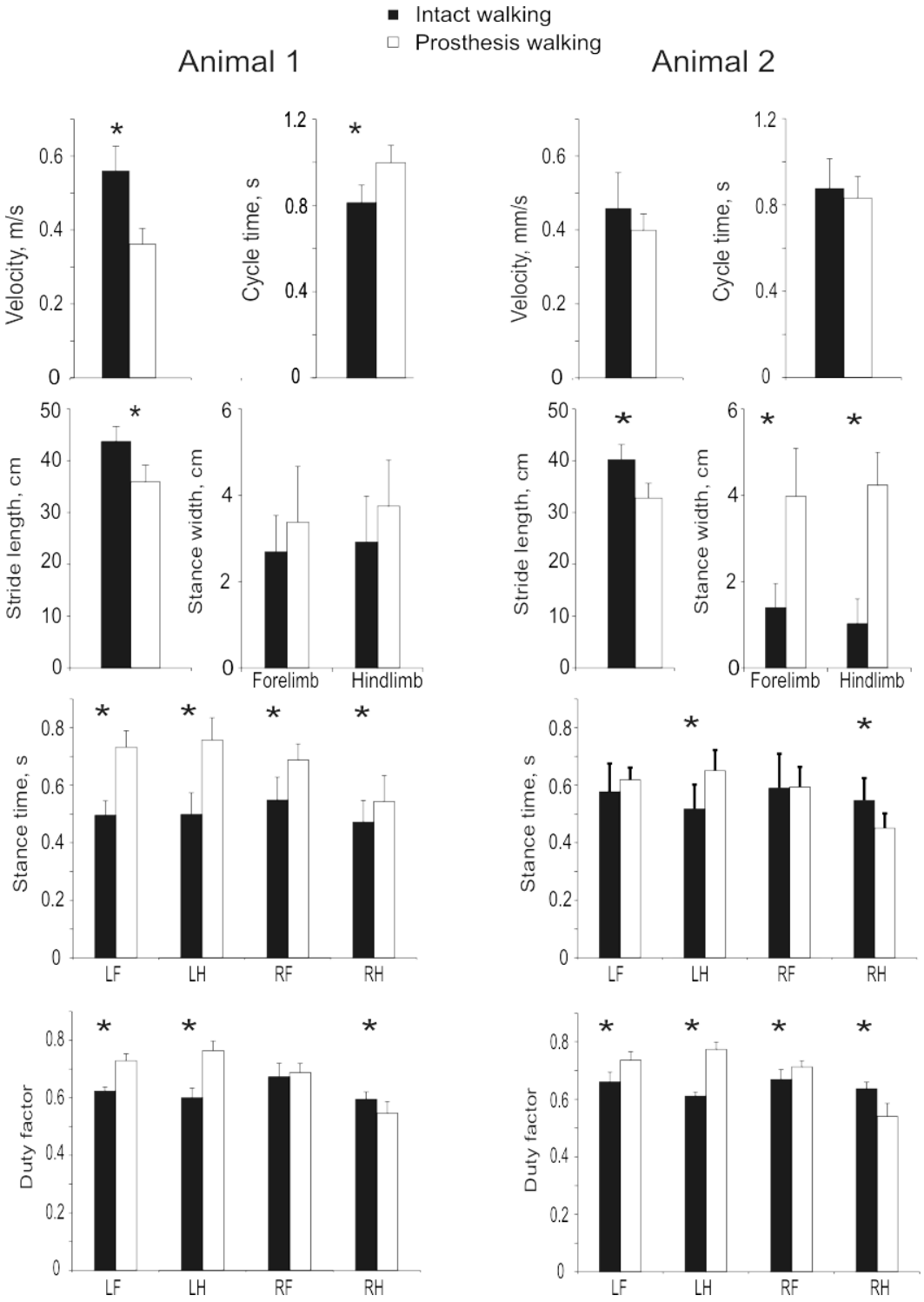

Figure 5.5 Stride parameters (mean+SD) of intact (filled bars) and prosthetic (unfilled bars) gait for cat 1 (left panels) and cat 2 (right panels). LF, LH, RF, and RH are left forelimb, left hindlimb, right forelimb, and right hindlimb, respectively; RH was implanted and had a DSA prosthesis on. Duty factor is the ration of stance time and cycle time. * indicates significant differences between intact and prosthetic conditions ($p < 0.05$). The number of analyzed cycles was between ## and ## for each condition.

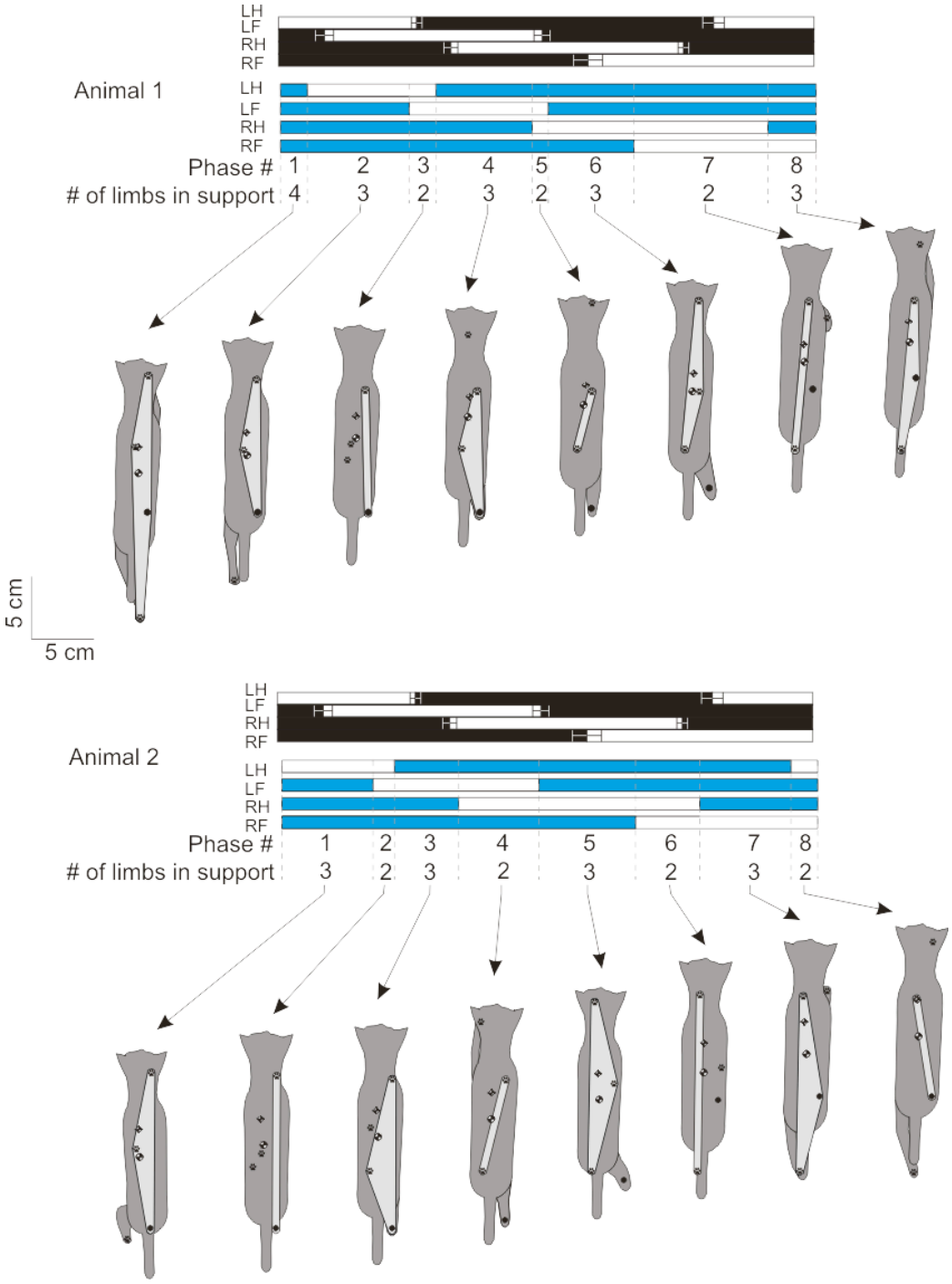

Figure 5.6 Support pattern (sequence of phases with different number of limbs on the ground) during intact (black) and prosthesis (blue) walking and representative base of support areas for each phase for cat 1 (top panel) and cat 2 (bottom panel). Filled bars indicate stance and unfilled bars swing. LH, LF, RH and RF are left hindlimb, left forelimb, right (prosthetic) hindlimb and right forelimb, respectively. The top row of numbers between dashed lines indicate the phase of gait; the second row, the number of limbs on the ground in a given phase. Dorsal cat views show the base of support area (light gray) relative to the paws on the ground and the center of mass and extrapolated center of mass.

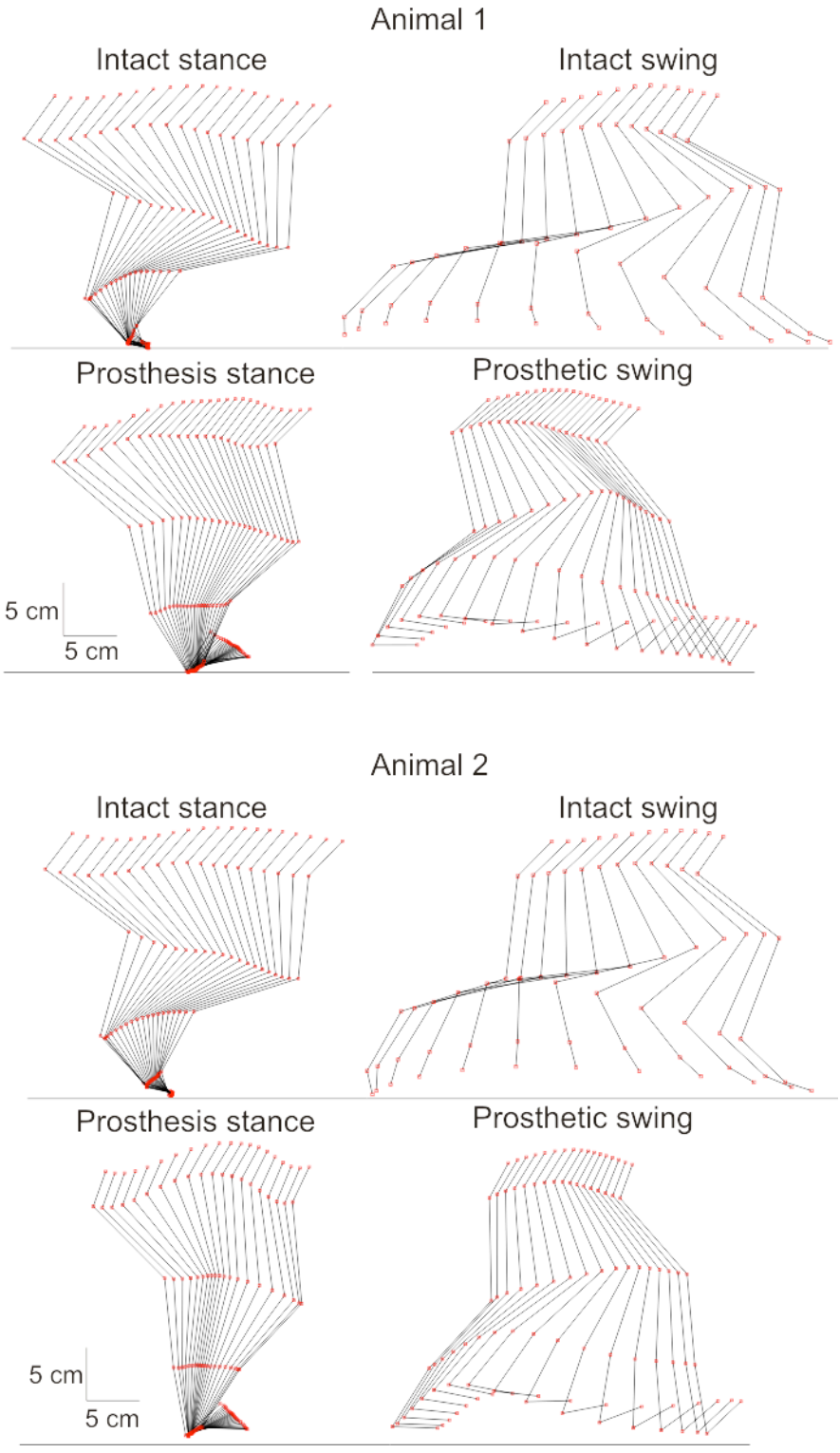

Figure 5.7 Stick figures of the right hindlimb from representative trials of animal 1 (top 4 panels) and animal 2 (bottom 4 panels) during intact and prosthetic walking. Stance and swing phases are shown separately. Red squares represent the marker locations.

Limb support pattern (sequence of phases with different number of limbs on the ground) showed substantial differences during prosthetic gait. Cat 1 used a limb support pattern 4-3-2-3-2-3-2-3, which was different from a pattern used in intact condition, i.e. 3-2-3-2-3-2-3-2 (Fig. 5.6). In this animal the most substantial difference was an increased stance contribution (duty factor) from the left hindlimb, followed by the left forelimb (Fig. 5.5). Cat 2 used a limb support pattern (3-2-3-2-3-2-3-2) typical for moderate walking speeds (see Chapter 2&3; also (Beloozerova *et al.*, 2010)). Both cats increased the time spent in 3-4-legged support and reduced time of 2-legged support during prosthetic gait (Fig. 5.6).

The prosthetic right hindlimb demonstrated qualitatively different kinematics compared to the intact limb. The knee and hip joints of the prosthetic limb were more extended during stance and much less flexed during swing; consequently, the pelvis, thigh and the residual shank were oriented more vertically and the pelvis vertical position was higher during prosthetic walking (Fig. 5.7).

5.3.3. Dynamic stability

Average indices of dynamic stability calculated for each phase of gait and for the total gait cycle had negative values in several phases, i.e. in these phases the animals were dynamically unstable (Fig. 5.8A, B). The dynamic stability of cat 1 during prosthetic walking was significantly different from that of intact walking in phases 2, 4, 5 and 6. For example, in phases 2, 4 and 6 margins of body instability increased (stability indices became more negative) and in phase 5 stability increased during prosthetic walking ($p < 0.05$, Fig. 5.8A). Dynamic stability averaged over the whole cycle slightly but significantly improved after the surgery. Cat 2 showed no changes in dynamic

stability between intact and prosthetic walking for individual phases or for total cycle stability (Fig. 5.8, $p>0.05$).

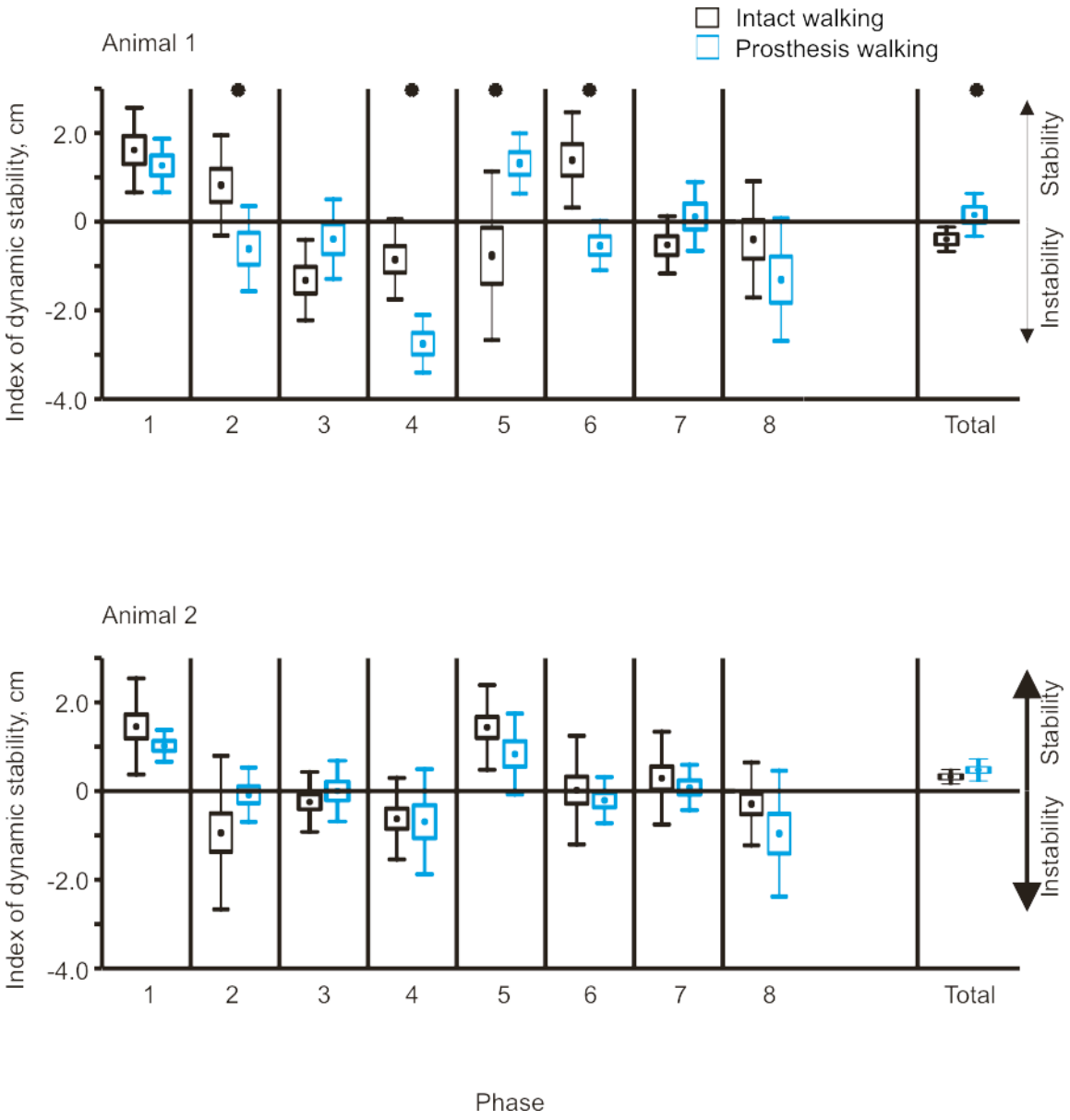

Figure 5.8 Dynamic stability index for each phase and the whole cycle of intact (black) and prosthetic (blue) gait. A) Stability index for cat 1. B) Stability index for cat 2 . * Indicates significant differences between intact and prosthetic conditions ($p < 0.05$). Phase numbers correspond to Fig. 5.6. Boxes indicate $\pm$ 1 standard error of measurement and vertical bars indicate $\pm$ 1 SD.

5.3.4. Kinetics of prosthetic gait

During walking, the animals loaded the prosthesis less than the intact right hindlimb prior to implantation. During intact walking, a peak vertical force on the hindlimb was 43% and 52% body weight (BW) for cat 1 and cat 2, respectively (Fig. 5.9 and 5.10). After surgery the prosthesis was loaded to 33% and 20% BW for cat 1 and cat 2, or 78% and 38% of the load on the same hindlimb prior to surgery. It should be noted however that in terms of absolute peak vertical forces the prosthetic limb of cat 1 was loaded similarly to load on the intact right hindlimb before surgery (13.1 vs. 14.2 N, respectively) due to an increase in mass of animal 1 (see above). The anterior-posterior forces on the prosthetic hindlimb also decreased in comparison with intact forces (Figs 5.9 and 5.10, left panels). Specifically, the prosthetic limb of cat 1 exerted lower breaking forces for much longer time (approximately two thirds of the stance duration compared to about one third of stance in intact conditions), but very little propulsive force (Fig. 5.9). Cat 2 exerted essentially no braking or propulsive forces in the anterior-posterior direction (Fig. 5.10).

The ground reaction forces applied to the other intact limbs during prosthetic walking demonstrated marked changes compared to intact conditions. The vertical loading of the left contralateral hind- and forelimb increased above the forces seen in intact conditions (Figs. 5.9 and 5.10, right panels), while the vertical loading on the right ipsilateral forelimb remained similar or decreased slightly. The left hindlimb increased peak vertical loading by 13% BW in cat 1 and 17% BW in cat 2. The anterio-posterior forces on the intact limbs during prosthetic walking were typically lower than prior to implantation except the left contralateral hindlimb, whose breaking force was only

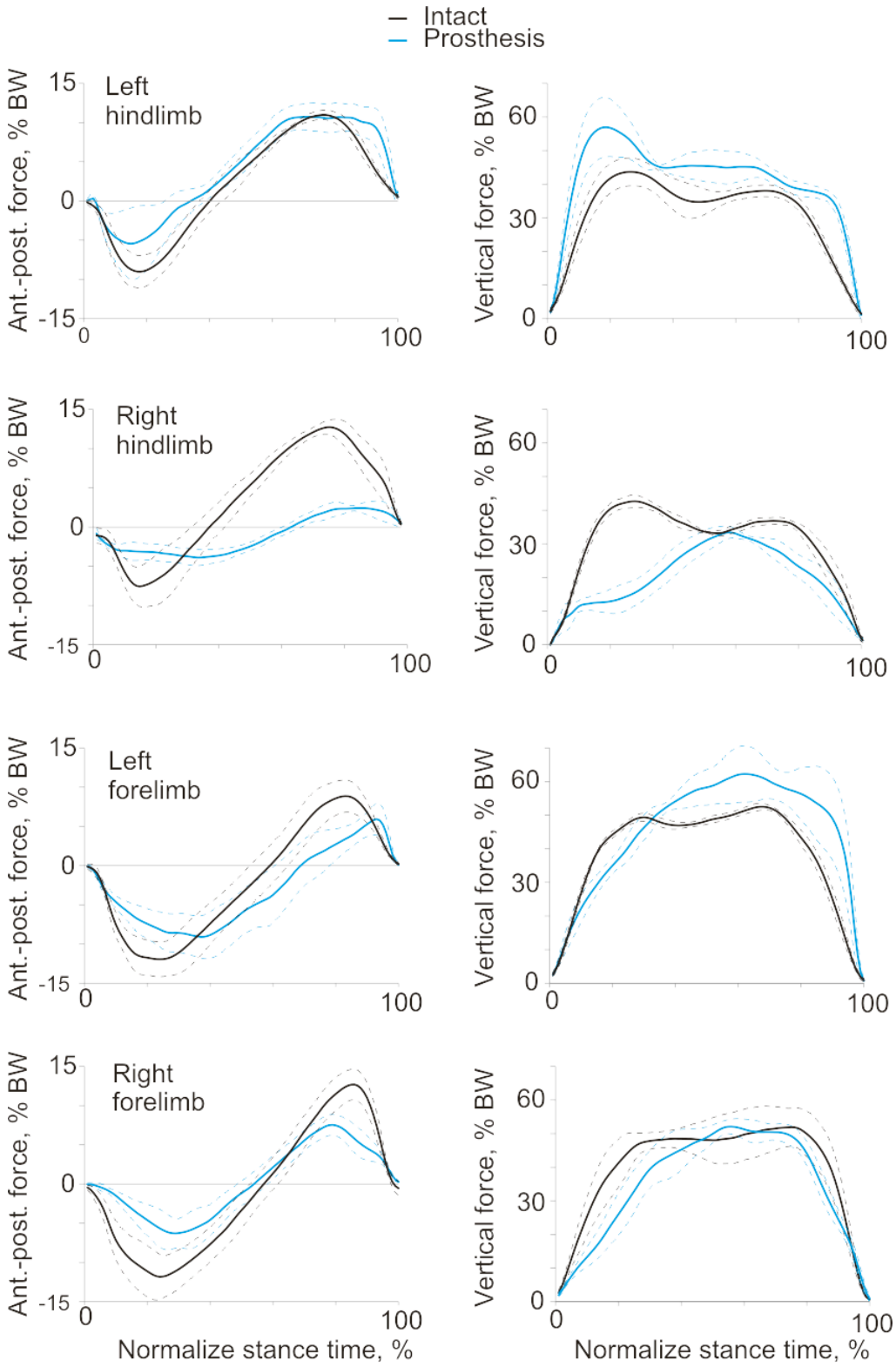

Figure 5.9 Mean anterior-posterior (left) and vertical (right) ground reaction forces acting on individual limbs of cat 1 during intact (black lines) and prosthetic (blue lines) gait conditions. Dashed lines indicate + SD.

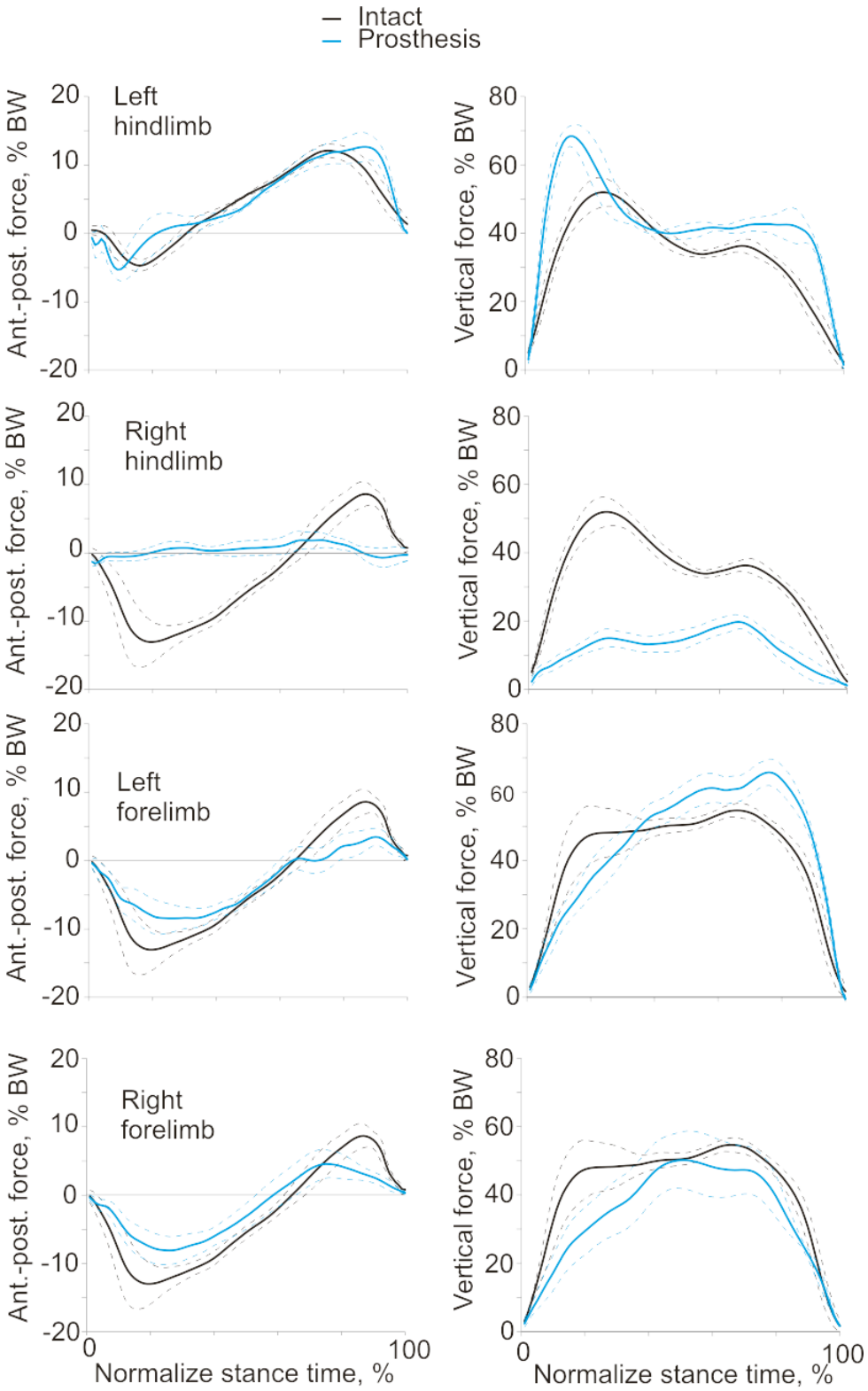

Figure 5.10 Mean anterior-posterior (left) and vertical (right) ground reaction forces acting on individual limbs of cat 2 during intact (black lines) and prosthetic (blue lines) gait conditions. Dashed lines indicate + SD.

slightly reduced, but propulsive force was higher in terminal stance (Figs. 5.9 and 5.10).

Joint moments were calculated based on the ground reaction forces, limb kinematics and inertial parameters of each limb (Hoy & Zernicke, 1985) or prosthesis (Table 5.1). The resulting joint moments (Fig. 5.11) demonstrated that the prosthetic limb hip and knee muscle moment contributions are lower than during intact walking. The contralateral hindlimb, conversely, increased hip and knee moments thus providing the necessary torque production to propel the body forward and prevent falling.

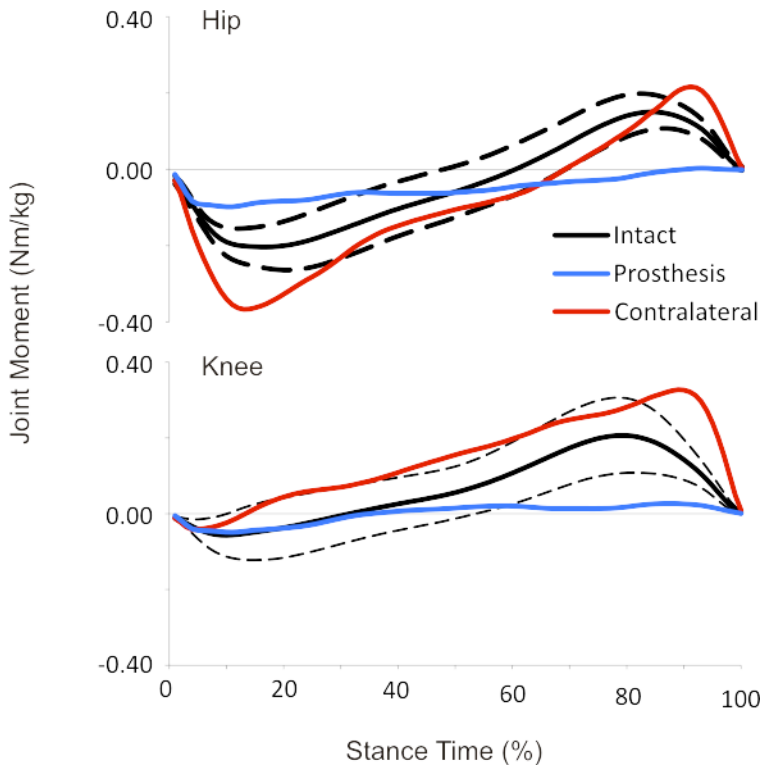

Figure 5.11 Joint moments for the hip (top) and knee (bottom) during stance phase of intact (black; mean ± SD), and prosthetic gait for cat 1. The prosthetic hindlimb is shown in blue and the contralateral hindlimb is shown in red.

5.4. Discussion

5.4.1. Study objectives

The goal of the study was to develop a feline experimental model for detailed analysis of skin and bone integration with a porous titanium implant that is physiologically loaded during locomotion with a DSA prosthesis. The surgical, rehabilitation and recording procedures and prosthetic devices developed in this study allowed two experimental animals to adopt DSA prostheses for locomotion and wear them for 9 weeks without clinical signs of distress, pain or infection. Full-body mechanical analysis of prosthetic gait revealed how the animals adapted to the prosthesis. Histological analysis of the porous titanium implants harvested at the end of the study demonstrated bone and skin ingrowth inside the implants. The obtained results confirmed expectations about tissue ingrowth into the implant and stability of prosthetic locomotion.

5.4.2. Integration of porous titanium implant with the residual bone and skin

The findings of this study (Figs 5.3-4, 5.7-10, Table 5.2) suggest that the porous titanium implants can serve as a reliable attachment point for an external prosthesis. Both implants demonstrated signs of integration with bone and one studied implant showed signs of integration with skin. There was at least mild bone growth into each quadrant of the proximal implant sections with more ingrowth seen in distal sections, which were in closer contact with the marrow cavity wall. The skin ingrowth appeared to follow the implant into the distal end of the marrow canal. The lack of intimate bone-implant contact at the distal end of the implant might have been due to bone resorption and osteoporotic bone in the residual tibia. Both animals demonstrated substantial loading of the prosthesis attached to the percutaneous implant during locomotion.

These results are in agreement with previous studies that demonstrated bone and skin integration with similar porous titanium implants (See Chapter 4; also (Pitkin *et al.*, 2007b; Pitkin *et al.*, 2009)) or solid titanium implants coated with porous titanium (Pendegrass *et al.*, 2006a; Isackson *et al.*, 2011; Jeyapalina *et al.*, 2012) in rats, a cat, rabbits, goats and sheep. Although osseointegration of solid titanium implants with bone has been well established in animal models and human patients (Branemark, 1983; Ysander *et al.*, 2001; Pitkin *et al.*, 2007b; Hagberg & Brånemark, 2009; Shelton *et al.*, 2011), skin integration with porous percutaneous implants has not been well documented. A limited number of studies have suggested the potential for these implants to form a skin barrier to pathogens at the skin-implant interface (Pendegrass *et al.*, 2006a; Pitkin *et al.*, 2007b; Isackson *et al.*, 2011; Jeyapalina *et al.*, 2012). The results of this study support this suggestion.

One limitation to the study was the fact that pore size was relatively small (40-100μm) and the optimum pore size for bone integration tends to be somewhere between 100-400μm (for review see (Kienapfel *et al.*, 1999)). It is known however, that bone ingrowth will occur with a variety of pore sizes, even if pore sizes are smaller (see RESULTS; also (Itala *et al.*, 2001)). It should be noted though that increasing pore size tends to reduce the shear stress that may form at the implant bone interface due to increased area; however, with completely porous implants, as pore size increases implant strength decreases. Further, given the geometry of the current implants it is likely that much of the loading seen is compressive loading where the forces will be distributed geometrically along the medullary canal assuming tight fit during implantation (For example, just after implantation compressive loads can be applied without implant

movement though no ingrowth is present). Tensile loads then would be the primary consideration for shear stress on the ingrowth and would be exerted during swing phase of walking. The resulting loads would be small (approximately the weight of the prosthesis) and should not create large shear forces. In the future however, it may be necessary to create implants with regions of differing pore sizes, where the region to be implanted in the bone contains larger pores and the skin smaller pores such as those shown here and in Chapter 4.

An advantage of the animal model developed in this study compared to the majority of animal models used previously is that it allows for an investigation of percutaneous implant properties after the animal has loaded it within physiological ranges during every day standing and locomotion with a prosthesis. Such a model is necessary for a meaningful translation of animal experimentation results to clinical studies and practice.

5.4.3. Prosthetic gait

Both implanted animals demonstrated stable prosthetic walking with normal speeds. As in another recent study of quadrupedal prosthetic locomotion (Shelton *et al.*, 2011), the animals in this study loaded the prosthetic limb less than before surgery or than other intact limbs after surgery. The analysis of loads exerted by the contralateral fore- and hindlimb and the ipsilateral forelimb (Figs. 5.9 and 5.10) suggests that the animal shifted body weight (CoM) to the contralateral side. Left hindlimb increased its propulsive force, whereas the other two intact limbs decreased their braking forces during prosthetic gait. This compensation strategy was employed by both animals and apparently helps the animals to maintain normal walking speed. Although the magnitude of

unloading of the prosthetic limb is similar to the previous study on sheep (Shelton *et al.*, 2011), the mechanism of this decrease is likely different. The ankle joint that provides a major contribution to energy generation for intact locomotion (Prilutsky *et al.*, 1996; Prilutsky *et al.*, 2011) was substituted with a passive prosthesis. In the sheep study, a much smaller metacarpophalangeal joint was removed. Thus, I propose that the decrease in loading on the prosthetic limb was a compensation strategy to allow the intact limbs to contribute more to propulsion. This explanation is supported by the greater magnitudes of the resultant muscle moments at joints of the intact limbs during prosthetic walking (Fig. 5.11). In addition, the stance duration and duty factor of the intact limbs increased during prosthetic gait, apparently compensating for the deficits in the right hind prosthetic limb.

5.4.4 Conclusions

Despite the number of advantages of bone-anchored prostheses, their use in patients is limited due to the lack of complete skin-implant integration. The objective of the present study was to develop an animal model that would permit both detailed investigations of prosthetic gait and histological analysis of the skin-implant-bone interface after physiological loading of the implant during standing and walking. The two animals adopted the bone-anchored prosthesis for standing and locomotion, although loads on the prosthetic limb decreased by 22% and 62%. The animals shifted weight to the contralateral side and increased propulsion forces by the contralateral hindlimb. Margins of dynamic stability were generally similar between intact and prosthetic gait indicating that dynamic stability could be maintained. Histological analysis of the implants demonstrated both bone and skin ingrowth. The developed animal model to study prosthetic gait and tissue integration, further demonstrated that a porous titanium

implant may permit bone and skin integration thus facilitating prosthetic gait. Future studies with this model will help optimize implant properties, prosthesis design and rehabilitation procedures.

CHAPTER 6

GENERAL CONCLUSIONS

Locomotor and postural control is remarkably proficient at preventing falls and recovering from perturbations. The adaptive nature of the central nervous system allows stable movement performance even during highly constrained and unstable situations. While control of balance involves coordination of sensory input and motor output at many different levels of the central nervous system, the resulting motor behavior is generally fluid and graceful. However, the neural and biomechanical mechanisms of stability control during locomotion are still not well understood. Therefore, the overall goal of my research was to determine the motor strategies involved in maintaining dynamic stability during intact and prosthetic locomotion. Specifically, I aimed to better understand the role of motor cortex and limb coordination in control of dynamic stability and develop an animal model to study dynamic stability during prosthetic gait with a prosthesis directly attached to the residual limb. In this chapter, I will discuss the key findings and their applicability to the larger body of knowledge and address inherent limitations and future directions of the research.

6.1 Summary of findings

Aim 1 of the study was to investigate the biomechanical mechanisms of control of static and dynamic stability during locomotion in the intact locomotor system of the cat (Chapters 2 and 3). This was accomplished by comparing stability of normal walking with stability in two perturbed walking conditions. In the first experiment, cats walked with increased stance width (Wide walking). I hypothesized that the increased base of

support would result in increased dynamic and static stability of walking. Margins of stability were measured as the distance from the center of mass (CoM) or extrapolated center of mass (XCoM) to the edge of the base of support (Fig, 2.1). I further expected to see a reduction in the overall motor cortex activity, as a more stable gait should need less motor cortex involvement. The results of this experiment did not support my initial hypothesis. The animals were less stable in 6 out of 8 phases of wide walking compared to unconstrained walking and only 2 of the 6 phases showed a significant increase in stability. Further, neuronal discharge rate from the right forelimb representation in the primary motor cortex showed significant changes during the swing phase only.

The second experiment of Aim 1 sought to evaluate static and dynamic stability of walking with a narrowed base of support (Narrow walking). I hypothesized that stability would decrease during narrow walking due to the increased likelihood that the CoM and XCoM would fall outside the base of support. The stability results of this experiment did not support the hypothesis, as dynamic stability was not poorer than during narrow walking. Furthermore, cortical activity demonstrated relatively small but significant changes during swing phase.

Aim 2 of my dissertation was to develop an animal model to study dynamic stability of prosthetic gait with a prosthesis directly attached to the residual limb (DSA prosthesis) and to investigate integration of skin and bone with a percutaneous porous titanium implant used for prosthetic attachment. In order to address this aim, I first needed to determine how the porous titanium implants would integrate with skin. This work is presented in Chapter 4. The effects of implant pore size, nano-surface modifications and duration of implantation on the length and rate of implant extrusion

and skin ingrowth were evaluated in a rat model. The results demonstrated that all porous implants regardless of pore size, surface or implantation duration exhibited signs of tissue ingrowth. However, the small pore implants were extruded at a slower rate than the larger pore implants. Implantation time was the only significant factor associated with tissue ingrowth. That is, the longer the implants were implanted the greater the pore fill fraction.

Based on these results, small pore implants with no surface modification were chosen for use in a feline animal model to study DSA prostheses and prosthetic gait stability. Using this model, implantation and rehabilitation procedures were developed to closely mimic the clinical procedures established (see Chapter 5.2 for details) (Brånemark *et al.*, 2001). The results presented in Chapter 5,demonstrate principally that the adapted procedures were successful in rehabilitating 2 cats with a DSA prosthesis. Furthermore, the histological evidence confirmed bone and skin ingrowth into the pores of both implants. The biomechanical gait analysis demonstrated that the cats will loaded the prosthesis and implant, but that these loads were 78% and 38% of intact gait loading in two cats, respectively. The results also indicate that the cats used a limb support pattern that is heavily reliant on the limbs contralateral to the prosthetic limb. Further, the analysis of dynamic stability showed that during prosthetic gait stability was similar or greater than during intact gait.

6.2 Implications of findings

Base of support and speed of locomotion influence dynamic stability

The results from Aim 1 demonstrate that the size and shape of the base of support influence the margins of stability during gait. Previous research has shown that adjusting

the base of support in humans alters the margins of stability; increasing stance width increases medial-lateral stability and decreasing stance width does not have a significant effect (McAndrew Young & Dingwell, 2012b). However, the effects of changes in base of support on the margins of stability in the intact and prosthetic gait in a quadrupedal animal model were unknown. Chapters 2, 3 and 5 provided this knowledge. First, the results indicate that the calculated stability index is a viable option for measuring stability in the quadruped. For instance, during narrow walking the cat increases stability (that is moving the projection of the CoM or XCoM closer to the center of the base of support) possibly as a safety measure in case a loss of balance occurs during gait; i.e. anticipating and planning to respond to a perturbation if one occurs. Conversely, during wide walking, stability margins decrease likely because of two reasons. First with the wide base of support, accurate regulation of the stability margin becomes less critical. Coupled with this is the fact that the body has to undergo significant left and right displacements (Fig. 2.5A). Chapter 5 demonstrates results from gait on a DSA prosthesis that indicate that dynamic stability can be maintained within intact ranges though this seems to be achieved at the expense of walking velocity. For instance, cat 1 reduced velocity and changed limb support pattern, which resulted in a slight but significant increase in stability.

Spinal pathways may be regulated in locomotor control

It is well established that various reflex pathways are used during gait to aid in stance to swing transitions, prevent tripping, maintain balance and help handle loading (Zehr & Stein, 1999) and the results presented here support this idea. It is also possible that spinal pathways can be up or down regulated to produce the desired movement (e.g.

(Chen *et al.*, 2006)). As an example, during wide walking, the apparent inhibition of the lateral gastrocnemius and soleus presumably by the medial gastrocnemius (Fig. 2.8) is upregulated to provide increased laterally directed force. Similar results have been seen in reflex pathways that are involved in responding to noxious stimulus on the lateral border of the paw and have been termed sural nerve reflex ((Nichols *et al.*, 1993). These pathways may be excited through cortical pathways or it may be solely due to the increased lateral force and thus pressure on the lateral aspect of the paw pad. Also shown in Chapters 2 and 3 was an increased activity of the flexor muscles during swing phase. These muscles are typically considered flexors and act together synergistically to enable flexion of the limb. The increased activity in these muscles is likely due to increased excitability of the flexor half-center of the central pattern generator through supraspinal mechanisms and visuomotor processing. Furthermore, based on the mechanical and EMG analyses of ankle muscles, it appears that many of the muscles commonly referred to as gross "extensors" or "flexors" have substantial out of plane moment contributions that may aid in achieving the task goals (Lawrence *et al.*, 1993). It is also possible that the elevated activity of the primary motor cortex during swing (i.e. the phase with increased dynamic instability) may regulate pathways to improve stability and control paw placement.

Contributions from the primary motor cortex in regulating dynamic stability is rather low

Decerebrate animals with intact brain stem have been shown to maintain balance during perturbations (Musienko *et al.*, 2008; Honeycutt & Nichols, 2010; Musienko *et al.*, 2012), suggesting that postural control during locomotion can be regulated through

brain stem and spinal cord functions to a large extent. The primary motor cortex appears to be involved in control of complex locomotor behaviors such as obstacle avoidance and precise stepping (Beloozerova & Siorta, 1993; Drew *et al.*, 2002; Beloozerova *et al.*, 2010). During the wide and narrow walking, recorded motor cortex activity demonstrated significant firing rate changes during swing phase. Based on previous work, altered activity during swing phase tends to be associated with accurate stepping (Beloozerova *et al.*, 2010). Therefore, during walking with altered stance width the changes in motor cortex activity appear to be associated with selection of paw placements to improve stability control. Further, individual neurons showed substantial changes and lumping all the activity together may not reflect the distinct nature of the motor cortex as different regions process different information and regulate different pathways. It is unlikely that each PTN is controlling an individual muscle and highly likely that groups of neurons are responsible for regulating different spinal pathways as was touched on previously. Therefore, in future analysis it may be necessary to do some type of cluster analysis dependent on both spatial and temporal firing parameters. These results might demonstrate groups of neurons highly correlated with the increased flexor activity (which was shown in the hindlimbs and is presumably present in the forelimbs) and possibly groups of neurons correlated with task goals such as endpoint control and stability.

Quadrupeds may utilize instability to move

The results of stability analysis suggest that the cat may use gravity and linear momentum to aid in the movement. For example, to move laterally during wide walking, the animal shifts the CoM outside the support area and "falls" under the action of gravitational force in the desired direction until the contralateral limbs "catch" the body

similar to results seen in the turtle (Jayes & Alexander, 1980). The findings also indicate that, during the diagonal support phases of walking, cats may purposefully destabilize the body in the direction of progression thereby using the center of mass linear momentum. Specifically, as the cat moves the extrapolated center of mass crosses the edge of the base of support and moves forward until the forelimb in swing makes contact with the ground ahead of the extrapolated center of mass. These results can be seen in Fig. 2.3 and 3.3 for walking with a support pattern of 3-2-3-2-3-2-3-2 and back the idea of efficient locomotion in quadrupeds (Griffin *et al.*, 2004). Griffin et al further demonstrated that in dogs peak propulsive force occurs during mid swing of each forelimb. These results tend to agree with the idea of destabalization during mid-to-late swing of the forelimbs based on the fact that the cat CoM is accelerating possibly to provide this instability. Other work, in human crawling, has shown destabalization during swing of the forelimb as well (Babic *et al.*, 2001). While this gait may not have features of an inverted pendulum, it does provide further evidence that destabalization during swing of the forelimbs (or arm in this case) is a common feature of quadrupedal gait. In human walking, it has been postulated that a CoM destabilization strategy is used for gait initiation and locomotion (Winter, 1995). These results are in agreement with this postulate. Additionally, based on the analysis of stability in the frontal plane, it is reasonable to assume that the cat is using a similar strategy to move in multiple planes (frontal and sagittal) (Fig 2.3-2.4, and 3.3-3.4). Overall it seems clear that the cat uses the motion of the CoM in both the sagittal and frontal planes even to aid stability control and forward and lateral movement.

Furthering this idea, I would also propose that if quadrupeds utilize instability to move, that the next phase of gait needs to be dynamically stable, i.e. the phase in which

the forelimb contacts the ground after the diagonal support phase. This dynamically stable phase is needed to prevent further destabilization and possibly sets the stage for where future paw placements are needed. Therefore Foot or paw placement is critical because failure place the limb ahead of, in this case, the extrapolated center of mass would result in further instability. For instance, is someone steps out of a slow moving vehicle, he/she can recover from the initial perturbation. However if vehicle speed increases, the person will fall after the initial contact because he/she cannot slow the body down enough with the next step (i.e. there is too much momentum to overcome). Subsequently, it would be interesting to examine stability when paw placement is changed during mid swing (e.g. during ladder walking when a rung is moved) given sufficient forward speed. In this case the quadruped would need to make stability adjustments, such as increasing the braking force in the forelimb thereby temporarily decreasing velocity, to compensate for the change which might further elucidate the role of paw placement in the control of stability.

Implantation time increases pore fill fraction in percutaneous porous titanium implants

Chapter 4 investigated how pore size, implantation time and nanotubular surface treatments influence skin integration with porous titanium. The results revealed that implantation time had the greatest influence on skin ingrowth. Further, implants with larger pore size were extruded faster compared to implants with smaller pore size (Fig 4.5 and Table 4.3). There was no correlation between tissue ingrowth and measured implant porosity or ingrowth and implant extrusion rate suggesting that other factors, which were

not accounted for, influence implant extrusion rate. Based on these results, porous titanium implants with small pore size range may be ideal for skin integration.

Locomotion asymmetry confirmed in quadrupedal prosthetic gait

The results from Chapter 5 confirmed results of human studies that prosthetic gait is asymmetrical yet stable. In humans the prosthetic limb is loaded less than the intact limb. The asymmetry can cause overuse injuries in the contralateral limb. Therefore rehabilitation procedures should focus not only on balancing the load between the limbs, but also on equalizing the duty factor between limbs. More studies are needed to address issues of restoring symmetry between limbs and the developed animal model of prosthetic gait will aid this research

6.3 Limitations

Several limitations of the studies can be identified. Stability of locomotion was not tested through unexpected perturbations (e.g. lateral movement of walkway or application of a rapid lateral force), a typical paradigm of assessing the mechanisms of the balance control system. While this is a good way to evaluate whether and how the motor system responds to specific perturbations, it does not assess how the motor system plans and adapts to novel, but expected mechanical conditions. Given that instability increases with decreasing base of support, the intact balance control system appears incorporates a stability safety factor. Additionally, the measure of dynamic stability may not be correct. The model assumes that an inverted pendulum gait. In humans, the inverted pendulum model is clearer because only a single limb is in contact with the ground during much of the gait cycle. However, in quadrupeds there are multiple limbs in contact with the ground during any phase. While inverted pendulum mechanics have

been shown to exist in quadrupeds (Fig 2.11 and (Griffin *et al.*, 2004)), the theory is not as well defined. Unfortunately, the dynamic stability calculations currently available assume a simplified model (e.g. (Hurmuzlu & Basdogan, 1994)), which utilize a rigid segment model that appears have similarities to an inverted pendulum model. Therefore, potential violations to the rigid segment assumptions may exist in quadrupeds due to changes in flexion or extension of joints such as the ankle or knee in the hindlimb or elbow and wrist in the forelimb or due to multiple limbs in contact with the ground.

The margins of stability may not be directly perceived by the physiological receptors. In order to asses this information, the supraspinal areas of the central nervous system responsible for balance control would need to integrate position and velocity of the center of mass relative to the base of support. While in theory it is possible to determine the position and velocity of the CoM from sensory feedback and visual cues, it us not clear whether the margins of stability are a variable that the CNS directly senses and controls. Another possibility is that in phases of dynamic instability, the CoM is accelerating in the direction of maximum instability, and this acceleration can be detected by the vestibular system and proprioceptors in the limbs on the ground.

Prosthetic gait in general was slower than typical quadrupedal gait. Slower walking speeds discussed in section 5.4, tends to increase stability. However, to compare intact and prosthetic gait more accurately, similar walking speeds would be necessary. Therefore in future experiments, recording walking at a variety of speeds on a treadmill may be beneficial to detecting changes in prosthetic gait.

Only two pore sizes were chosen for the experiment in Chapter 4 to study skin integration with porous titanium; 40-100 μm and 100-160 μm. It is known from literature

that pore sizes smaller than 40 μm are ineffective at providing tissue ingrowth (Winter, 1974). Using larger pore sizes than may increase skin ingrowth; however increasing pore size decreases strength of the implants and may lead to premature implant failure. In bone integration there is also an optimal pore size range (100-400 μm) (Kienapfel *et al.*, 1999). Therefore, the two pore sizes chosen were thought to provide the best possibility for tissue ingrowth and implant strength that could be translated to developing an animal model of direct skeletal attachment. Additionally, 6 weeks was chosen as the maximal implanted time. Longer duration could be used to determine the long-term survivability of the implants, however, given the increased extrusion rate for the large pore implants, it is likely that only the small and nano implants would have remained in the skin. Therefore, in future development, it may be necessary to develop implants, which have optimal pore size regions for both skin and bone integration and that are implanted for longer periods of time.

Despite the fact that 2 cats were rehabilitated on a DSA prosthesis, the low animal numbers do not provide statistical power generalize the results of prosthetic gait. Given that the goal was to develop an animal model, this limitation was expected. However, in future studies where the detailed mechanics of DSA gait in a feline model are required, a larger sample of animals will be obtained

6.4 Future Directions

The results of this work provide the framework for many potential studies. Principally, the developed animal model will allow investigation into the long-term skin-implant-bone integration and adaptations of cortical control adaptations to prosthetic training and gait. It would also be important to record from other areas of the brain

known to be involved in balance control – cerebellum, basal ganglia, reticular formation – during the same tasks. Also, recording EMG from more prominent frontal plane muscles may give more specific insight into how they are controlled during gait and how their function changes when limb frontal plane angles are altered and muscle moments in the frontal plane increase. Measurements of pull-off force from skin integrated with porous titanium would provide useful information to understand how well the skin is attached to the implant. Further, challenging the skin implant interface with external pathogens would provide better evidence regarding the ability of the skin-implant barrier to prevent infection. Finally, adding to the total animal numbers in the prosthetic gait study would provide significantly more statistical power as well as help develop better rehabilitation protocols, which are be applicable to human amputees.

REFERENCES

Adell R, Hansson BO, Brånemark PI & Breine U. (1970). Intra-osseous anchorage of dental prostheses. II. Review of clinical approaches. *Scandinavian journal of plastic and reconstructive surgery* **4,** 19-34.

Albrektsson T & Johansson CB. (2001). Osteoinduction, osteoconduction and osseointegration. *European Spine Journal* **10,** S96-S101.

Armstrong DM & Marple-Horvat DE. (1996). Role of the cerebellum and motor cortex in the regulation of visually controlled locomotion. *Can J Physiol Pharmacol* **74,** 443-455.

Aschoff HH, Kennon RE, Keggi JM & Rubin LE. (2010). Transcutaneous, distal femoral, intramedullary attachment for above-the-knee prostheses: an endo-exo device. *The Journal of bone and joint surgery American volume* **92 Suppl 2,** 180-186.

Babic J, Karcnik T & Bajd T. (2001). Stability analysis of four-point walking. *Gait & Posture* **14,** 56-60.

Barnett CT, Vanicek N & Polman RC. (2012). Postural responses during volitional and perturbed dynamic balance tasks in new lower limb amputees: A longitudinal study. *Gait Posture*.

BBC News. (2010). Bionic feet for amputee cat.

Bellmann M, Schmalz T & Blumentritt S. (2010). Comparative biomechanical analysis of current microprocessor-controlled prosthetic knee joints. *Arch Phys Med Rehabil* **91,** 644-652.

Beloozerova IN, Farrell BJ, Sirota MG & Prilutsky BI. (2010). Differences in movement mechanics, electromyographic, and motor cortex activity between accurate and non-accurate stepping. *Journal of neurophysiology* **103,** 2285-2300.

Beloozerova IN & Siorta MG. (1993). The role of the motor cortex in the control of accuracy of locomotor movements in the cat. *Journal of Physiology* **461,** 1-25.

Beloozerova IN, Sirota MG, Orlovsky GN & Deliagina TG. (2005). Activity of pyramidal tract neurons in the cat during postural corrections. *Journal of neurophysiology* **93,** 1831-1844.

Beloozerova IN, Sirota MG, Orlovsky GN & Deliagina TG. (2006). Comparison of activity of individual pyramidal tract neurons during balancing, locomotion, and scratching. *Behav Brain Res* **169,** 98-110.

Bishop PO, Burke W & Davis R. (1962). The identification of single units in central visual pathways. *J Physiol* **162,** 409-431.

Bobyn JD, Wilson GJ, MacGregor DC, Pilliar RM & Weatherly GC. (1982). Effect of pore size on the peel strength of attachment of fibrous tissue to porous-surfaced implants. *Journal of biomedical materials research* **16,** 571-584.

Bolton DA, Williams L, Staines WR & McIlroy WE. (2012). Contribution of primary motor cortex to compensatory balance reactions. *BMC neuroscience* **13,** 102.

Bolton DaE & Misiaszek JE. (2009). Contribution of hindpaw cutaneous inputs to the control of lateral stability during walking in the cat. *Journal of Neurophysiology* **102,** 1711-1724.

Bolton DaE, Tse ADY, Ballermann M, Misiaszek JE & Fouad K. (2006). Task specific adaptations in rat locomotion : Runway versus horizontal ladder. *Behavioural Brain Research* **168,** 272-279.

Bonding P. (2000). Titanium implants for bone-anchored hearing aids--host reaction. *Acta Oto-Laryngologica Supplementum* **543,** 105-107.

Branemark PI. (1983). Osseointegration and its experimental background. *Journal of Prosthetic Denistry* **50,** 399-410.

Brånemark PI, Adell R, Breine U, Hansson BO, Lindström J & Ohlsson A. (1969). Intra-osseous anchorage of dental prostheses. I. Experimental studies. *Scandinavian journal of plastic and reconstructive surgery* **3,** 81-100.

Brånemark PI & Albrektsson T. (1982). Titanium implants permanently penetrating human skin. *Scandinavian journal of plastic and reconstructive surgery* **16,** 17-21.

Brånemark R, Brånemark PI, Rydevik B & Myers RR. (2001). Osseointegration in skeletal reconstruction and rehabilitation: a review. *Journal of rehabilitation research and development* **38,** 175-181.

Brodell JD, Axon DL & Evarts CM. (1986). The Robert Jones bandage. *Journal of bone and Joint Surgery* **68,** 776-779.

Brown TG. (1914). On the Nature of the Fundamental Activity of the Nervous Centres. *Journal of Physiology* **49,** 18-36.

Buckley JG, O'Driscoll D & Bennet SJ. (2002). Postural sway and active balance performance in highly active lower-limb amputees. *American Journal of Physical Medicine and Rehabilitation* **81,** 13-20.

Bunderson NE, McKay JL, Ting LH & Burkholder TJ. (2010). Directional constraint of endpoint force emerges from hindlimb anatomy. *Journal of Experimental Biology* **213,** 2131-2141.

Burkett B, Smeathers J & Barker T. (2003). Walking and running inter-limb asymmetry for Paralympic trans-femoral amputees, a biomechanical analysis. *Prosthetics and orthotics international* **27,** 36-47.

Burlachkova NI, Ioffe, M.E. . (1979). On the functions of the cortical motor area in precise movement organization. *Acta Neurobiol Exp (Wars)* **39,** 27-39.

Centers for Disease Control and Prevention. (2003). Wed-based injury statistics query and reporting system (WISQARS) [Online]. National Center for Injury Prevention and Control, Centers for Disease Control and Prevention. , online.

Cervelli V, Bottini D-J, Arpino a, Grimaldi M, Rogliani M & Gentile P. (2008). Bone-anchored implant in cosmetic finger reconstruction. *Annales de chirurgie plastique et esthétique* **53,** 365-367.

Chamberlin ME, Fulwider BD, Sanders SL & Medeiros JM. (2005). Does fear of falling influence spatial and temporal gait parameters in elderly persons beyond changes associated with normal aging? *Journal of Geronol A Biol Sci Med Sci* **60,** 1163-1167.

Chehroudi B & Brunette DM. (2002). Subcutaneous microfabricated surfaces inhibit epithelial recession and promote long-term survival of percutaneous implants. *Biomaterials* **23,** 229-237.

Chen F, Lo S, Meng N, Lin C & Chou L. (2006). Effects of wrist position and contration on wrist flexors H-reflex, and its functional implications. *Journal of electromyography and kinesiology* **16,** 440-447.

Chou TGR, Petti CA, Szakacs J & Bloebaum RD. (2010). Evaluating antimicrobials and implant materials for infection prevention around transcutaneous osseointegrated implants in a rabbit model. *Journal of biomedical materials research Part A* **92,** 942-952.

Curtze C, Hof AL, Postema K & Otten B. (2010). Over rough and smooth: Amputee gait on an irregular surface. *Gait & posture* **33,** 292-296.

Curtze C, Hof AL, Postema K & Otten B. (2012). The relative contributions of the prosthetic and sound limb to balance control in unilateral transtibial amputees. *Gait Posture* **36,** 276-281.

Davis SD, Gibbons DF, Martin RL, Levitt SR, Smith J & Harrington RV. (1972). Biocompatibility of ceramic implants in soft tissue. *Journal of biomedical materials research* **6,** 425-449.

Day KV, Kautz Sa, Wu SS, Suter SP & Behrman AL. (2012). Foot placement variability as a walking balance mechanism post-spinal cord injury. *Clinical biomechanics (Bristol, Avon)* **27,** 145-150.

Deliagina TG, Beloozerova IN, Zelenin PV & Orlovsky GN. (2008). Spinal and supraspinal postural networks. *Brain Res Rev* **57,** 212-221.

Dichgans J & Fetter M. (1993). Compartmentalized cerebellar functions upon the stabilization of body posture. *Rev Neurol (Paris)* **149,** 654-664.

Dingwell JB, Cusumano JP, Sternad D & Cavanagh PR. (2000). Slower speeds in patients with diabetic neuropathy lead to improved local dynamic stability of continuous overground walking. *Journal of biomechanics* **33,** 1269-1277.

Donlan RM. (2001). Biofilms and device-associated infections. *Emerg Infect Dis* **7,** 277-281.

Dorland's Illustrated Medical Dictionary. (2007).

Drew T, Andujar JE, Lajoie K & Yakovenko S. (2008). Cortical mechanisms involved in visuomotor coordination during precision walking. *Brain Res Rev* **57,** 199-211.

Drew T, Jiang W, Kably B & Lavoie S. (1996). Role of the motor cortex in the control of visually triggered gait modifications. *Can J Physiol Pharmacol* **74,** 426-442.

Drew T, Jiang W & Widajewicz W. (2002). Contributions of the motor cortex to the control of the hindlimbs during locomotion in the cat. *Brain Res Brain Res Rev* **40,** 178-191.

Drillis R, Contini R & Bluestein M. (1964). Body segment parameters; a survey of measurement techniques. *Artificial Limbs* **25,** 44-66.

Drygas KA, Taylor R, Sidebotham CG, Hugate RR & Mcalexander H. (2008). Transcutaneous tibial implants: a surgical procedure for restoring ambulation after amputation of the distal aspect of the tibia in a dog. *Veterinary Surgery* **37,** 322-327.

Dufosse M, Macpherson J, Massion J & Sybirska E. (1985). The postural reaction to the drop of a hindlimb support in the standing cat remains following sensorimotor cortical ablation. *Neurosci Lett* **55,** 297-303.

Dunlap P, Perera S, VanSwearingen JM, Wert D & Brach JS. (2012). Transitioning to a narrow path: the impact of fear of falling in older adults. *Gait Posture* **35,** 92-95.

Duong TT, Englander J, Wright J, Cifu DX, Greenwald BD & Brown AW. (2004). Relationship between strength, balance, and swallowing deficits and outcome after traumatic brain injury: a multicenter analysis. *Archives of physical medicine and rehabilitation* **85,** 1291-1297.

Ehrenfest DMD, Coelho PG, Kang B-S, Sul Y-T & Albrektsson T. (2010). Classification of osseointegrated implant surfaces: materials, chemistry and topography. *Trends in biotechnology* **28,** 198-206.

Farell BJ, Beloozerova IN & Prilutsky BI. (2008). Three dimensional kinematics and kinetics of the center of mass of the cat during walking on a narrow walkway. In *North American Congress on Biomechanics*, ed. Ashton-Miller JA, Hughes RE & Andrews DM, pp. Abstract 421. Ann Arbor, MI.

Farrell BJ, Bulgakova M, Sirota MG, Prilutsky BI & Beloozerova IN. (2011). Frontal plane mechanics and activity of motor cortex during locomotion tasks with challenging requirements for lateral stability. In *Society for Neuroscience, 2011*, pp. Program No. 710.710. 2011 Neuroscience Meeting Planner. Washington, DC. Online.

Farrell BJ, Kistenberg RS, Dalton JF, Strong A, Pitkin M & Prilutsky BI. (2012a). Evaluation of skin and bone integration with a porous titanium pylon after prosthetic gait rehabilitation in the cat. In *4th International Conference: Advances in Orthopaedic Osseointegration*. San Francisco, CA.

Farrell BJ, Pitkin M, Popat K & Prilutsky BI. (2012b). Effect of pore size, implantation time and nano-surface properties on rat skin ingrowth into porous titanium. In *4th International Conference on Advances in Orthopaedic Osseointegration*. San Francisco, CA.

Feldman DS & von Recum aF. (1985). Non-epidermally induced failure modes of percutaneous devices. *Biomaterials* **6,** 352-356.

Fridman A, Ona I & Isakov E. (2003). The influence of prosthetic foot alignment on trans-tibial amputee gait. *Prosthetics and Orthotics International* **27,** 17-22.

Frossard L, Gow DL, Contoyannis B, Ewins D, Sullivan J, Haggstrom E & Branemark R. (2002). Loading Applied to the Implant of Transfemoral Amputees Fitted with a Direct Skeletal Fixation during Load Bearing Exercises. *Proceedings of the Fourth Australasian Biomechanics Conference***,** 114-115.

Frossard L, Stevenson N, Smeathers J, Häggström E, Hagberg K, Sullivan J, Ewins D, Gow DL, Gray S & Brånemark R. (2008). Monitoring of the load regime applied

on the osseointegrated fixation of a trans-femoral amputee: a tool for evidence-based practice. *Prosthetics and orthotics international* **32,** 68-78.

Frossard LA. (2010). Load on osseointegrated fixation of a transfemoral amputee during a fall: Determination of the time and duration of descent. *Prosthetics and orthotics international* **34,** 472-487.

Fukano Y, Usui ML, Underwood RA, Isenhath S, Marshall aJ, Hauch KD, Ratner BD, Olerud JE & Fleckman P. (2010). Epidermal and dermal integration into sphere-templated porous poly(2-hydroxyethyl methacrylate) implants in mice. *Journal of biomedical materials research Part A* **94,** 1172-1186.

Full RJ, Kubow T, Schmitt J, Holmes P & Koditschek D. (2002). Quantifying dynamic stability and maneuverability in legged locomotion. *Integrative and comparative biology* **42,** 149-157.

Fuller JH & Schlag JD. (1976). Determination of antidromic excitation by the collision test: problems of interpretation. *Brain Res* **112,** 283-298.

Fung J & Macpherson JM. (1995). Determinants of Postural Orientation in Quadrupedal Stance. *Journal of Neuroscience* **15,** 1121-1131.

Fung J & Macpherson JM. (1999). Attributes of Quiet Stance in the Chronic Spinal Cat. *Journal of Neurophysiology* **82,** 3056-3065.

Galibin OV, Protasov MV, Chikhovskaya YV, Belyaeva I & Pitkin M. (2007). Study of Growth Processes in Bone and Skin Tissues in Porous Implants Designed for Fixation of External Prosthesis after Amputation of Extremities. *Cell and Tissue Biology* **1,** 272-275.

Galvez-Lopez E, Maes LD & Abourachid A. (2011). The search for stability on narrow supports: an experimental study in cats and dogs. *Zoology (Jena)* **114,** 224-232.

Glencross DJ. (1977). Control of skilled movements. *Psychological bulletin* **84,** 14-29.

Gray J. (1968). *Animal locomotion*. Weidenfeld & Nicolson, London.

Gregor RJ, Smith DW & Prilutsky BI. (2006). Mechanics of slope walking in the cat: quantification of muscle load, length change, and ankle extensor EMG patterns. *J Neurophysiol* **95,** 1397-1409.

Griffin TM, Main RP & Farley CT. (2004). Biomechanics of quadrupedal walking: how do four-legged animals achieve inverted pendulum-like movements? *J Exp Biol* **207,** 3545-3558.

Grosse-Siestrup C & Affeld K. (1984). Design criteria for percutaneous devices. *Journal of biomedical materials research* **18,** 357-382.

Hagberg K & Brånemark R. (2009). One hundred patients treated with osseointegrated transfemoral amputation prostheses—Rehabilitation perspective. *Rehabilitation* **46,** 331-344.

Hagberg K, Häggström E, Uden M & Brånemark R. (2005). Socket versus bone-anchored trans-femoral prostheses: Hip range of motion and sitting comfort. *Prosthetics and Orthotics International* **29,** 153-163.

Hall CW, Adams LM & Ghidoni JJ. (1975). Development of skin interfacing cannula. *Transactions - American Society for Artificial Internal Organs* **21,** 281-288.

Hall CW & Ghidoni JJ. (1978). Indirect percutaneous cannula construction. *The Journal of surgical research* **25,** 122-128.

Hallemans A, Ortibus E, Meire F & Aerts P. (2010). Low vision affects dynamic stability of gait. *Gait & posture* **32,** 547-551.

Hasan Z. (2005). The Human Motor Control System ' s Response to Mechanical Perturbation : Should It , Can It , and Does It Ensure Stability ? *Journal of Motor Behavior* **37,** 484-493.

Henry SM, Fung J & Horak FB. (2001). Effects of stance width on multidirectional postural responses. *Journal of Neurophysiology* **85,** 559-570.

Hildebrand M. (1965). Symmetrical gaits of horses. *Science* **150,** 701-708.

Hodgson JA. (1983). The relationship between soleus and gastrocnemius muscle activity in conscious cats--a model for motor unit recruitment? *J Physiol* **337,** 553-562.

Hof AL. (2008). The 'extrapolated center of mass' concept suggests a simple control of balance in walking. *Hum Mov Sci* **27,** 112-125.

Hof aL, Gazendam MGJ & Sinke WE. (2005). The condition for dynamic stability. *Journal of biomechanics* **38,** 1-8.

Hof AL, van Bockel RM, Schoppen T & Postema K. (2007). Control of lateral balance in walking. Experimental findings in normal subjects and above-knee amputees. *Gait & posture* **25,** 250-258.

Hol aM, van Grinsven S, Lucas C, van Susante JLC & van Loon CJM. (2010). Partial versus unrestricted weight bearing after an uncemented femoral stem in total hip arthroplasty: recommendation of a concise rehabilitation protocol from a

systematic review of the literature. *Archives of orthopaedic and trauma surgery* **130,** 547-555.

Holder-Powell HM & Rutherford OM. (2000). Unilateral Lower-Limb Effect on Balance Injury : Its Long-Term Effect on Balance. *Archives of Physical Medicine Rehabilitation* **81,** 265-268.

Honeycutt CF & Nichols TR. (2010). The decerebrate cat generates the essential features of the force constraint strategy. *J Neurophysiol* **103,** 3266-3273.

Hoy MG & Zernicke RF. (1985). Modulation of limb dynamics in the swing phase of locomotion. *J Biomech* **18,** 49-60.

Hurley G, McKenney R, Robinson M, Zadravec M & Pierrynowski M. (1990). The role of the contralateral limb in below-knee amputee gait. *Prosthetics and Orthotics International* **14,** 33-42.

Hurmuzlu Y & Basdogan C. (1994). On the measruement of dynamic stability of human locomotion. *Journal of Biomechanical Engineering* **116,** 30-36.

Ioffe ME, Chernikova LA & Ustinova KI. (2007). Role of cerebellum in learning postural tasks. *Cerebellum* **6,** 87-94.

Isackson D, McGill LD & Bachus KN. (2011). Percutaneous implants with porous titanium dermal barriers: an in vivo evaluation of infection risk. *Med Eng Phys* **33,** 418-426.

Itala AI, Ylanen HO, Ekholm C, Karlsson KH & Aro HT. (2001). Pore diameter of more than 100 μm is not requisite for bone ingrowth in rabbits. *Journal of Biomedical Materials Research* **58,** 679-683.

Jacobs JV & Horak FB. (2007). Cortical control of postural responses. *J Neural Transm* **114,** 1339-1348.

Jacobs R, Brånemark R, Olmarker K, Rydevik B, Van Steenberghe D & Brånemark PI. (2000). Evaluation of the psychophysical detection threshold level for vibrotactile and pressure stimulation of prosthetic limbs using bone anchorage or soft tissue support. *Prosthetics and orthotics international* **24,** 133-142.

Jankowska E. (2008). Spinal interneuronal networks in the cat : Elementary components. *Brain Research Reviews* **57,** 46-55.

Jansen Ja & de Groot K. (1988). Guinea pig and rabbit model for the histological evaluation of permanent percutaneous implants. *Biomaterials* **9,** 268-272.

Jansen Ja, Paquay YG & van der Waerden JP. (1994). Tissue reaction to soft-tissue anchored percutaneous implants in rabbits. *Journal of biomedical materials research* **28,** 1047-1054.

Jansen Ja, van der Waerden JP, van der Lubbe HB & de Groot K. (1990). Tissue response to percutaneous implants in rabbits. *Journal of biomedical materials research* **24,** 295-307.

Jayes AS & Alexander RM. (1980). The gaits of chelonians: walking techniques for very low speeds. *Journal of zoology* **191,** 353-378.

Jeyapalina S, Beck JP, Bachus KN, Williams DL & Bloebaum RD. (2012). Efficacy of a porous-structures titanium subdermal barrier for preventing infection in percutaneous osseointegrated prostheses. . *Journal of Orthopaedic Research* **30,** 1304-1311.

Jonsson S, Caine-Winterberger L & Branemark R. (2011). Osseointegration amputation prostheses on the upper limbs: methods, prosthetics and rehabilitation. *Prosthetics and Orthotics International* **35,** 190-200.

Kang NV, Pendegrass CJ, Marks L & Blunn GW. (2010). Osseocutaneous Integration of an Intraosseous Transcutaneous Amputation Prosthesis Implant Used for Reconstruction of a Transhumeral Amputee: Case Report. *The Journal of hand surgery* **35,** 1130-1134.

Karayannidou A, Beloozerova IN, Zelenin PV, Stout EE, Sirota MG, Orlovsky GN & Deliagina TG. (2009). Activity of pyramidal tract neurons in the cat during standing and walking on an inclined plane. *J Physiol* **587,** 3795-3811.

Karayannidou a, Deliagina TG, Tamarova Za, Sirota MG, Zelenin PV, Orlovsky GN & Beloozerova IN. (2008). Influences of sensory input from the limbs on feline corticospinal neurons during postural responses. *The Journal of Physiology* **586,** 247-263.

Kienapfel H, Sprey C, Wilke A & Griss P. (1999). Implant Fixation by Bone Ingrowth. *Journal of Arthroplasty* **14**.

Knowles NG, Miyashita Y, Usui ML, Marshall AJ, Pirrone A, Hauch KD, Ratner BD, Underwood Ra, Fleckman P & Olerud JE. (2005). A model for studying epithelial attachment and morphology at the interface between skin and percutaneous devices. *Journal of biomedical materials research Part A* **74,** 482-488.

Koc E, Tunca M, Akar A, Erbil aH, Demiralp B & Arca E. (2008). Skin problems in amputees: a descriptive study. *International journal of dermatology* **47,** 463-466.

Köhler P, Lindh L & Björklind A. (1989). Bacteria on stumps of amputees and the effect of antiseptics. *Prosthetics and orthotics international* **13,** 149-151.

Krouchev N, Kalaska JF & Drew T. (2006). Sequential activation of muscle synergies during locomotion in the intact cat as revealed by cluster analysis and direct decomposition. *J Neurophysiol* **96,** 1991-2010.

Krouskop TA, Brown HD, Gray K, Romovacek GR, Spira M & Runyan RS. (1988). Bacterial challenge study of a porous carbon percutaneous implant. *Biomaterials* **9,** 398-404.

Lalonde R & Strazielle C. (2007). Brain regions and genes affecting postural control. *Prog Neurobiol* **81,** 45-60.

Lammers AR & Biknevicius AR. (2004). The biodynamics of arboreal locomotion: the effects of substrate diameter on locomotor kinetics in the gray short-tailed opossum (Monodelphis domestica). *J Exp Biol* **207,** 4325-4336.

Lauer AC, Elder JT & Weiner ND. (1997). Evaluation of the hairless rat as a model for in vivo percutaneous absorption. *Journal of Pharmaceutical Sciences* **86,** 13-18.

Lawrence JH, 3rd, Nichols TR & English AW. (1993). Cat hindlimb muscles exert substantial torques outside the sagittal plane. *Journal of Neurophysiology* **69,** 282-285.

Lee WCC, Frossard La, Hagberg K, Haggstrom E, Brånemark R, Evans JH & Pearcy MJ. (2007). Kinetics of transfemoral amputees with osseointegrated fixation performing common activities of daily living. *Clinical biomechanics (Bristol, Avon)* **22,** 665-673.

Levy SW. (1992). Skin Problems of the Amputee. In *Atlas of Limb Prosthetics: Surgical, Prosthetic and Rehabilitation Principles*, 2nd edn, ed. Bowker H & Michael J. American Academy of Orthopedic Surgeons, Rosemont, IL.

Levy SW. (1995). Amputees: skin problems and prostheses. *Cutis; cutaneous medicine for the practitioner* **55,** 297-301.

Loram ID, Maganaris CN & Lakie M. (2007). The passive, human calf muscles in relation to standing: the short range stiffness lies in the contractile component. *J Physiol* **584,** 677-692.

Lundborg G, Brånemark PI & Rosén B. (1996). Osseointegrated thumb prostheses: a concept for fixation of digit prosthetic devices. *The Journal of hand surgery* **21,** 216-221.

MacKinnon CD & Winter Da. (1993). Control of whole body balance in the frontal plane during human walking. *Journal of biomechanics* **26,** 633-644.

Macpherson J & Fung J. (1999). Weight support and balance during perturbed stance in the chronic spinal cat. *Journal of Neurophysiology* **82,** 3066-3081.

Macpherson JM, Everaert DG, Stapley PJ & Ting LH. (2007). Bilateral vestibular loss in cats leads to active destabilization of balance during pitch and roll rotations of the support surface. *J Neurophysiol* **97,** 4357-4367.

Maki BE. (1997). Gait changes in older adults: predictors of falls or indicators of fear. *Journal of the American Geriatrics Society* **45,** 313-320.

Maki BE & McIlroy WE. (1997). The role of limb movements in maintaining upright stance: the "change-in-support" strategy. *Physical therapy* **77,** 488-507.

Maki BE & McIlroy WE. (2007). Cognitive demands and cortical control of human balance-recovery reactions. *J Neural Transm* **114,** 1279-1296.

Manter JT. (1938). The Dynamics of Quadrupedal Walking. *Journal of Experimental Biology* **15,** 522-540.

Manurangsee P, Isariyawut C, Chatuthong V & Mekraksawanit S. (2000). Osseointegrated finger prosthesis: An alternative method for finger reconstruction. *The Journal of hand surgery* **25,** 86-92.

Markin SN, Klishko AN, Shevtsova Na, Lemay Ma, Prilutsky BI & Rybak Ia. (2010). Afferent control of locomotor CPG: insights from a simple neuromechanical model. *Annals of the New York Academy of Sciences* **1198,** 21-34.

Markin SN, Lemay MA, Prilutsky BI & Rybak IA. (2012). Motoneuronal and muscle synergies involved in cat hindlimb control during fictive and real locomotion: a comparison study. *J Neurophysiol* **107,** 2057-2071.

Matthews PBC. (2004). Historical analysis of the neural control of movement from the bedrock of animal experimentation to human studies. *Journal of applied physiology (Bethesda, Md : 1985)* **96,** 1478-1485.

McAndrew PM, Wilken JM & Dingwell JB. (2011). Dynamic stability of human walking in visually and mechanically destabilizing environments. *Journal of biomechanics* **44,** 644-649.

McAndrew Young PM & Dingwell JB. (2012a). Voluntarily changing step length or step width affects dynamic stability of human walking. *Gait & posture* **35,** 472-477.

McAndrew Young PM & Dingwell JB. (2012b). Voluntary changes in step width and step length during human walking affect dynamic margins of stability. *Gait & posture*.

Miller S, Van Der Burg J & Van Der Meche F. (1975). Coordination of movements of the kindlimbs and forelimbs in different forms of locomotion in normal and decerebrate cats. *Brain Res* **91,** 217-237.

Miller WC, Deathe AB, Speechley M & Koval J. (2001a). The influence of falling, fear of falling, and balance confidence on prosthetic mobility and social activity among individuals with a lower extremity amputation. *Arch Phys Med Rehabil* **82,** 1238-1244.

Miller WC, Speechley M & Deathe B. (2001b). The prevalence and risk factors of falling and fear of falling among lower extremity amputees. *Arch Phys Med Rehabil* **82,** 1031-1037.

Misiaszek JE. (2006a). Control of Frontal Plane Motion of the Hindlimbs in the Unrestrained Walking Cat. *Journal of Neurophysiology* **96,** 1816-1828.

Misiaszek JE. (2006b). Neural control of walking balance: IF falling THEN react ELSE continue. *Exercise Sport Science Review* **34,** 128-134.

Mori S. (1987). Integration of posture and locomotion in acute decerebrate cats and in awake, freely moving cats. *Progress in Neurobiology* **28,** 161-195.

Müller U, Imwinkelried T, Horst M, Sievers M & Graf-Hausner U. (2006). DO HUMAN OSTEOBLASTS GROW INTO OPEN-POROUS TITANIUM ? *European Cells and Materials* **11,** 8-15.

Murdoch G. (1969). Balance in the amputee. *Physiotherapy* **55,** 405-408.

Murphy EF. (1973). History and philosophy of attachment of prostheses to the musculo-skeletal system and of passage through the skin with inert materials. *Journal of biomedical materials research* **7,** 275-295.

Musienko P, Courtine G, Tibbs JE, Kilimnik V, Savochin A, Garfinkel A, Roy RR, Edgerton VR & Gerasimenko Y. (2012). Somatosensory control of balance during locomotion in decerebrated cat. *J Neurophysiol* **107,** 2072-2082.

Musienko PE, Zelenin PV, Lyalka VF, Orlovsky GN & Deliagina TG. (2008). Postural performance in decerebrated rabbit. *Behav Brain Res* **190,** 124-134.

Nederhand MJ, Van Asseldonk EH, van der Kooij H & Rietman HS. (2012). Dynamic Balance Control (DBC) in lower leg amputee subjects; contribution of the regulatory activity of the prosthesis side. *Clin Biomech (Bristol, Avon)* **27,** 40-45.

Nichols TR & Houk JC. (1976). Improvement in linearity and regulation of stiffness that results from actions of strech reflex. *Journal of Neurophysiology* **39,** 119-142.

Nichols TR, Lawrence JH, 3rd & Bonasera SJ. (1993). Control of torque direction by spinal pathways at the cat ankle joint. *Experimental Brain Research* **97,** 366-371.

Nilles JL & Lapitsky M. (1973). Biomechanical investigations of bone-porous carbon and porous metal interfaces. *Journal of biomedical materials research* **7,** 63-84.

Pantall A, Gregor RJ & Prilutsky BI. (2012). Stance and swing phase detection during level and slope walking in the cat: Effects of slope, injury, subject and kinematic detection method. *Journal of biomechanics* **45,** 1529-1533.

Pendegrass CJ, Goodship AE & Blunn GW. (2006a). Development of a soft tissue seal around bone-anchored transcutaneous amputation prostheses. *Biomaterials* **27,** 4183-4191.

Pendegrass CJ, Goodship AE, Price JS & Blunn GW. (2006b). Nature's answer to breaching the skin barrier: an innovative development for amputees. *Journal of anatomy* **209,** 59-67.

Pendegrass CJ, Gordon D, Middleton CA, Sun SNM & Blunn GW. (2008). Sealing the skin barrier around transcutaneous implants. *Journal of Bone and Joint Surgery* **90B,** 114-121.

Peramo A & Marcelo CL. (2010). Bioengineering the skin-implant interface: the use of regenerative therapies in implanted devices. *Annals of biomedical engineering* **38,** 2013-2031.

Perry EL, Beck JP, Williams DL & Bloebaum RD. (2009). Assessing Peri-Implant Tissue Infection Prevention in a Percutaneous Model. *Journal of Biomedical Materials Research Part B: Applied Biomaterials***,** 397-408.

Pezzin L. (2004). Use and satisfaction with prosthetic limb devices and related services ,. *Archives of Physical Medicine and Rehabilitation* **85,** 723-729.

Pitkin M & Raykhtsaum G. (2012). Skin Integrated Device. US Patent.

Pitkin M, Raykhtsaum G, Galibin OV, Protasov MV, Chihovskaya JV & Belyaeva IG. (2006). Skin and bone integrated prosthetic pylon: A pilot animal study. *The Journal of Rehabilitation Research and Development* **43,** 573.

Pitkin M, Raykhtsaum G, Pilling J, Galibin O, Protasov MV, Chihovskaya J, Belyaeva I, Blinova M, Yudintseva M, Potokin I, Pinaev G, Moxson V & Duz V. (2007a).

Porous composite prosthetic pylon for integration with skin and bone. *Journal of Rehabilitation Research & Development* **44,** 723-738.

Pitkin M, Raykhtsaum G, Pilling J, Galibin OV, Protasov MV, Chihovskaya JV, Belyaeva IG, Blinova MI, Yudintseva NM, Potokin I, Pinaev GP, Moxson V & Duz V. (2007b). Porous composite prosthetic pylon for integration with skin and bone. *Journal of Rehabilitation Research and Development* **44,** 723-738.

Pitkin M, Raykhtsaum G, Pilling J, Shukeylo Y, Moxson V, Duz V, Lewandowski J, Connolly R, Kistenberg RS, Dalton JF, IV, Prilutsky BI, Jacobson S & Western C. (2009). Mathematical modeling and Mechanical and histopathological testing of porous prosthetic pylon for direct skeletal attachment. *Journal of Rehabilitation Research & Development* **46,** 315-330.

Pollock aS, Durward BR, Rowe PJ & Paul JP. (2000). What is balance? *Clinical rehabilitation* **14,** 402-406.

Prilutsky BI, Herzog W & Allinger TL. (1996). Mechanical power and work of cat soleus, gastrocnemius and plantaris muscles during locmotion: possible functioncal significance of muscle design and force patterns. *Journal of Experimental Biology* **199,** 801-814.

Prilutsky BI & Klishko NA. (2011). Control of locomotion: Lessons from whole-body biomechanical analysis. In *Motor control: Theories experiments and applications*, ed. Danion F & Latash ML, pp. 197-218. Oxford University Press, Oxford.

Prilutsky BI, Maas H, Bulgakova M, Hodson-Tole EF & Gregor RJ. (2011). Short-term motor compensations to denervation of feline soleus and lateral gastrocnemius result in preservation of ankle mechanical output during locomotion. *Cells, tissues, organs* **193,** 310-324.

Prilutsky BI, Sirota MG, Gregor RJ & Beloozerova IN. (2005). Quantification of motor cortex activity and full-body biomechanics during unconstrained locomotion. *Journal of neurophysiology* **94,** 2959-2969.

Puckett SD, Lee PP, Ciombor DM, Aaron RK & Webster TJ. (2010). Nanotextured titanium surfaces for enhancing skin growth on transcutaneous osseointegrated devices. *Acta Biomaterialia* **6,** 2352-2362.

Rossignol S. (2006). Plasticity of connections underlying locomotor recovery after central and/or peripheral lesions in the adult mammalts. *Philosophical transactions Royal Society London* **B Biol Sci, 361,** 1647-1671.

Rougier A. (1987). The hairless rat: a relevant animal model to predict *in vivo* percutaneous absorption in humans? *Journal of investigative dermatology* **88,** 577-581.

Ruckh T, Porter JR, Allam NK, Feng X, Grimes CA & Popat KC. (2009). Nanostructured tantala as a template for enhanced osseointegration. *Nanotechnology* **20,** 045102.

Schmid M, Conforto S, Lopez L & D'Alessio T. (2007). Cognitive load affects postural control in children. *Experimental brain research Experimentelle Hirnforschung Expérimentation cérébrale* **179,** 375-385.

Schmidt A & Fischer MS. (2010). Arboreal locomotion in rats - the challenge of maintaining stability. *J Exp Biol* **213,** 3615-3624.

Schneider CA, Rasband WS & Eliceiri KW. (2012). NIH Image to ImageJ: 25 years of image analysis. *Nature Methods* **9,** 671-675.

Schrager Ma, Kelly VE, Price R, Ferrucci L & Shumway-Cook A. (2008). The effects of age on medio-lateral stability during normal and narrow base walking. *Gait & posture* **28,** 466-471.

Schreuders PD, Salthouse TN & von Recum aF. (1988). Normal wound healing compared to healing within porous Dacron implants. *Journal of biomedical materials research* **22,** 121-135.

Scrivens JE, Ting LH & Deweerth SP. (2006). Effects of stance width on control gain in standing balance. In *28th IEEE*, pp. 4055-4057. New York.

Segal AD, Orendurff MS, Czerniecki J, Shofer JB & Klute GK. (2010). Local dynamic stability of amputees wearing a torsion adapter compared to a rigid adapter during straight-line and turning gait. *Journal of Biomechanics* **43,** 2798-2803.

Shelton TJ, Beck JP, Bloebaum RD & Bachus KN. (2011). Percutaneous osseointegrated prostheses for amputees: Limb compensation in a 12-month ovine model. *Journal of biomechanics* **44,** 2601-2606.

Sherman Ra. (1999). Utilization of prostheses among US veterans with traumatic amputation: a pilot survey. *Journal of rehabilitation research and development* **36,** 100-108.

Sherrington CS. (1910). Flexion-reflex of the limb, crossed extension-reflex, and reflex stepping and standing. *J Physiol* **40,** 28-121.

Shik ML, Severin FV & Orlovskii GN. (1966). Control of walking and running by means of electric stimulation of the midbrain. *Biofizika* **11,** 659-666.

Shinder ME & Taube JS. (2010). Differentiating ascending vestibular pathways to the cortex involved in spatial cognition. *Journal of vestibular research : equilibrium & orientation* **20,** 3-23.

Shkuratova N & Taylor N. (2008). The influence of age on gait parameters during the transition from a wide to a narrow pathway. *Physiotherapy research international : the journal for researchers and clinicians in physical therapy* **13,** 75-83.

Smith JL, Carlson-Kuhta P & Trank TV. (1998). Forms of Forward Quadrupedal Locomotion . III . A Comparison of Posture , Hindlimb Kinematics , and Motor Patterns for Downslope and Level Walking. *Journal of Neurophysiology* **79,** 1702-1716.

Snik AFM, Mylanus EaM, Proops DW, Wolfaardt JF, Hodgetts WE, Somers T, Niparko JK, Wazen JJ, Sterkers O, Cremers CWRJ & Tjellström A. (2005). Consensus statements on the BAHA system: where do we stand at present? *The Annals of otology, rhinology & laryngology Supplement* **195,** 2-12.

Stapley PJ & Drew T. (2009). The pontomedullary reticular formation contributes to the compensatory postural responses observed following removal of the support surface in the standing cat. *J Neurophysiol* **101,** 1334-1350.

Stapley PJ, Ting LH, Kuifu C, Everaert DG & Macpherson JM. (2006). Bilateral Vestibular Loss Leads to Active Destabilization of Balance During Voluntary Head Turns in the Standing Cat. *Journal of Neurophysiology* **95,** 3783-3797.

Staubach KH & Grundei H. (2001). [The first osseointegrated percutaneous prosthesis anchor for above-knee amputees]. *Biomedizinische Technik Biomedical engineering* **46,** 355-361.

Stevens NJ. (2006). Stability, limb coordination and substrate type: the ecorelevance of gait sequence pattern in primates. *Journal of experimental zoology Part A, Comparative experimental biology* **305,** 953-963.

Stynes G, Kiroff GK, Morrison WaJ & Kirkland Ma. (2008). Tissue compatibility of biomaterials: benefits and problems of skin biointegration. *ANZ journal of surgery* **78,** 654-659.

Sullivan J, Uden M, Robinson KP & Sooriakumaran S. (2003). Rehabilitation of the trans-femoral amputee with an osseointegrated prosthesis : the United Kingdom experience. *Prosthetics and Orthotics International* **27,** 114-120.

The Bulletin Online. (2005). Groundbreaking surgery puts cat on its (three) feet.

Tillander J, Hagberg K, Hagberg L & Brånemark R. (2010). Osseointegrated titanium implants for limb prostheses attachments: infectious complications. *Clinical orthopaedics and related research* **468,** 2781-2788.

Ting LH, Blickhan R & Full RJ. (1994). Dynamic and static stability in hexapedal runners. *The Journal of experimental biology* **197,** 251-269.

Ting LH, van Antwerp KW, Scrivens JE, McKay JL, Welch TD, Bingham JT & Deweerth SP. (2009). Neuromechanical tuning of nonlinear postural control dynamics. *Chaos* **19,** 026111.

Tjellström A & Håkansson B. (1995). The bone-anchored hearing aid. Design principles, indications, and long-term clinical results. *Otolaryngologic clinics of North America* **28,** 53-72.

Tjellström A, Rosenhall U, Lindström J, Hallén O, Albrektsson T & Branemark PI. (1983). Five-Year Experience with Skin-Penetrating Bone-Anchored Implants in the Temporal Bone. *Acta Oto-Laryngologica* **95,** 568-575.

Torcasio a, van Lenthe GH & Van Oosterwyck H. (2008). The importance of loading frequency, rate and vibration for enhancing bone adaptation and implant osseointegration. *European cells & materials* **16,** 56-68.

Torralba K & Quismorio F, Jr. (2009). Soft tissue infections. *Rheumatic diseases clinics of North America* **35,** 45-62.

Torres-Oviedo G, Macpherson JM & Ting LH. (2006). Muscle synergy organization is robust across a variety of postural perturbations. *J Neurophysiol* **96,** 1530-1546.

Torres-Oviedo G & Ting LH. (2010). Subject-specific muscle synergies in human balance control are consistent across different biomechanical contexts. *J Neurophysiol* **103,** 3084-3098.

Underwood RA, Usui ML, Zhao G, Hauch KD, Takeno MM, Ratner BD, Marshall AJ, Shi X, Olerud JE & Fleckman P. (2011). Quantifying the effect of pore size and surface treatment on epidermal incorporation into percutaneously implanted sphere-templated porous biomaterials in mice. *Journal of biomedical materials research Part A* **98,** 499-508.

Viswanathan A & Sudarsky L. (2012). Balance and gait problems in the elderly. *Handbook of clinical neurology / edited by PJ Vinken and GW Bruyn* **103,** 623-634.

von Recum AF. (1984). Applications and failure modes of percutaneous devices: a review. *Journal of biomedical materials research* **18,** 323-336.

von Recum AF & Park JB. (1981). Permanent percutaneous devices. *Critical reviews in bioengineering* **5,** 37-77.

Walmsley B, Hodgson JA & Burke RE. (1978). Forces produced by medial gastrocnemius and soleus muscles during locomotion in freely moving cats. *J Neurophysiol* **41,** 1203-1216.

Whelan PJ. (1996). CONTROL OF LOCOMOTION IN THE DECEREBRATE CAT. *Progress in Neurobiology* **49,** 481-515.

Williams DL, Bloebaum RD, Beck JP & Petti Ca. (2010). Characterization of bacterial isolates collected from a sheep model of osseointegration. *Current microbiology* **61,** 574-583.

Wilson AB. (1992). History of Amputation Surgery and Prosthetics. In *Atlas of Limb Prosthetics: Surgical, Prosthetic and Rehabilitation Principles*, 2 edn, ed. Bowker H & Michael J. American Academy of Orthopedic Surgeons, Rosemont, IL.

Winter DA. (1995). Human balance and posture control during standing and walking. *Gait & Posture* **3,** 193-214.

Winter GD. (1974). Transcutaneous implants: reactions of the skin-implant interface. *Journal of biomedical materials research* **8,** 99-113.

Yakovenko S, Mushahwar V, VanderHorst V, Holstege G & Prochazka A. (2002). Spatiotemporal activation of lumbosacral motoneurons in the locomotor step cycle. *J Neurophysiol* **87,** 1542-1553.

Young RP, Scott SH & Loeb GE. (1993). The distal hindlimb musculature of the cat: multiaxis moment arms at the ankle joint. *Exp Brain Res* **96,** 141-151.

Ysander M, Branemark R, Olmarker K & Myers RR. (2001). Intramedullary osseointegration : Development of a rodent model and study of histology and neuropeptide changes around titanium implants. *Journal Of Rehabilitation Research And Development* **38,** 183-190.

Zarzecki P, Blum PS, Bakker DA & Herman D. (1983). Convergence of sensory inputs upon projection neurons of somatosensory cortex: vestibular, neck, head, and forelimb inputs. *Exp Brain Res* **50,** 408-414.

Zatsiorsky VM. (2002). *Kinetics of human motion*. Human Kinetics, Champaign, IL.

Zehr EP & Stein RB. (1999). What function do reflexes serve during human locomotion? *Progress in Neurobiology* **59,** 185-205.

Zelenin PV, Beloozerova IN, Sirota MG, Orlovsky GN & Deliagina TG. (2010). Activity of red nucleus neurons in the cat during postural corrections. *The Journal of neuroscience : the official journal of the Society for Neuroscience* **30,** 14533-14542.